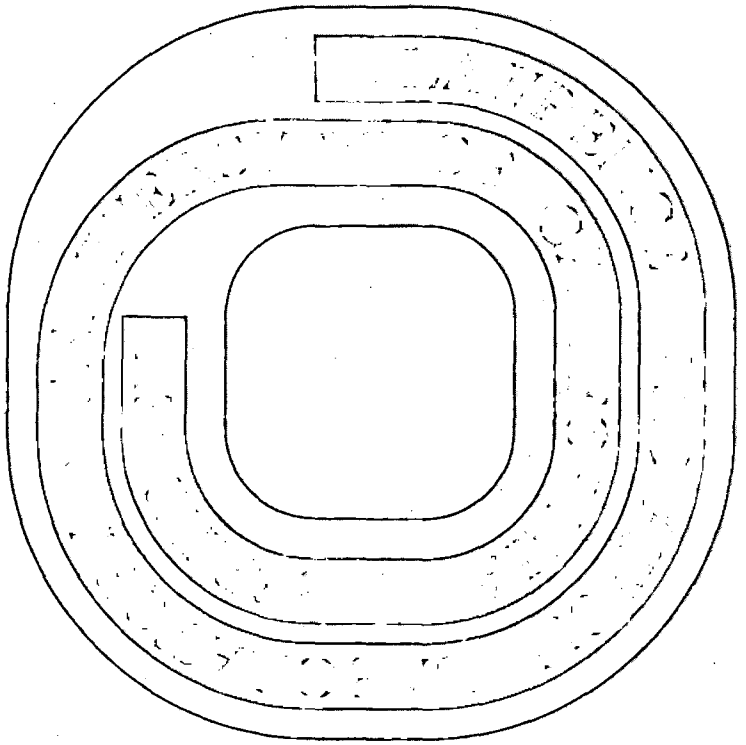

CHARGED PION PRODUCTION IN PROTON-PROTON INTERACTIONS BETWEEN 13 AND 28.5 GeV/c

Dennis Baird Smith

(Ph. D. Thesis)

March 1971

AEC Contract No. W-7405-eng-48

DISCLAIMER

Charged Pion Production in Proton-Proton Interactions Between 13 and 28.5 GeV/c

Abstract

Dennis Baird Smith

Multiparticle production is examined using 40 000 inelastic proton-proton interactions seen in the B.N.L. Hydrogen Bubble Chamber at five incident beam momenta: 13, 18, 21, 24, and 28.5 GeV/c. We present cross sections for various inelastic topologies. Using the sample of positively charged track momenta, we find that we can estimate both the π^+ and proton momentum distributions.

The cross sections for π^- production in the reaction $pp \rightarrow \pi^-$ + anything are given. For small values of π^- laboratory momentum, we find that the π^- production differential cross section is independent of beam energy, indicating that the Hypothesis of Limiting Fragmentation already holds at our energies.

The transverse and longitudinal center-of-mass momentum distributions of both π^+'s and π^-'s are given for each inelastic topology and for each beam momentum. One parameter functions successfully describe each distribution. The topology and beam energy dependence of all the longitudinal c.m. momentum spectra can be described by two parameters. The transverse momentum distributions are consistent with a high energy limit that is independent of topology and that agrees well with a picture of "hadronic boiling."

Contents

I. INTRODUCTION

The high energy interactions of hadrons produce pions copiously. This thesis documents an experimental study of multiple charged pion production in high energy proton-proton interactions.

Many aspects of proton-proton interactions have already been studied extensively.[1,2] Some of these studies have concentrated on the more accessible final states, particularly elastic proton-proton scattering.[3,4] At high energies (above 6 GeV/c), total and elastic cross section measurements show that the inelastic final states account for three-quarters of the proton-proton interactions.[5,6] Counter experiments at high energies have approached the study of particle production by measuring individually the momentum spectrum of each species of outgoing charged particle ("inclusive" experiments).[7-12] While succeeding in observing most of the inelastic events, these experiments do not determine the number of remaining particles in the final state.

Bubble chamber experiments, while observing the simultaneous production of all final charged particles, have often relied on kinematic reaction fitting (balancing energy and momentum) to identify those reactions with no more than one neutral particle among the outgoing particles.[13] Although information is obtained about all outgoing particles in these reactions, at high beam energies these analyses studied only a small fraction of the total number of inelastic events. Two other analyses have examined all final charged particles.[4,14]

In this experiment we determine the charged pion production in non-strange proton-proton interactions classified by the total number of charged particles in the final state. In November 1966, 70 000 pictures of proton-proton interactions were taken in the 80-Inch B.N.L.

Hydrogen Bubble Chamber at five widely separated beam momenta: 13, 18, 21, 24, and 28.5 GeV/c.[15] At each momentum the flux of incident protons was approximately 1/2 event/proton. Section II of this thesis describes the analysis of the 40 000 non-strange inelastic topology events: from the scan of this film we found the events (and the number of outgoing charged particles for each); from the measurements of these events we determined the momentum spectra of the charged pions. We limit this analysis to the charged pion production in final states containing four or more charged particles: excluding obvious strange particle production, we do not identify specific final states of exclusive reactions nor do we discuss our neutral particle production.[16]

In Section III the π^- laboratory production cross sections summed over topology are presented. We examine the beam energy dependence of these cross sections to test the Hypothesis of Limiting Fragmentation.[17] In Section IV we give the π^+ and π^- momentum spectra for each topology. We successfully parameterize all of the c.m. momentum distributions.

II. EXPERIMENTAL PROCEDURES

We first discuss the exposure of the film, then the scan for inelastic events, and finally the measurement of the charged tracks in these events to determine the laboratory momentum of the charged final particles.

A. Recording the Events

Protons accelerated to beam energies by the A.G.S. were scattered off an internal target. Beam C4 (the RF Separated Beam run in the unseparated mode) guided protons from the forward elastic peak to the 80-Inch Liquid Hydrogen Bubble Chamber.[18] A special camera was prepared for the chamber with all three views on the same reel of 46 mm film ("LRL format" --as contrasted to the BNL camera with each view on its own reel of 70 mm film).[19] This camera was used to take 70 000 triads divided into roughly equal numbers of triads with 13, 18, 24, 21, and 28.5 GeV/c incident beam momenta.

B. Scanning the Film

The film was brought back to the Lawrence Radiation Laboratory for analysis. The film was scanned for specific topologies.[20] The topology of an event is defined by the number of outgoing charged tracks ("prongs") and the presence or absence of visible strange particle decays. A two-prong event without a decay is called an "elastic topology." The scanner sees an incident beam track and only two outgoing tracks.

Strange particle decays are indicated by either a "kink" in the track of an outgoing charged particle which decays or a "Vee" pointing back at the interaction vertex from the decay of an outgoing neutral particle. They cause the event to be classified as having a "strange" topology; independent of the number of prongs.

Four or more final charged particles indicate inelastic particle production and, if there are no visible decays, the events are recorded as having an "inelastic topology."

In this thesis, we will only analyze events of inelastic topology, excluding those of strange topology. Henceforth, by "pp interactions," we mean non-strange pp interactions.

The film was divided into two portions within each momentum interval. Approximately one-third was scanned exhaustively for the number of incident beam tracks. All of the film was scanned for the inelastic topology events.[20] Both scans were performed twice. Any disagreement between the two scanners was resolved if necessary by a third "conflict" scan.

The scan resulted in 40 000 inelastic topology events. We saw appreciable numbers of events with four through fourteen prongs! Figure 1 shows a typical multi-pronged event.

C. Topological Cross Sections

The results of the beam track scans were used to determine the cross sections by topology for four or more final state charged particles. The determination of pathlength and the calculation of cross sections are described in Appendix A. Figure 2 displays the cross sections (also given in Table I) as a function of incident beam momenta. Fits to the four-, six-, and eight-prong production are the results of calculations by G. F. Chew and A. Pignotti using a multi-peripheral bootstrap model containing two parameters and are shown as solid curves on Figure 2. (The dashed lines through the 10-, 12-, and 14-prong values are our freehand curves.)

D. The Laboratory Momenta of the Charged Particles

We next determined the laboratory momentum of each outgoing track.

1. Measuring Procedure

The track image on the three views of the bubble chamber film was approximated by measuring machines as three sets of points along the images. These three sets of points were then used to reconstruct the charged particle's trajectory through the 80-Inch Bubble Chamber. The curvature and angles of the trajectory in the bubble chamber's magnetic field determine the laboratory momentum of the particle.

We measured the events by the Franckenstein II (except for the 13 GeV/c four prongs which were first measured by the Spiral Reader I). The measured track momenta were produced by the procedure described in Figure 3. We made "second measurements" of the events which failed to pass this procedure.

2. Modifications to SIOUX

Optical and magnetic constants appropriate to the 80-Inch Hydrogen

Bubble Chamber were introduced into the program SIOUX.[26-28] We used the μ^+ range from 200 stopping π^+ decays to find the range-energy scale factor.[29] To check SIOUX's estimates of the uncertainties ("errors") in the measured momentum values, we used a sample of events corresponding to the reaction $pp \rightarrow pp\pi^+\pi^-$. Minimum error estimates, or floors, in the curvature measurements and in the angle measurements were necessary to give us the theoretical χ^2 distribution for four constraints.

This sample of events from the reaction $pp \rightarrow pp\pi^+\pi^-$ also allowed us to determine our incident beam momenta to better than 0.1 %. We determined our five beam momenta to be: 12.88, 18.00, 21.08, 24.12, and 28.44 GeV/c. The spread about a central value was designed to be less than 0.5 % in the unseparated mode of the RF separated beam.

3. Rate of Successful Track Measurement

Tracks were omitted from the final sample in several ways. Using criteria which did not bias the sample, the scanners ruled seven per cent of the events unmeasurable.[20]

Entire events were rejected in PANAL, MATCH, and SIOUX. The passing rate and the number of passing events are given for each beam momentum and topology in Table II. (More than 94 % of the events with four through eight prongs passed; this fraction drops with increasing numbers of tracks.)

Individual track measurements failed in SIOUX. Table III and IV give the numbers of positive and negative track momenta out of the total number of positive and negative tracks in events which passed SIOUX. (Roughly three percent of the positive and two percent of the negative tracks fail SIOUX.)

Finally, additional tracks which passed TVGP were rejected for

poor measurements. The main difficulties were with the fast outgoing tracks which were confused with adjacent beam tracks and also a small number of short tracks. These problems were only important in our sample of positive tracks. Figure 4 shows the distribution in inverse laboratory momenta for positive tracks from 28 GeV/c four prongs. We removed 2.7% of the track momenta (shown shaded) from this sample. The relative contribution of these tracks to the transverse and longitudinal laboratory momentum spectra is shown in Figure 5. We rejected less than 2.2% of the positive tracks for all other topologies and beam momenta. Figure 6 shows the distribution in inverse laboratory momentum for negative tracks in 28 GeV/c four-prong events. Fewer than 0.3% of the negative tracks have inverse momenta smaller than that of the beam.

E. Contamination in the Sample of Charged Pion Momenta

Most negative tracks will be π^-. Other negatively charged hadron may be in the sample: K^-, Σ^-, Ξ^-, Ω^-, and $\bar{p}$, and $\overline{\Sigma^+}$. We expect a K^- contamination of less than four percent of the π^- production from the rate of K^- to π^- production at 19 GeV/c.[8] Events with Σ^- decays are not present in our sample of non-strange inelastic topology events.[30] Cross sections for producing the last four are expected to be small at these energies.[7,8,11]

The positive track sample contains significant numbers of both π^+ and protons. Reference 8 reported K^+ production to be seven percent of the π^+. Nearly all K^+ contamination from YK production is absent from our sample, since we see the decaying hyperon in the bubble chamber. By arguments similar to those above for the negative baryons, we may neglect the other positive baryons.

F. Separation of π^+ and Proton Momentum Distributions

Since an unknown mixture of the reactions:

$$pp \rightarrow pp + N\,\pi^+ + N\,\pi^- + \text{unseen } \pi^o\text{'s}$$
$$pn + (N+1)\pi^+ + N\,\pi^- + \text{unseen } \pi^o\text{'s}$$
$$nn + (N+2)\pi^+ + N\,\pi^- + \text{unseen } \pi^o\text{'s}$$

produces our sample of non-strange events with 2N+2 final charged particles ($N \geq 1$), our positive tracks are an undetermined combination of π^+ and protons. In only a small fraction of the events does energy-momentum balance or ionization distinguish among the various reactions possible.[31] Thus we introduce a new approach to the separation of π^+ and proton momenta.[32]

The tracks moving backwards in the laboratory can only be π^+, not protons. Events producing a proton which moves backwards in the laboratory fail to conserve energy. When the proton goes backward in the laboratory, the remaining final particles have a combined momentum greater than that of the beam. However, baryon conservation gives these remaining particles a combined mass of at least that of the beam nucleon so that their energy is greater than that of the target, so we have gained energy!

We use these known pions and the forward-backward symmetry of proton-proton interactions in the c.m. to separate out the π^+ spectrum as explained in the following discussion (the details of the procedure used are discussed in Appendix B):

The laboratory spectrum of backward pions is transformed to the c.m. We reflect this spectrum about the origin and transform it to the laboratory to estimate the number of π^+ in a region of forward laboratory momenta. Subtracting this distribution from the laboratory momentum spectrum of all positively charged tracks gives

the corresponding forward proton spectrum.

This laboratory distribution of protons is transformed to the c.m., reflected and transformed to the laboratory to estimate the momentum spectrum of the protons with low values of laboratory momenta. These slow protons can be subtracted from the positive tracks in the laboratory frame to give us the corresponding portion of the slowly forward moving π^+ spectrum.

This procedure iterates to determine the entire π^+ and proton spectrum.

For this procedure to be useful, the number of iterations had to be low, since the errors rise with the absolute sum of the numbers subtracted to determine the π^+ spectrum. The maximum number of iterations, which increases with increasing transverse momentum, is three for tracks with transverse momenta less than 0.6 GeV/c at 28 GeV/c beam momentum.

III. NEGATIVE PION PRODUCTION

Our sample of events with four and more prongs contains all π^- production. Here we put them all together to study the non-strange "inclusive" reaction $pp \rightarrow \pi^- +$ anything.

A. π^- Production Cross Section and Average π^- Multiplicity

Using the cross section for production of n final π^-'s, σ_n, as given in Table I, the cross section for π^- production through the reaction $pp \rightarrow \pi^- +$ anything is $\sigma_\pi = \sum_n n\sigma_n$. The average π^- multiplicity, σ_π/σ_T, where σ_T is the total proton-proton cross section, is shown in Figure 7.

B. Laboratory Differential Production Cross Sections for π^-

The forward-backward symmetry of proton-proton interactions in the overall c.m. enables us to give a complete description of the π^- production spectra using only those π^- moving backwards in the c.m. After checking that our c.m. π^- momentum distribution was forward-backward symmetric, we reflected the forward π^- c.m. momenta and transformed them back to the laboratory frame to double the statistics of our π^- laboratory momenta distributions.

The momenta of the π^- are decomposed into a momentum component along the beam direction (its longitudinal momentum $p_\parallel$) and a component in the plane perpendicular to the beam direction (its transverse momentum $p_\perp$).

We calculated the cross section, $\frac{d^2\sigma}{dp_\perp dp_\parallel} = \sum_n F_n(\underline{p}) n\sigma_n$, where, in (2n+2)-pronged events with cross section σ_n, $n\sigma_n$ is the relative production of π^- and $F_n(\underline{p})$ is the fraction of these π^- falling into the laboratory momentum interval, $\Delta p_\perp \Delta p_\parallel$. Our bins have width $\Delta p_\perp = \Delta p_\parallel = 0.1$ GeV/c.

This cross section was evaluated in the laboratory frame to check predictions of several current theories. These cross sections are expected to become constant at high energies independent of the incident beam momentum except for changes in the kinematic boundaries. We tested that $\frac{d^2\sigma}{dp_\perp dp_\parallel}$ was constant using the kinematic region of π^- production at 13 GeV/c which is overlapped by those of the four other beam momenta.

For each bin of laboratory momentum, $\Delta p_\perp \Delta p_\parallel$, the magnitude of the cross sections at the five incident beam momenta were ordered from first first through fifth. Figure 8 shows the distributions in rank as a function of beam momentum. For example, the left column of Figure 8 gives the number of times the largest cross section occurs at each beam momentum. The results show little correlation of rank with beam energy.

As a further test of the prediction, we used the χ^2-test to see if, for each bin, $\Delta p_\perp \Delta p_\parallel$, the measurements of the cross section, $\frac{d^2\sigma}{dp_\perp dp_\parallel}$, can be represented by a single average value.

For each bin the minimum χ^2 and corresponding confidence level are shown in Table VI. In Figure 9, we display a histogram of our χ^2 for four degrees of freedom. The least-squares averages of the cross sections are shown in Table VII.

The models of multi-particle production which predict the beam energy independence of these cross sections are: the multi-peripheral model,[34] the "parton" model,[35] and the "Hypothesis of Limiting Fragmentation."[17] As the beam energy increases, these theories are expected to describe pion production over ever-widening ranges of laboratory momenta, so that the number of pions satisfying the hypotheses can increase without bound. But in our range of laboratory π^- momenta.

our measured cross sections are those expected for all higher beam energies.

C. Average π^- Transverse Momentum

The average of all π^- transverse momenta is shown as a function of incident beam momentum in Figure 10. In this energy range, the average transverse momenta have reached only ~80% of the constant value reported at much higher (TeV) energies.[36]

IV. CHARGED PION PRODUCTION BY TOPOLOGY

A. Rate of Charged Pion Production

The number of events classified by the numbers of final charged particles, i.e., our charged multiplicity distribution, is given in Table IX for each of our beam momenta.

Using the π^+ momentum spectrum estimated by the methods described in Section II-F, we found the average number of π^+ per event. In Table X we list the difference between the number of π^+ and π^- per event for each topology and beam momentum. The excess number of π^+ per event over the number of π^- appears to be somewhat independent of charged multiplicity at our highest momenta. At 28 GeV/c the incident nucleons for four prongs and above have a probability of .37 ± .02 for exchanging their positive charge.

B. Transverse and Longitudinal Charged Pion Center-of-Mass Momenta

Figure 11 shows the transverse and longitudinal c.m. momentum distributions for pions of both charges, at each of the five beam momenta, and for all non-strange inelastic topologies. We display the data in separate histograms of c.m. momentum, $\frac{dN}{dp_\perp}$, $\frac{dN}{dp_\parallel}$, summing over the dependence on the other momentum component. (The backward π^- c.m. momenta were reflected and added to the forward c.m. π^- momenta to double our statics for our forward π^- c.m. momentum distribution.)

We studied the shape of the pion momentum distributions (the differential cross sections can be found from the topology cross sections in Table I) and found that we can represent each histogram by functions of the form:

$$\frac{dN}{dp_\perp} = N_T \frac{a_\perp^{5/2}\, p_\perp^{3/2}\, e^{-a_\perp p_\perp}}{(3/4)\ \sqrt{\pi}} \qquad (1)$$

$$\frac{dN}{dp_\parallel} = N_T\, a_\parallel\, e^{-a_\parallel p_\parallel} \qquad (2)$$

where N_T is the total number of tracks). These functions, suggested by the thermodynamical model,[37,38] had been used earlier by Elbert et al., to obtain good fits to the distributions of c.m. momentum components of pions produced in 24 GeV/c π^-p interactions.[14]

The χ^2 minimization procedure was used to determine the best fit parameters. In fitting the π^+ histograms, it was necessary to determine M_i, the absolute sum of the quantities subtracted to determine N_i, the number of π^+. The error in N_i is taken as $\delta N_i = \sqrt{M_i}$. For the π^- histograms the error is taken to be $\delta N_i = \sqrt{N_i}$.

Since the Poisson distribution is asymmetric for small numbers, we only considered bins where $N_i \geq 5$ for the χ^2 fits. With one adjustable parameter, the number of degrees of freedom is one less than the number of bins used.

There were approximately 30 degrees of freedom for the 4 and 6 prongs' longitudinal c.m. momentum distributions and about 20 for the remaining distributions. Figure 12 shows a histogram of confidence levels from the fits. Although the distribution peaks at zero, only four of the 94 fits have confidence levels of less than .01 and the lowest confidence level we found was 8×10^{-4}, showing that all of the distributions are reasonably fitted.

The coefficients $a_\perp$ and $a_\parallel$ for the π^+ and π^- distributions are given in Table XI for every combination of beam momentum and charged multiplicity. The π^+ and π^- coefficients can be seen to be close in value

(within 10%). However, at each beam energy, the coefficients describing π^+ transverse momentum distributions are consistently greater than those describing the π^-.

Because of the better statistics, we study the topology and beam momentum dependence of the π^- transverse and longitudinal c.m. momentum distribution coefficients. For each beam momentum, Figure 13 shows the longitudinal and transverse coefficients as a function of topology. A linear fit is adequate to describe the dependence on the number of charged prongs. The results of the fits are superimposed on the data of Figure 13 as solid curves. With the same functional forms (1) and (2), the fits of 24 GeV/c π^-p interactions by Elbert et al. also showed a linear dependence on the number of charged prongs.

The coefficients $a_{\parallel}$ of our longitudinal c.m. momentum distributions are shown in Figure 14 for all topologies as a function of beam momentum. The variation of the coefficients $a_{\parallel}$ with the total c.m. energy, W_{cm}, and the number of π^- per event, n, is well represented by the function: $a_{\parallel}(n,W_{cm}) = \frac{c+dn}{W_{cm}}$. A fit to our 24 π^- longitudinal coefficients gives $\chi^2 = 27$ for $c = 10.2 \pm 0.2$ and $d = 5.4 \pm 0.1$ The curves corresponding to the fit are shown superimposed on Figure 14. It would be interesting to see if these coefficients are capable of describing the shape of charged pion momentum distributions by topology at much higher energies.

Figure 15 shows the transverse coefficients as a function of beam momentum for all topologies. The total reaction energy dependence of the transverse coefficients was fit separately for each topology to the function form:

$$a_{\perp}(n,W_{cm}) = e(n) + \frac{f(n)}{W_{cm}} \qquad (3)$$

Our fits are superimposed on Figure 15. Fitting the coefficients e(n) and f(n) with a linear dependence on topology gives

$$e(n) = (6.3 \pm 0.5) + (-0.3 \pm 0.3)n$$

$$f(n) = (5.9 \pm 3.2) + (5.3 \pm 1.8)n$$

The only significant topology dependence is from the energy-dependent term and agrees well with that of the longitudinal coefficient,

$$a_{\parallel}(n,W_{cm}) = \frac{(10.2 \pm 0.2) + (5.4 \pm 0.1)n}{W_{cm}}$$

If the energy dependence of equation (3) holds, the asymptotic values of the coefficients $a_{\perp}$ at high energy are consistent with being independent of the topology.

In the statistical thermodynamic model of R. Hagedorn, the thermodynamic production of particles reaches a maximum temperature T_o = 160 MeV at the "boiling point of hadronic matter."[37] For descriptions of the transverse momentum distributions by the function (1), the temperature T_o gives a limiting value of $a_{\perp} = 6.25$.

V. CONCLUSIONS

In our survey of inelastic non-strange proton-proton interactions over a wide range of beam energies, we found many aspects of multiple charged pion production which could be described simply.

The cross section for production of π^-'s with slow laboratory momenta via the reaction $pp \rightarrow \pi^- +$ anything is constant independent of the beam momentum. The Hypothesis of Limiting Fragmentation holds for π^- production at our energies.

For different numbers of final charged particles, the shapes of secondary charged pion transverse and longitudinal c.m. momentum distributions can be accurately summarized by one-parameter functions.

In our energy range, the transverse momentum spectra appear to be undergoing a transition to an asymptotic distribution whose shape is independent of the charged multiplicity and beam momentum.

The shapes of all of our longitudinal c.m. momentum distributions are described by a simple two-parameter function which shows the dependence on beam momentum and number of final charged particles.

ACKNOWLEDGMENTS

My parents have encouraged me throughout my education.

Many people have given invaluable assistance in this experiment. Robert J. Sprafka adapted the analysis programs to the B. N. L. 80-Inch Hydrogen Bubble Chamber. Wallace E. Hendricks was extremely competent in coordinating our scanning and measuring. Jared Anderson, in addition to proposing the experiment with Janos Kirz and T. B. Day, actively encouraged our effort with useful advice. Jon Aymong gave enthusiastic and intensive help in the analysis.

Professor Ronald Ross patiently provided guidance and helped me to develop a more mature and thorough view of the experiment.

The staff of Group A was very cooperative, providing much assistance at all stages of this analysis, and the physicists readily offered good advice on many difficulties.

In addition, I would like to thank L. W. Alvarez and R. Muller for many stimulating discussions of physics.

APPENDICES

A. Calculations of the Topology Cross Sections

We completed a conflict scan of our film for all topologies except two prongs. The scanners counted the beam tracks in a portion of the film at each beam momentum. This appendix describes our calculation of the non-strange (excluding two prongs) topology cross sections at our five momenta.

1. Determination of topology cross section

The partial cross sections were calculated as

$$\sigma_i = \frac{N_i \ \sigma_T}{N_{bt} \ (1-e^{-L \rho N_a \sigma_T / M})} \qquad (1)$$

where

1) N_i is the number of particles of a given topology in this portion of the film corrected for scanning inefficiencies.
2) σ_T is the total proton-proton cross section.
3) N_{bt} is the number of entering beam tracks.
4) L is the length of a track down the whole bubble chamber = 139 $\pm$ 1 cm.
5) ρ is the density of hydrogen in the BNL 80-inch bubble chamber = 0.06138 $\pm$ 0.00065 gm/cm^3.
6) N_a is Avogadro's number = 6.02252 x 10^{23}/mole.
7) M is the proton's gram atomic weight = 1.0073 gm/mole.

Equation (1) follows from the usual definition of a partial cross section; $\sigma_i = \frac{N_i}{(P \rho N_a / M)}$, where P is the total path length. The total path length is calculated from the attenuation of the total number of beam tracks, N_{bt}, as they travel down the bubble chamber of length L: $P = \int_0^L N_{bt} \ e^{-x/\lambda} \ dx$, where $1/\lambda = N_a \rho \sigma_T / M$.

2. Values used in the calculation of the topology cross sections

a. Scanning efficiencies and the total number of events. Non-strange topologies have no decays or "Vee's" in the scan volume. Multi-prongs with associated electron-positron pairs were taken as normal multi-prongs if the pair had both tracks minimum ionizing and had momenta less than 110 MeV/c. If a pair had a 0° opening angle and momenta less than 1.5 BeV/c, it was also treated as an associated $e^{\pm}$.

For each topology and at each momentum, the total number of events was inferred from the efficiencies ϵ_1, ϵ_2, for the first or second scanner finding an event in the (assumed) statistically independent sample of all the events seen by the other scanner. Then the probability of the conflict scan's missing an event may be taken as $(1-\epsilon_1)(1-\epsilon_2)$, which Table XII shows is less than 0.0006 for all topologies and beam momenta. The efficiency of the conflict scan's finding an event is $1-(1-\epsilon_1)(1-\epsilon_2)$. The total number of events is then the total number seen by the conflict scan divided by its efficiency for finding an event. (This discussion is identical to that of reference 39 except that the efficiency of a scanner is defined as the total number that scanner sees out of all events seen by the conflict scan.) The error in the total number of events, taken as the square root, disregards the errors in the efficiencies.

According to reference 40, either scanner's ruling a frame unscannable resulted in all events in the frame being deleted. This convention should not affect the total number of events, but we found it slightly affected the number of events seen with many prongs.

b. Beam track count. The scanners counted all the beam tracks according to the instructions of reference 20.

c. Length of non-interacting beam track. We used the conventions of reference 20 to determine the desired fiducial volume corresponding to grids 3-26 on the scan table. On one scan table, using measured events' reconstructed vertex locations, we found events under the lines between grids 2 and 3 and grids 26 and 27. The difference in the vertex y coordinates yielded 139 cm in space, which we use as a fiducial length. Then with some events lying under these grid lines we examined the effects of:

1) different scan tables
2) distortion caused by grid or film not moving in the focal plane of its lens.
3) three different grid alignment criteria given in reference 20 .

We concluded that an error of ± 1/6 grid zone or ± 1 cm reconstructed in bubble chamber space was appropriate. (This corresponds to a .7 $^{o}/_{o}$ error in the number of μb event.) The entry angle of the beam and the protons' curvature in the magnetic field give a systematic extra track length of .3 $^{o}/_{o}$.

A Master List tally by grid zone showed no decline in the number of events in our extreme grid zones.

d. Hydrogen Density, Avogadro's Number, and Proton Mass in amu. Reference 29 gives our value of the density of liquid hydrogen in the BNL 80-inch bubble chamber:

0.06138 ± 0.00065 gm/cm^3.

Reference 41 gives Avogadro's number and the proton's atomic mass. (We took the errors on both of these numbers to be zero.)

e. Dependence on σ_T.

Because our bubble chamber is only 1/5 of an interaction length for protons in hydrogen, the variation of the number of μb/ event,

$$\frac{\sigma_T}{N_{bt}\,(1-e^{-L\rho N_a\,\sigma_T/M})} ,$$

is small with respect to any variation of the input parameter, σ_T . For example, a change of σ_T from 39 mb to 30 or 50 mb changes the μb/ event by ± 2.5 $^{o}/_{o}$. We chose our σ_T from the results of reference 5 since they had measurements close to all of our momenta. The relatively large uncertainty (± 1.5 mb) of these measurements does not trouble us since it accounts for a fractional error of only .4 $^{o}/_{o}$ in our expression.

B. Procedure for Separating π^+ and Proton Momentum Spectra

We prepared histograms of the pion and proton c.m. momenta from the sample of positive tracks' laboratory momenta by the following procedure:

(1) Transform the laboratory momentum to the c.m. with a pion mass and, if the longitudinal component of c.m. momentum is negative, continue with (2), otherwise go to (4).

(2) Reflect the c.m. momentum forward, transform the momentum to the laboratory as a pion, transform it to the c.m. as a proton, and enter it in the proton histograms with negative weight.

(3) Reflect the c.m. momentum backward, transform to the laboratory as a proton, transform the c.m. as a pion, and include in the pion histograms with positive weight. If the longitudinal component of the c.m. momentum is negative iterate the procedure (i.e., return to (2)), otherwise stop.

(4) Transform the initial laboratory momentum to the c.m. as a proton: if the c.m. longitudinal momentum is positive continue with 5), otherwise stop.

(5) Reflect the c.m. momentum backwards, transform it to the laboratory as a proton, transform it to the c.m. as a pion, and give it negative weight in the pion distributions

(6) Reflect it forward and transform it to the laboratory as a pion, transform it to the c.m. as a proton and enter it in the proton histograms with positive weight. If the longitudinal c.m. momentum of the proton is positive, iterate the procedure (i.e., go to (5)), otherwise stop.

REFERENCES AND FOOTNOTES

1. Odette Benary, LeRoy R. Price and Gideon Alexander, NN and ND Interactions (Above 0.5 GeV/c) - A Compilation, Particle Data Group UCRL-20 000 NN (1970).
2. H. Yukawa, ed., Experimental Data on Hadron Interactions in GeV Region, Supplement of the Progress of Theoretical Physics Extra Number (1967).
3. A. N. Diddens, E. Lillethun, G. Manning, A. E. Taylor, T. G. Walker, and A. M. Wetherell, Phys. Rev. Lett. 9, 108 (1962); K. J. Foley, S. J. Lindenbaum, W. A. Love, S. Ozaki, J. J. Russell, and L. C. L. Yuan, Phys. Rev. Lett. 11, 425 (1963); P. Breitenlohner, P. Egli, H. Hofer, W. Koch, M. Nikolic, J. Pahl, A. Pallinger, E. Pallinger, M. Schneeberger, R. Schneeberger, H. Winzeler, G. Czapek and G. Kellner, Phys. Lett. 7, 73 (1963).
4. P. Dodd, M. Jobes, J. Kinson, B. Tallini, B. R. French, H. J. Sherman, I. O. Skillicorn, W. T. Davies, M. Derrick and D. Radojicic, Pion Production by 24 GeV/c Protons in Hydrogen, in Proceedings of the Aix-en-Provence International Conference on Elementary Particles, Vol. I, Sept. 1961, p. 433.
5. A. Ashmore, G. Cocconi, A. N. Diddens, and A. M. Wetherell, Phys. Rev. Lett. 5, 576 (1960).
6. G. Bellettini, G. Cocconi, A. N. Diddens, E. Lillethun, J. Pahl, J. P. Scanlon, J. Walters, A. M. Wetherell and P. Zanella, Phys. Rev. Lett. 14, 164 (1965); W. Galbraith, E. W. Jenkins, T. F. Kycia, B. A. Leontic, R. H. Phillips, A. L. Read, and R. Rubinstein, Phys. Rev. 138, B913 (1965); K. J. Foley, R. S. Jones, S. J. Lindenbaum, W. A. Love, S. Ozaki, E. D. Platner, C. A. Quarles, and E. H. Willen, Phys. Rev. Lett. 19, 857 (1967).
7. D. Dekkers, J. A. Geibel, R. Mermod, G. Weber, T. R. Willitts, K. Winter, B. Jordan, M. Vivargent, N. M. King, and E. J. N. Wilson, Phys. Rev. 137, B962 (1965).
8. A. N. Diddens, W. Galbraith, E. Lillethun, G. Manning, A. G. Parham, A. E. Taylor, T. G. Walker, and A. M. Witherell, Nuovo Cimento 31, 961 (1964).

9. E. W. Anderson, E. J. Bleser, G. B. Collins, T. Fujii, J. Menes, F. Turkot, R. A. Carrigan, R. M. Edelstein, N. C. Hein, T. J. McMahon, and I. Nadelhaft, Phys. Rev. Letters 19, 198 (1967).

10. J. L. Day, N. P. Johnson, A. D. Krisch, M. L. Marshak, J. K. Randolph, P. Schmueser, G. J. Marmer and L. G. Ratner, Phys. Lett. 23, 1055 (1969).

11. L. G. Ratner, K. W. Edwards, C. W. Akerlof, D. G. Crabb, J. L. Day, A. D. Krisch, and M. T. Lin, Phys. Rev. 166, 1353 (1968) and Phys. Rev. Letters 18, 1218 (1967).

12. D. G. Crabb, J. L. Day, A. D. Krisch, M. T. Lin, M. L. Marshak, J. G. Ashbury, L. G. Ratner and A. L. Read, Phys. Rev. Lett. 21, 830 (1968).

13. H. Boggild et al. (The Scandinavian Collaboration), Phys. Lett. 30B, 369 (1969); P. L. Connolly, I. R. Kenyon, R. R. Kinsey, and A. M. Thorndike, The Analysis of 28.5 GeV/c pp Interactions Producing 6 or More Charged Final Particles, BNL-13694, June 1969; R. Enrlich, R. Nieporent, R. J. Plano, J. B. Whittaker, C. Baltay, J. Feinman, P. Franzini, R. Newman, and N. Yeh, Phys. Rev. Lett. 21, 1839 (1968); W. E. Ellis, T. W. Morris, R. S. Panvini, and A. M. Thorndike, A. Description of Final States with Three, Four, and Five Particles in pp Interactions at 28.5 GeV/c, BNL-13671, June 1969; J. I. Rhode, R. A. Leacock, W. J. Kernan, R. A. Jespersen, and T. L. Schalk, Phys. Rev. 187, 1844 (1969); J. G. Rushbrooke and J. R. Williams, Phys. Rev. Lett. 22, 248 (1969).

14. J. W. Elbert, A. R. Erwin, S. Mikamo, D. Reeder, Y. Y. Chen, W. D. Walker, and A. Weinberg, Phys. Rev. Lett. 20, 124 (1968).

15. Analyses of this exposure have been reported previously by Z. Ming Ma, G. A. Smith, R. J. Sprafka, and G. T. Williamson, Phys. Rev. Lett. 24, 1031 (1970). Also see Z. Ming Ma, R. J. Sprafka, and G. A. Smith, Proton-Proton Elastic Scattering Between 13.0 and 28.4 GeV/c, Michigan State University, 1969; D. B. Smith, R. J. Sprafka, and J. A. Anderson, Phys. Rev. Lett. 23, 1064 (1969).

16. J. W. Elbert, A. R. Erwin, W. D. Walker and J. W. Waters, Nuclear Physics B19, 85 (1970).

17. J. Benecke, T. T. Chou, C. N. Yang, and E. Yen, Phys. Rev. 188, 2159 (1969); T. T. Chou and C. N. Yang, Phys. Rev. Lett. 25, 1072 (1970).

18. H. Foelsche, J. Lach, J. Sandweiss, and M. Gundzik, Optical Design of an RF Separated Beam for the BNL 80-In. Bubble Chamber, Brookhaven National Laboratory Report HF/JL/MG-1, July 1964.

19. Duane Norgren, 80" BNL Bubble Chamber Camera Stereo Image Calibration Object-Space Dimension, Lawrence Radiation Laboratory, Note UCID 2742, Jan. 1966.

20. R. J. Sprafka and W. E. Hendricks, Experiment 26 Scanning Instructions, Lawrence Radiation Laboratory, Alvarez Physics Memo No. 617, December 1966: addenda-#1, Jan. 1966; #2, Dec. 1966; #3, Jan. 1967; #4, April 1967.

21. G. F. Chew and A. Pignotti, Phys. Rev. 176, 2112 (1968).

22. M. S. Hutchinson, N. K. Ruiz, and W. O. Koellner, 6600 LYRIC III, Lawrence Radiation Laboratory Alvarez Programming Note P-148 (Revised), May 1968.

23. Alston, Berge, Braley, Campbell, Harvey, Hutchinson, and Schneider, Panal, Lawrence Radiation Laboratory Alvarez Physics Memo No. 358 (Revised), Feb. 1963. C. Toland Draper, MOTIF A 6600 Measurement Editor Program for Events Measured on the Franckensteins, Lawrence Radiation Laboratory Alvarez Programming Note P-169, Jan. 1968.

24. Alice J. Lee, Operation of Match 5 A Program Which Correlates Tracks in Three Views, Lawrence Radiation Laboratory Alvarez Programming Note P-165, July 1967. Sam Penny and M. Alston, Match (Fortran II Version), Lawrence Radiation Laboratory Alvarez Programming Note P-88 (Revised), June 1964.

25. F. T. Solmitz, A. D. Johnson, and T. B. Day, Three View Geometry Program, Lawrence Radiation Laboratory Alvarez Programming Note P-117, May 1965.

26. SIOUX refers to a program containing a collection of subroutines, among which are TVGP, described in reference 24, and SQUAR, des-

cribed in O. I. Dahl, T. B. Day, F. T. Solmitz, and N. L. Gould, SQUAW Kinematic Fitting Program, Lawrence Radiation Laboratory Alvarez Programming Note P-126, July 1968.

27. E. L. Hart, Optical Constants, Data-Box Format and Film Format of the B. N. L. 80" Hydrogen Bubble Chamber, Brookhaven National Report BC-04-3-B, March 1965.
28. B. B. Culwick, 80" Bubble Chamber 17 Kg Magnetic Field, Brookhaven National Laboratory Report BC-05-2-H (Revision I), Nov. 1965; addendum-Sept. 1966.
29. R. J. Sprafka and D. B. Smith, Determination of Optical Constants for H_2 in the BNL 80-Inch Bubble Chamber, Lawrence Radiation Laboratory Alvarez Physics Memo No. 632, Aug. 1967 (unpublished).
30. J. Bartke, W. A. Cooper, B. Czapp, H. Filthuth, Y. Goldschmidt-Clermont, L. Montanet, D. R. O. Morrison, S. Nilsson, Ch. Peyrou, and R. Sosnowski, Nuovo Cimento 29, 8 (1963).
31. Corrections for ionization losses introduce a mass dependence in the reconstructed lab momentum. Tracks with a significant difference in reconstructed momenta for the pion and proton hypotheses can be scanned for ionization to determine the correct lab momentum. We scanned tracks with a difference in reconstructed momenta comparable to our resolution ($\Delta P_{c.m.}$ = 50 MeV/c).
32. This procedure has previously been discussed by: J. Anderson, and D. Smith, A Method for Separation of the Proton and Pi Plus Momentum Distributions Produced in Proton-Proton Interactions, Lawrence Radiation Laboratory Alvarez Physics Memo No. 673, December 1968.
33. See L. W. Jones, A. E. Bussian, G. D. DeMeester, B. W. Loo, D. E. Lyon, Jr., J. G. Learned, F. E. Mills, D. D. Reeder, K. N. Erickson, and Bruce Cork, Phys. Rev. Lett. 25, 1679 (1970), for an experimental study of charged multiplicity over a much wider range of energies.
34. D. Amati, S. Fubini and A. Stanghellini, Phys. Lett. 1, 29 (1962). D. Amati, A. Stanghellini and S. Fubini, Nuovo Cimento XXVI, 896 (1962). Kenneth G. Wilson, Acta Physica Austriaca 17, 37 (1963). Geoffrey F. Chew, Multiperipheral Dynamics, UCRL-19437, Dec. 1969. Carleton E. DeTar, Phys. Rev. D 3, 128 (1971). S. C. Frautschi, Nuovo Cimento 28, 409 (1963).

35. R. P. Feynman, The Behavior of Hadron Collisions at Extreme Energies, in Third International Conference on High Energy Collisions, C. N. Yang et al., eds., (Gordon and Breach, Inc. New York, 1969), p. 237. Richard P. Feynman, Phys. Rev. Lett. 23, 1415 (1969).
36. D. H. Perkins, Observations on Cosmic Ray "Jet" Interactions in Nuclear Emulsions, in Progress in Elementary Particle and Cosmic Ray Physics, Vol. V, J. G. Wilson and S. A. Wouthuysen, Ed. (North-Holland Publishing Co., Amsterdam, 1960), p. 307. Kimeo Fujimura, NN Inelastic Processes, in reference 2, p. 282.
37. R. Hagedorn, Nuovo Cimento Suppl. 3, 2, 147 (1965); See also R. Hagedorn, CERN-TH-1228, Sept. 1970, and R. Hagedorn, Remarks on the Thermodynamical Model of Strong Interactions, in Proceedings of the Colloquium on High Multiplicity Hadronic Interactions, A. Krzywicki, et al., eds., (Ecole Polytechnique, Paris, 1970), p. IV.0.
38. G. A. Milekhin and I. L. Rozental, J. Exptl. Theoret. Phys. (U.S.S.R.) 33, 197 (1957); J. R. Wayland and T. Bowden, Nuovo Cimento 48A, 663 (1967).
39. Janos Kirz, Cross Section Measurement in Bubble Chambers, Lawrence Radiation Laboratory Alvarez Physics Memo No. 640, Jan. 1968.
40. W. Hendricks, Pi-66 BP-66 Conflict Procedures, Lawrence Radiation Laboratory Alvarez Physics Memo No. 627, June 1967.
41. N. Barash-Schmidt, A. Barbaro-Galtieri, C. Bricman, C. Y. Chien, T. Lasinski, L. R. Price, A. Rittenberg, M. Roos, A. H. Rosenfeld, P. Söding, and C. G. Wohl, Phys. Lett. 33B, 1 (1970).

Table I. Non-Strange Inelastic Topology Cross Sections (mb)*

Topology (number of prongs)	Beam Momentum (in GeV/c) 12.88	18.00	21.08	24.12	28.44
4	13.0 ±.4	12.8 ±.3	12.0 ±.3	11.8 ±.3	11.1 ±.3
6	3.9 ±.2	5.2 ±.2	5.9 ±.2	6.4 ±.2	6.4 ±.2
8	.55 ±.07	1.3 ±.1	1.8 ±.1	2.2 ±.1	2.5 ±.1
10	(.023±.008)	(.13 ±.02)	.37 ±.05	.27 ±.05	.80 ±.08
12	(.003±.003)	(.020±.006)	(.032±.008)	(.06 ±.01)	(.09 ±.02)
14	(.000±.003)	(.004±.003)	(.002±.002)	(.006±.004)	(.010±.005)

*Cross sections in parentheses calculated from scan of entire exposure

Table II. Number and Fraction of Measured Events Successfully Reconstructed

Number of Final Charged Tracks	Nominal Beam Momentum (in GeV/c) 13	18	21	24	28
4	4514	6207	5685	4351	3803
	.9566	.9717	.9775	.9714	.9682
6	1419	2632	2943	2400	2348
	.9692	.9627	.9681	.9635	.9690
8	208	627	837	808	894
	.9455	.9486	.9577	.9395	.9427
10	7	62	133	123	240
	.8750	.8857	.9500	.9111	.9266
12	1	5	12	12	28
	1.	.7143	.8571	.6316	.8485
14	0	2	0	2	3
	-	1.	-	1.	1.

Table III. Tabulation of Track Loss in Reconstruction Program SIOUX

Number of Positively Charged Tracks Actually Passing SIOUX
Number of Potential Positive Tracks from Passing Events

Number of Prongs	Nominal Beam Momentum (in GeV/c) 13	18	21	24	28.5
4	13351	18410	16835	12869	11203
	13542	18621	17055	13053	11409
6	5591	10358	11594	9450	9209
	5676	10528	11772	9600	9392
8	990	3070	4083	3951	4374
	1040	3135	4185	4040	4470
10	4	368	790	706	1424
	42	372	798	738	1440
12	7	35	84	84	196
	7	35	84	84	196
14	0	16	0	16	24
		16		16	24

Table IV. Tabulation of Track Loss
in Reconstruction Program SIOUX

Number of Negatively Charged Tracks Actually Passing SIOUX
Number of Potential Negative Tracks from Passing Events

Number of Prongs	Nominal Beam Momentum (in GeV/c)				
	13	18	21	24	28.5
4	4477	6173	5642	4314	3780
	4514	6207	5685	4351	3803
6	2812	5234	5848	4773	4668
	2838	5264	5886	4800	4696
8	597	1845	2461	2386	2648
	624	1881	2511	2424	2682
10	28	247	531	476	953
	28	248	532	492	960
12	5	25	60	60	139
	5	25	60	60	140
14		12		12	18
		12		12	18

Table V. Non-Strange Production of π^-:
Cross Section and Average Number per Event

Beam Momentum (in GeV/c)	13	18	21	24	28
Cross Section (mb)	22.6 ±.6	27.7 ±.7	30.7 ±.8	32.6 ±.8	35.3 ±.9
Average Number per Event (all ±.02)	.58	.70	.78	.84	.88

Table VI.

χ^2 (and Confidence Level) from Least Squares Fit to the Laboratory Differential Production Cross Sections for π^- for 0. GeV/c $\leq p_\perp \leq$ 0.7 GeV/c.

Central Value of 0.1 GeV/c Bin Transverse Momentum (in GeV/c)	-.35	-.25	-.15	-.05	.05	.15	.25	.35	.45	.55
.65					4.6 (.33)	2.5 (.64)	3.4 (.49)	5.7 (.22)	2.7 (.60)	9.1 (.06)
.55				4.6 (.33)	5.4 (.97)	6.1 (.19)	1.1 (.89)	2.1 (.72)	2.8 (.59)	3.3 (.51)
.45			1.5 (.82)	2.2 (.71)	1.7 (.80)	10.4 (.03)	.98 (.91)	4.4 (.35+)	.66 (.96)	5.8 (.21)
.35		4.0 (.41)	3.1 (.53)	2.7 (.61)	3.3 (.52)	3.2 (.53)	5.3 (.26)	1.8 (.78)	8.5 (.08)	5.4 (.25)
.25		3.5 (.48)	5.7 (.22)	2.7 (.62)	5.8 (.22)	3.2 (.53)	3.0 (.55+)	2.4 (.67)	3.6 (.46)	6.3 (.18)
.15		14.0 (.007)	12.0 (.017)	3.4 (.49)	4.1 (.39)	11.0 (.03)	4.6 (.33)	2.4 (.66)		
.05	.78 (.94)	6.1 (.19)	2.5 (.65)	1.6 (.81)	8.2 (.08)	4.0 (.41)	4.3 (.36)			

Central Value of 0.1 GeV/c Wide Bin in Longitudinal Component of Laboratory Momentum (in GeV/c)

Central Value of 0.1 GeV/c Bin Transverse Momentum (in GeV/c)	.65	.75	.85	.95	1.05	1.15	1.25	1.35	1.45
.65	9.2 (.06)	5.3 (.26)	1.7 (.80)	2.9 (.58)	4.3 (.37)	3.9 (.42)	2.7 (.61)	2.1 (.71)	4.0 (.41)
.55	5.6 (.23)	1.7 (.79)	2.1 (.72)	6.4 (.17)	1.7 (.80)	6.6 (.16)	18.9 (.0008)		
.45	7.2 (.13)	2.5 (.65)	9.3 (.05)	5.7 (.22)					
.35	4.4 (.36)	2.5 (.64)							

Central Value of 0.1 GeV/c Wide Bin in Longitudinal Component of Laboratory Momentum (in GeV/c)

Table VII.

Least Squares Average of the Laboratory Differential Production Cross Sections for π^- for 0. GeV/c $\leq p_\perp \leq$ 0.7 GeV/c.

Central Value of 0.1 GeV/c Bin Transverse Momentum (in GeV/c)	-.35	-.25	-.15	-.05	.05	.15	.25	.35	.45	.55
.65					.003 ±.001	.009 ±.002	.023 ±.003	.030 ±.004	.041 ±.004	.047 ±.005
.55				.003 ±.001	.020 ±.003	.033 ±.004	.060 ±.006	.085 ±.006	.110 ±.008	.118 ±.008
.45			.008 ±.002	.034 ±.004	.061 ±.006	.103 ±.007	.166 ±.009	.206 ±.010	.240 ±.011	.247 ±.011
.35		.004 ±.001	.036 ±.004	.098 ±.007	.167 ±.009	.287 ±.012	.386 ±.014	.469 ±.016	.473 ±.016	.496 ±.017
.25		.018 ±.003	.085 ±.006	.226 ±.011	.478 ±.016	.688 ±.020	.814 ±.022	.816 ±.022	.810 ±.022	.755 ±.021
.15		.022 ±.003	.121 ±.008	.423 ±.015	.889 ±.023	1.105 ±.026	1.156 ±.027	1.052 ±.026		
.05	.003 ±.001	.009 ±.002	.074 ±.006	.295 ±.012	.534 ±.017	.660 ±.020	.596 ±.018			

Central Value of 0.1 GeV/c Wide Bin in Longitudinal Component of Laboratory Momentum (in GeV/c)

Central Value of 0.1 GeV/c Bin Transverse Momentum (in GeV/c)	.65	.75	.85	.95	1.05	1.15	1.25	1.35	1.45
.65	.060 ±.006	.064 ±.006	.072 ±.006	.079 ±.006	.070 ±.006	.069 ±.006	.066 ±.006	.070 ±.006	.071 ±.006
.55	.151 ±.009	.134 ±.008	.129 ±.008	.131 ±.008	.127 ±.008	.123 ±.008	.122 ±.008	.113 ±.008	.105 ±.008
.45	.271 ±.012	.247 ±.011	.248 ±.011	.253 ±.012					
.35	.489 ±.016	.418 ±.015							

Central Value of 0.1 GeV/c Wide Bin in Longitudinal Component of Laboratory Momentum (in GeV/c)

Table VIII. Average π^- Transverse Momentum as a Function of Beam Energy

Beam Momentum (in GeV/c)	13	18	21	24	28.5
Average π^- Transverse Momentum (in GeV/c)	.294 ±.006	.308 ±.005	.309 ±.005	.314 ±.006	.318 ±.006

Table IX. Relative Numbers of Events by Topology

Number of Events Seen by Both Scanners

Momentum in GeV/c	12.88	18.00	21.08	24.12	28.44
topology (number of prongs)					
4	4796	6755	6150	4758	4068
6	1473	2827	3084	2548	2447
8	214	698	894	872	975
10	8	72	147	145	278
12	1	11	16	20	34
14	0	2	1	2	4

Table X.

Average Difference Between the Number of π^+ and the Number of π^- per Event

Number of Prongs	Nominal Beam Momentum (in GeV/c)				
	13	18	21	24	28.5
4	0.61 ±.04	0.66 ±.04	0.68 ±.04	0.79 ±.05	0.79 ±.05
6	0.40 ±.07	0.58 ±.06	0.61 ±.06	0.57 ±.06	0.66 ±.07
8	0.34 ±.20	0.44 ±.12	0.49 ±.11	0.65 ±.12	0.71 ±.11
10		0.01 ±.40	0.09 ±.28	0.64 ±.31	0.69 ±.22
12		0.20 ±1.55	-0.67 ±.97	0.67 ±1.13	0.07 ±.64

Table XI

Coefficients Describing Transverse Momentum Distributions of π^+ (in $(GeV/c)^{-1}$)

Number of Final Charged Tracks	Nominal Beam Momentum (in GeV/c)				
	13	18	21	24	28
4	8.69 ±.15	8.14 ±.13	7.92 ±.14	7.85 ±.15	7.97 ±.15
6	9.35 ±.20	8.20 ±.13	8.33 ±.13	8.08 ±.14	8.17 ±.15
8	9.69 ±.45	9.06 ±.24	9.21 ±.21	8.98 ±.22	8.48 ±.20
10		10.50 ±.93	9.82 ±.58	8.94 ±.47	8.78 ±.33
12		14.19 ±11.68	17.33 ±6.47	14.38 ±3.64	11.45 ±2.05

Coefficients Describing Transverse Momentum Distributions of π^- (in $(GeV/c)^{-1}$)

Number of Final Charged Tracks	Nominal Beam Momentum (in GeV/c)				
	13	18	21	24	28
4	8.15 ±.08	7.86 ±.07	7.72 ±.07	7.57 ±.08	7.44 ±.09
6	8.76 ±.12	8.18 ±.08	8.09 ±.07	7.92 ±.08	7.82 ±.08
8	10.25 ±.32	8.87 ±.15	8.80 ±.12	8.47 ±.12	8.19 ±.11
10	16.94 ±7.00	9.19 ±.51	9.60 ±.31	9.08 ±.32	9.16 ±.21
12		14.19 ±11.68	12.18 ±2.50	12.31 ±1.94	10.36 ±.84
14					14.18 ±13.46

Table XI. continued

Coefficients Describing Longitudinal Center-of-Mass Momentum Distributions of π^+ (in $(GeV/c)^{-1}$)

Number of Final Charged Tracks	Nominal Beam Momentum (in GeV/c) 13	18	21	24	28
4	3.21 ±.08	2.52 ±.06	2.29 ±.06	2.13 ±.06	2.02 ±.07
6	4.44 ±.15	3.59 ±.09	3.02 ±.08	2.82 ±.08	2.63 ±.08
8	5.35 ±.48	4.25 ±.17	4.06 ±.15	3.73 ±.14	3.33 ±.12
10		5.10 ±.96	5.46 ±.56	5.36 ±.57	4.02 ±.25
12			9.54 ±8.84	7.26 ±2.99	5.89 ±1.65

Coefficients Describing Longitudinal Center-of-Mass Momentum Distributions of π^- (in $(GeV/c)^{-1}$)

Number of Final Charged Tracks	Nominal Beam Momentum (in GeV/c) 13	18	21	24	28
4	3.04 ±.05	2.57 ±.04	2.39 ±.04	2.33 ±.04	2.12 ±.04
6	4.14 ±.08	3.56 ±.05	3.31 ±.04	3.01 ±.05	2.85 ±.05
8	5.27 ±.29	4.55 ±.12	4.10 ±.09	3.90 ±.09	3.44 ±.08
10	8.45 ±3.05	5.42 ±.49	4.37 ±.24	5.34 ±.31	4.06 ±.17
12		7.48 ±3.37	7.15 ±1.84	9.27 ±2.86	5.33 ±.82

Table XII

NUMBER OF EVENTS SEEN BY BOTH SCANNERS*

Momentum in GeV/c topology (number of prongs)	12.88	18.	21.08	24.12	28.44
4	1652	1860	1591	1597	1311
6	497	753	784	868	759
8	70	190	234	296	291
10	(1)	(23)	49	37	94
12	(1)	(2)	(4)	(8)	(14)
14	0	(0)	(0)	(0)	(1)

* Because of the small statistics of the entries shown in parentheses, the corresponding topology cross sections were calculated using the numbers of events seen in the scan of all the film. (The number of uncounted beam tracks was estimated from the relative numbers of frames.)

PROBABILITY OF SCANNER 1 MISSING AN EVENT
PROBABILITY OF SCANNER 2 MISSING AN EVENT

Momentum in GeV/c topology (number of prongs)	12.88	18.	21.08	24.12	28.44
4	.01317 .01234	.02443 .02369	.01480 .01463	.02228 .01976	.01819 .02089
6	.01021 .00953	.01061 .01238	.01102 .00649	.00824 .00981	.00654 .00981
8	.00467 .0	.01433 .01146	.00783 .00447	.01147 .01147	.01026 .00923
10	.125 .0	.01389 .01389	.01361 .00680	.02069 .01379	.01079 .0
12	.0 .0	.0 .0	.0 .0	.1 .0	.0 .0
14		.0 .0	.0 .0	.0 .0	.0 .0

Table XII. continued

Momentum	12.88	18.	21.08	24.12	28.44
total pp cross section (in mb) (all ± 1.5 mb)	39.0	39.7	39.4	38.7	39.9
total number of beam tracks	27326	31409	28640	29149	25397
$\mu b/_{event}$	7.87 ±.10	6.87 ±.08	7.53 ±.09	7.38 ±.09	8.50 ±.10

FIGURE CAPTIONS

Figure 1. Fourteen-prong in the B. N. L. 80-Inch Hydrogen Bubble Chamber.

Figure 2. (a) Topology cross sections as a function of beam momentum. The smooth curves through the four-, six-, and eight-prongs are the results of a fit to our data described in reference 21. Freehand (dashed) curves were drawn through the 10-, 12-, and 14-prongs. (b) Topology cross sections of the four-, six-, and eight-prongs on a larger scale (with freehand curves through them).

Figure 3. Description of the measuring procedure.

Figure 4. Inverse laboratory momentum of positively charged tracks from 28 GeV/c four-prongs.

Figure 5. (a) Transverse and (b) longitudinal laboratory momentum of positively charged tracks from 28 GeV/c four prongs.

Figure 6. Inverse laboratory momentum of negatively charged tracks from 28 GeV/c four prongs.

Figure 7. Average number of π^-'s per proton-proton interaction as a function of incident beam momentum.

Figure 8. Distribution of order of cross section magnitudes as a function of incident beam momentum.

Figure 9. Distribution of χ^2 from testing constancy of laboratory differential production cross sections for π^- (see text).

Figure 10. Average transverse momentum of π^- as a function of incident beam momentum.

Figure 11. Transverse and longitudinal c.m. momentum distributions of π^+ and π^- by topology and beam momentum. The curves superimposed on the data come from individual fits to each

distribution as described in the text.

Figure 12. Distributions in the confidence level from the fits to the transverse and longitudinal c.m. momentum distributions described in the text.

Figure 13. Topology dependence of (a) longitudinal coefficient $a_{\parallel}$ and (b) transverse coefficient $a_{\perp}$.

Figure 14. Longitudinal coefficient $a_{\parallel}$ as a function of beam momentum for each topology. The smooth curves are the result of a fit to the coefficients of all topologies and beam momenta described in the text.

Figure 15. Transverse coefficient $a_{\perp}$ as a function of incident beam beam momentum for each topology. The beam energy dependence of the coefficients was fitted separately for each topology to give the smooth curves (see text).

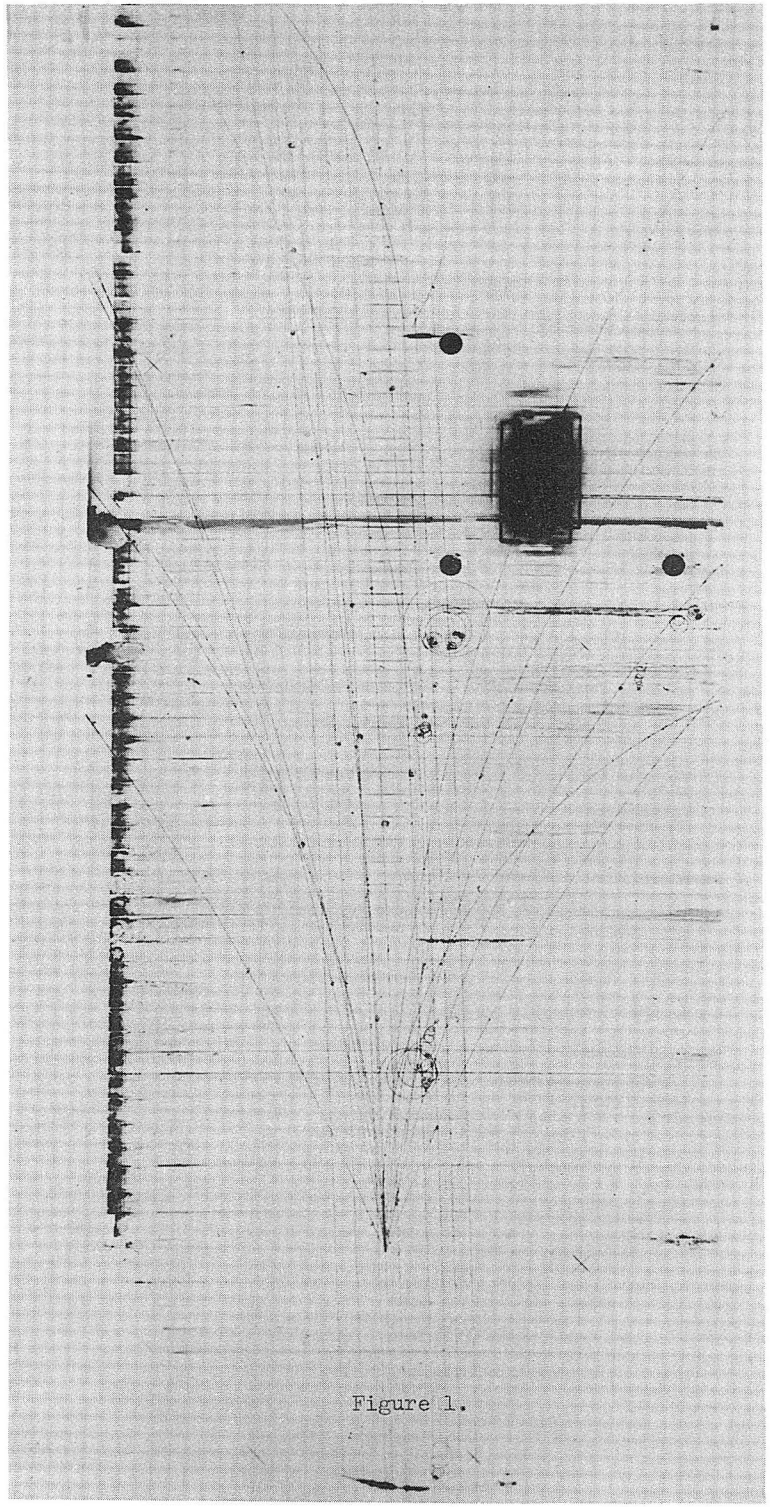

Figure 1.

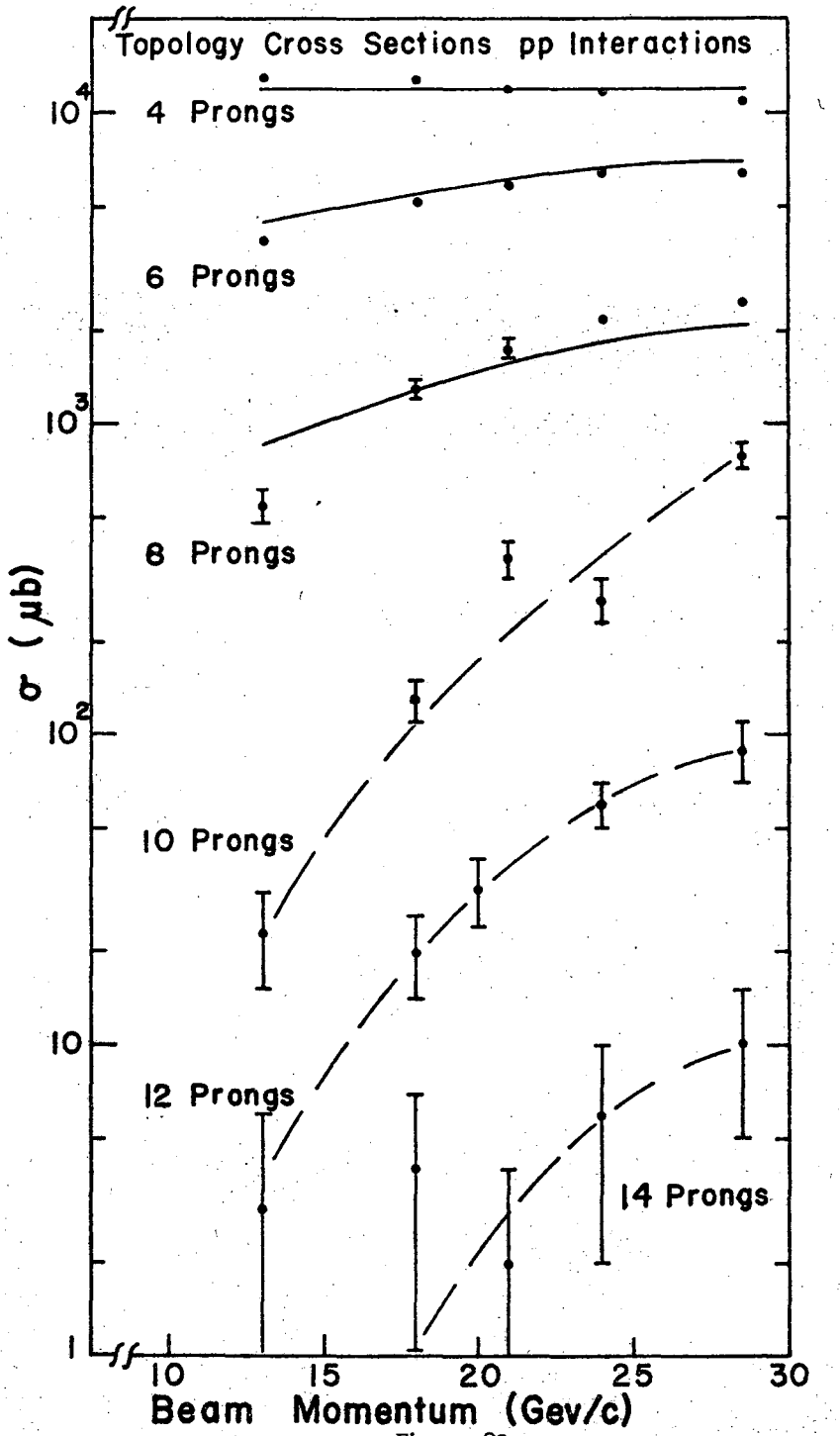

Figure 2a.

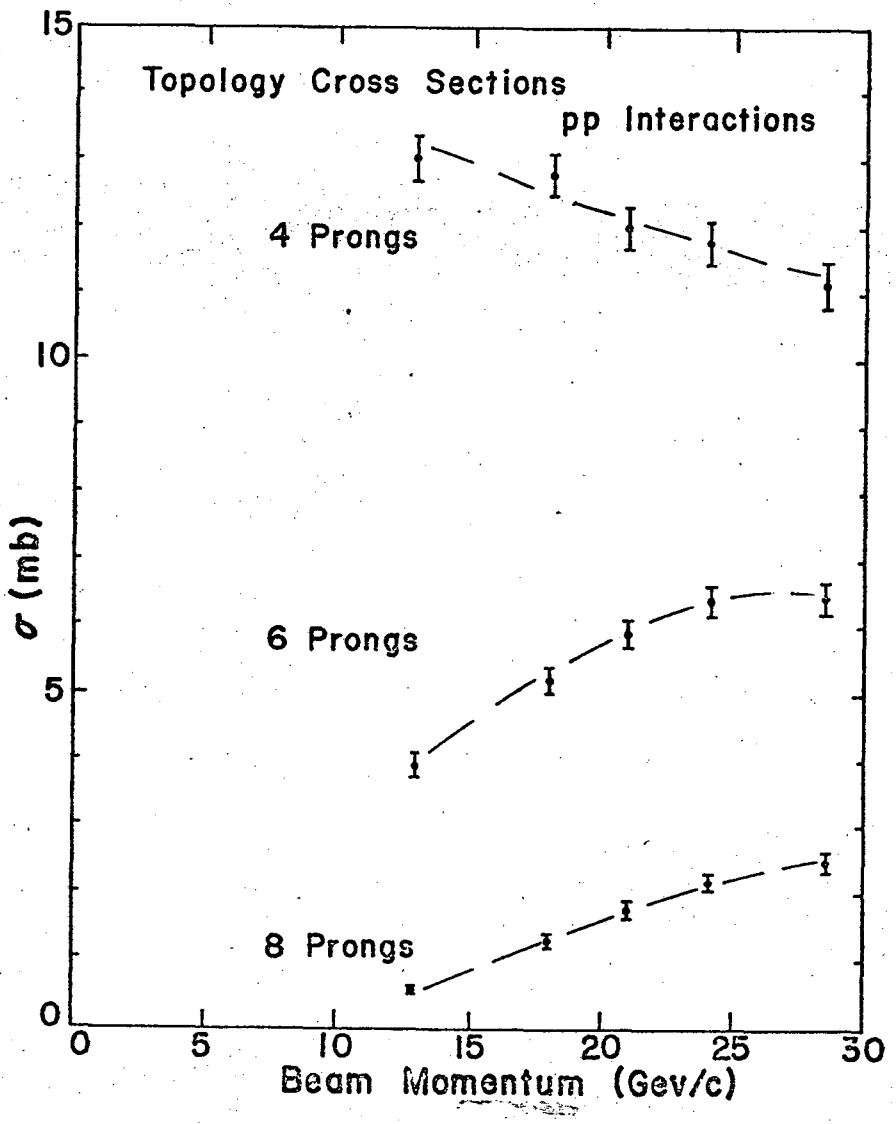

Figure 2b

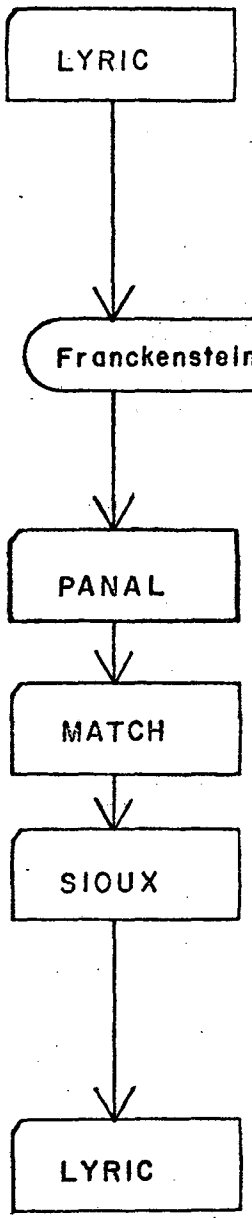

reads initial "Master List" (list of conflict scanned multi-prongs) to give both a "Measurement ReQuest" (tape listing events to be measured) and an intermediate Master List annotated with the measurement requests

records sets of points along the image of the track in each of the three views on a "Data Measurement Tape"

checks consistency and fiducial volume to give a carefully formatted tape

finds most likely association of track images in three views

uses its Three View Geometry subroutines to reconstruct the trajectory of three dimensional tracks from the sets of points from track images to put out a "Soo Tape" of measured momenta with errors

compares the Soo Tape with the measurement requests on the intermediate Master List to give a "Data Summary Tape" of measurements and a final Master List with results of multi-prong measurements

Figure 3.

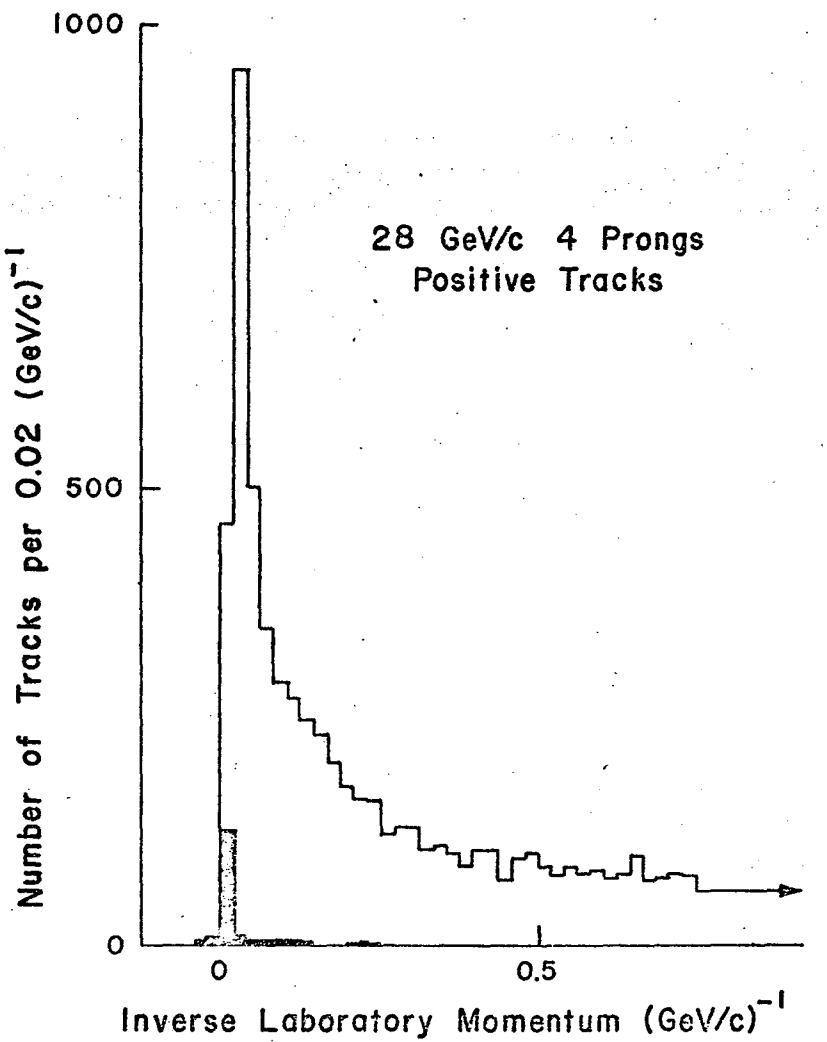

Figure 4

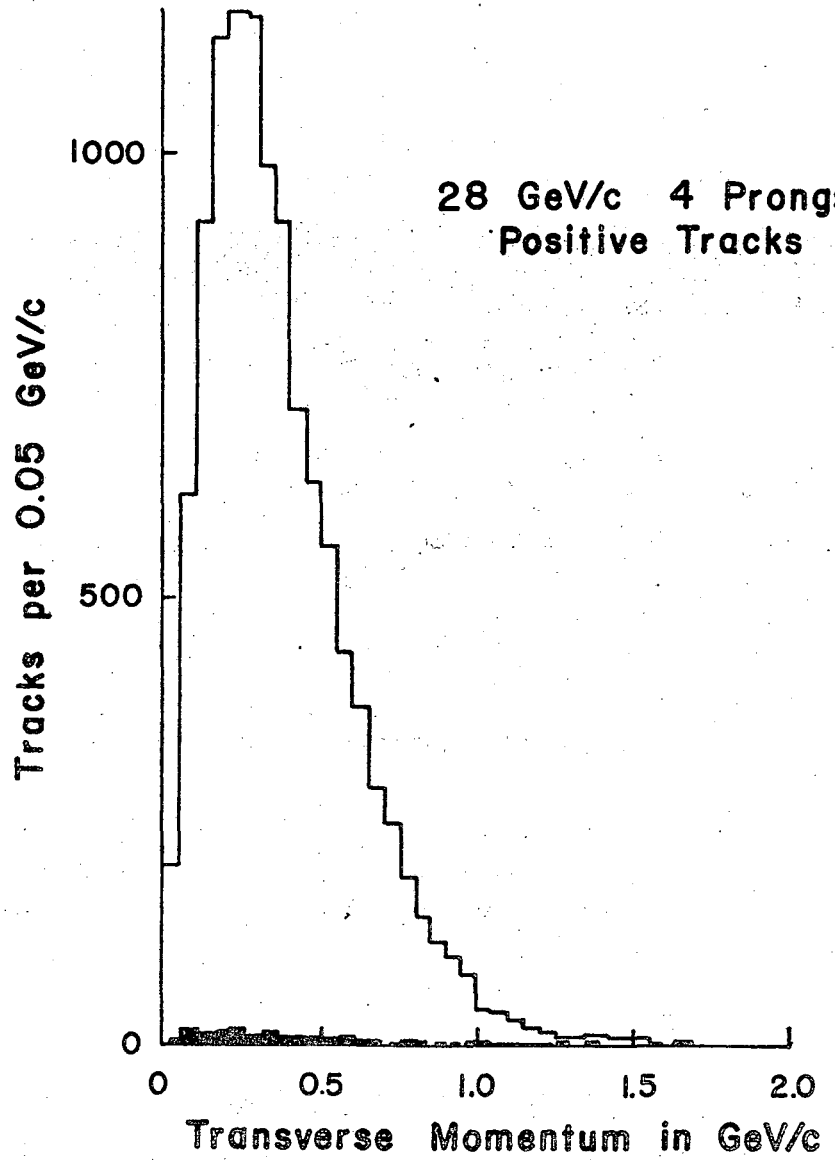

Figure 5a.

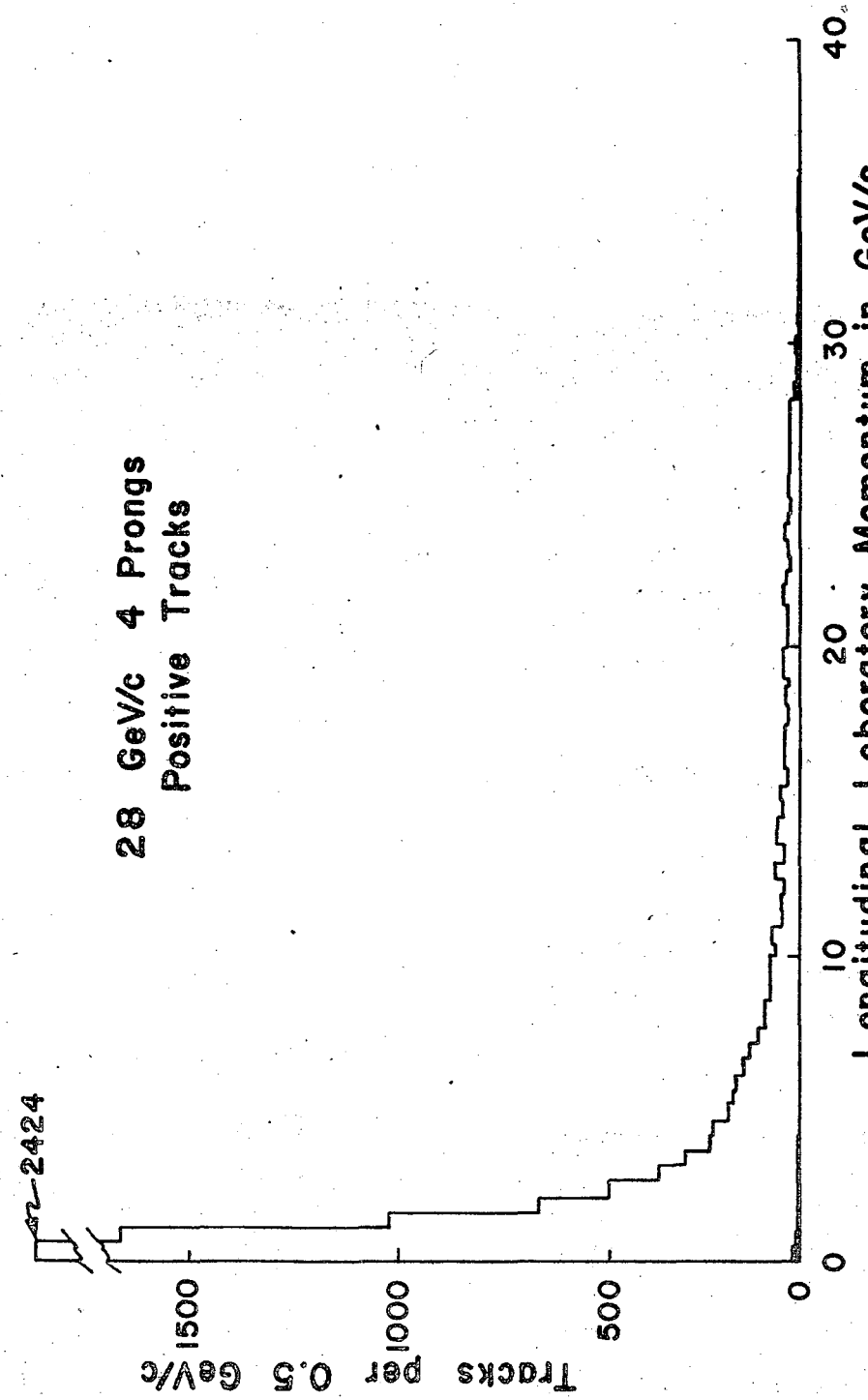

Figure 5b.

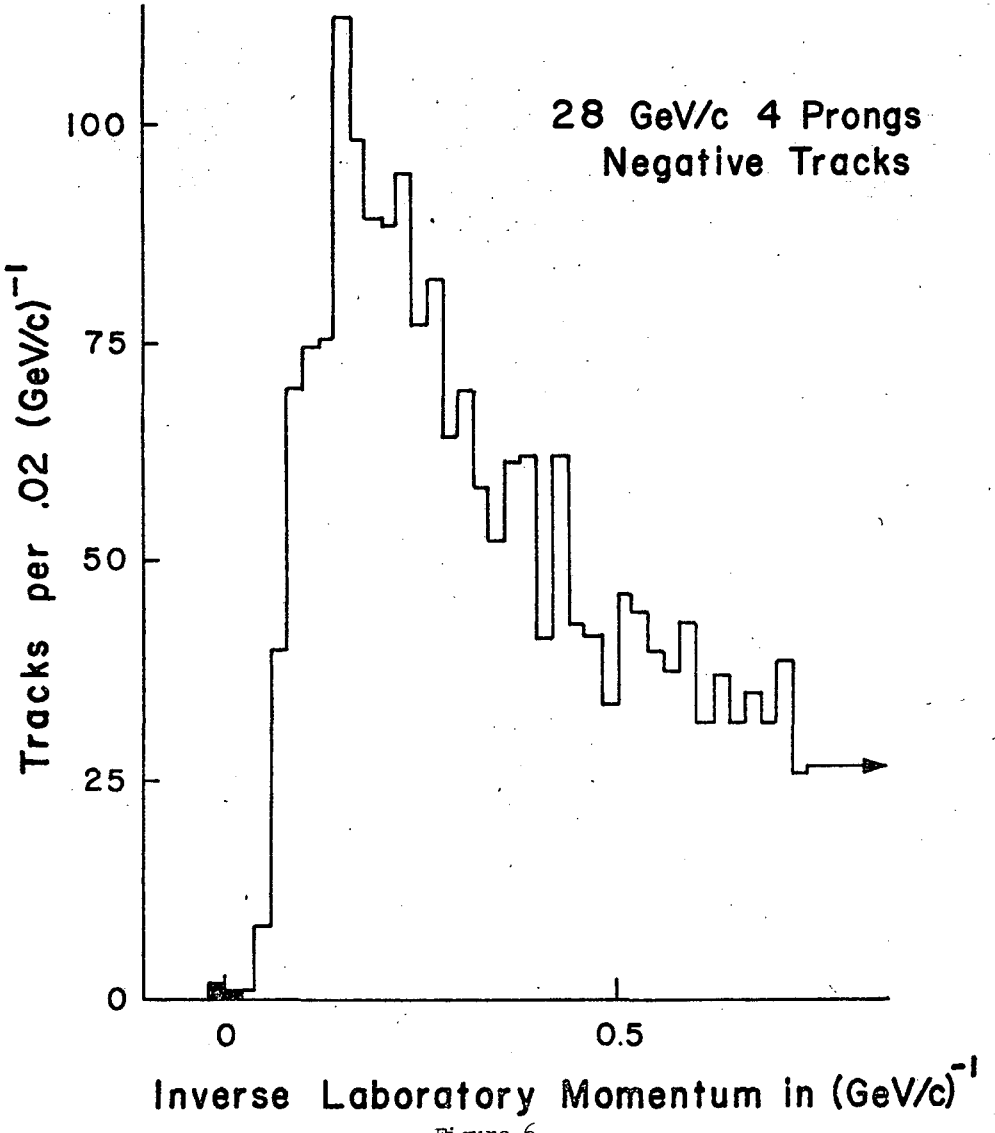

Figure 6.

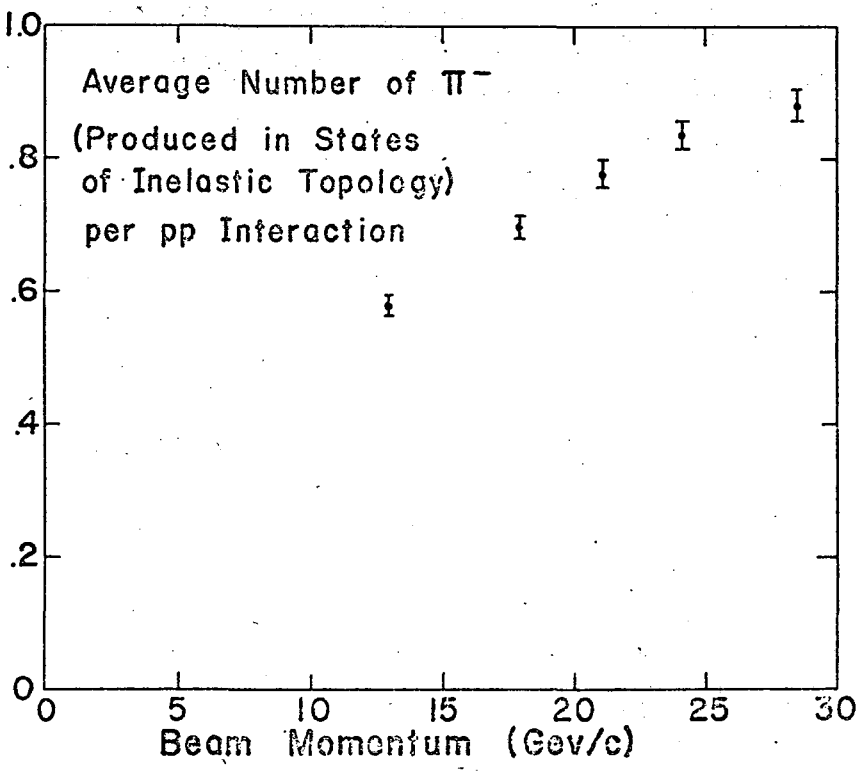

Figure 7

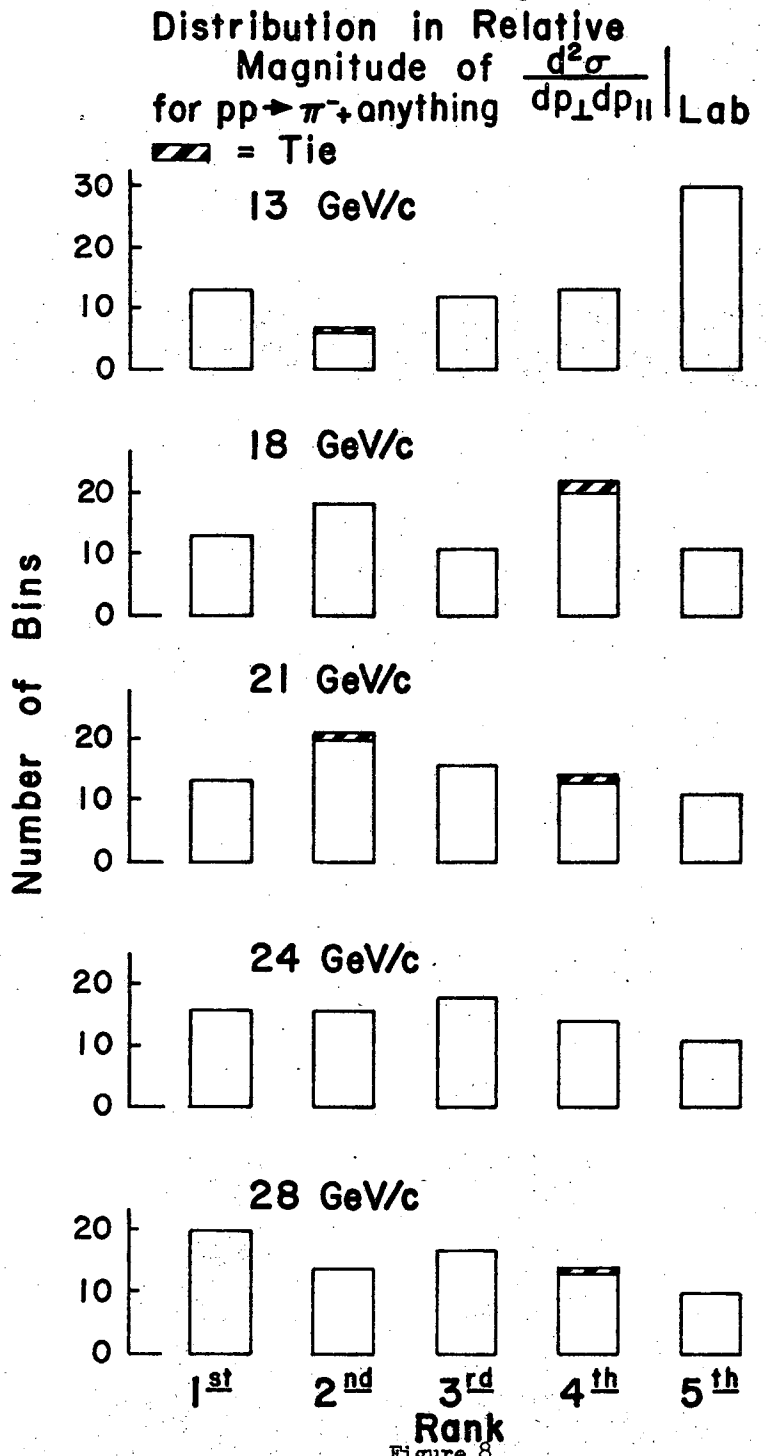

Figure 8.

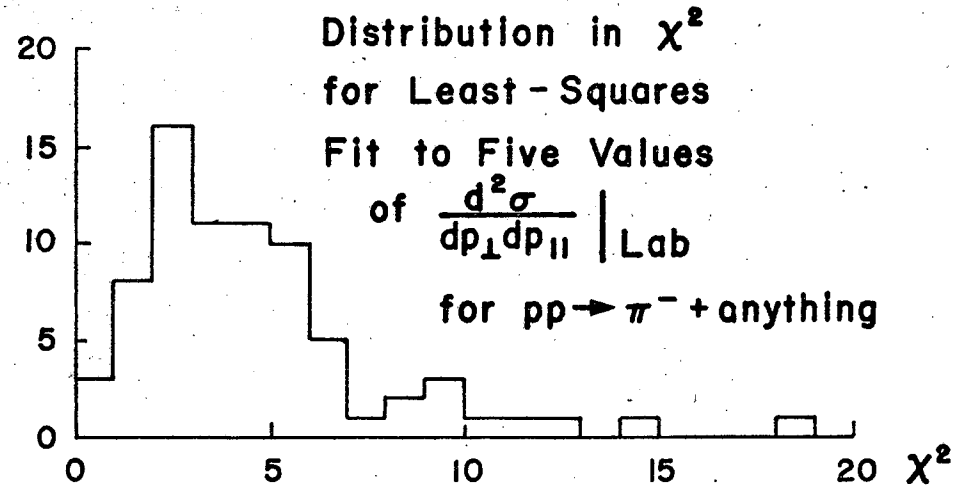

Figure 9.

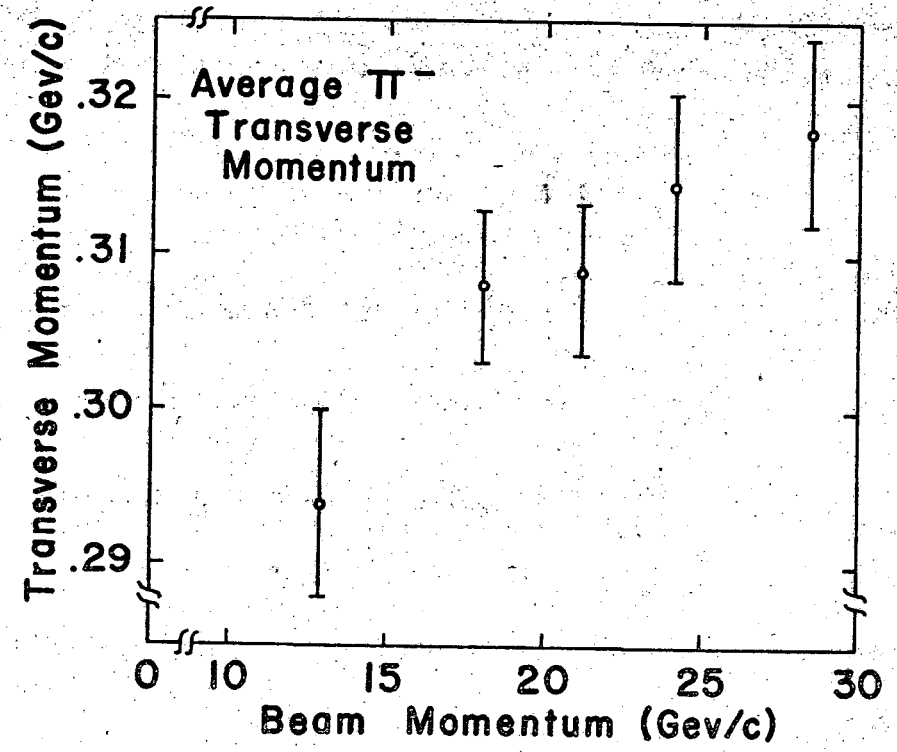
Average π^-
Transverse
Momentum
Transverse Momentum (Gev/c)
.32
.31
.30
.29
0
10
15
20
25
30
Beam Momentum (Gev/c)

Figure 10.

Smith. LBL 20632 (71)

J. V. Allaby – CERN (1974)

P. L. 37B, 435 (71)
38B, 51 (72)

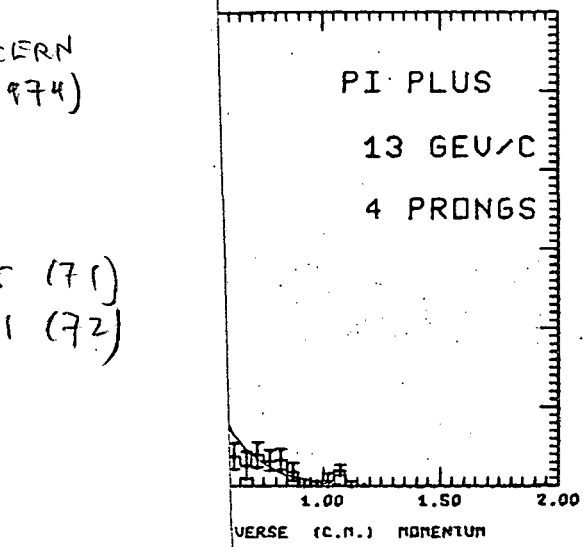

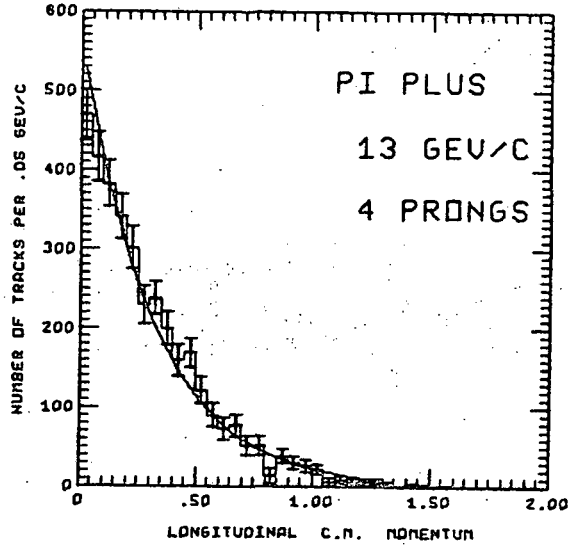

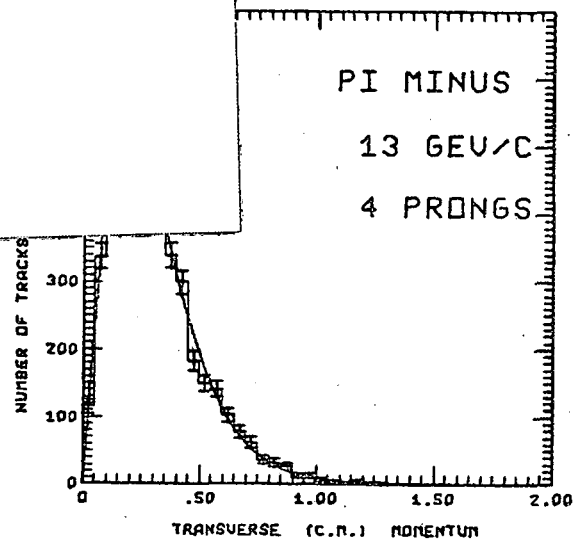

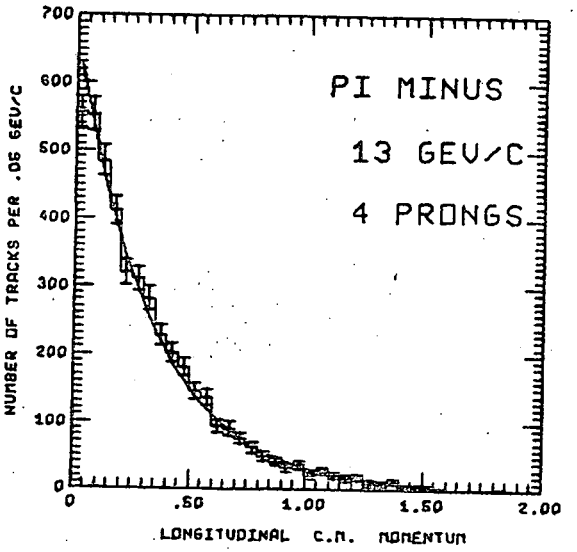

Figure 11.

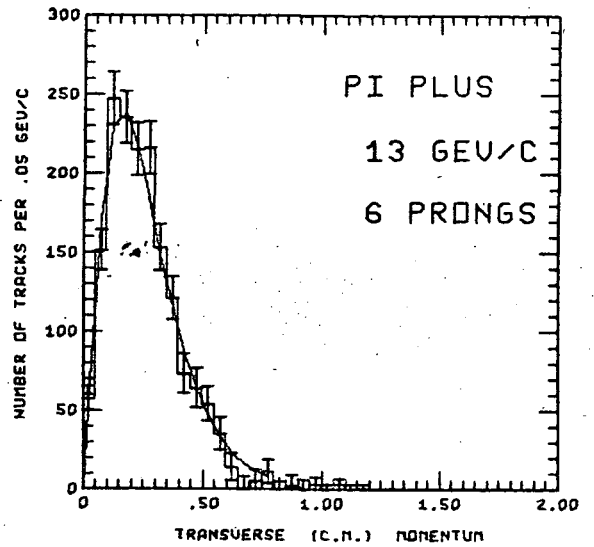
PI PLUS
13 GEV/C
6 PRONGS
NUMBER OF TRACKS PER .05 GEV/C
TRANSVERSE (C.M.) MOMENTUM
0
50
100
150
200
250
300
.50
1.00
1.50
2.00

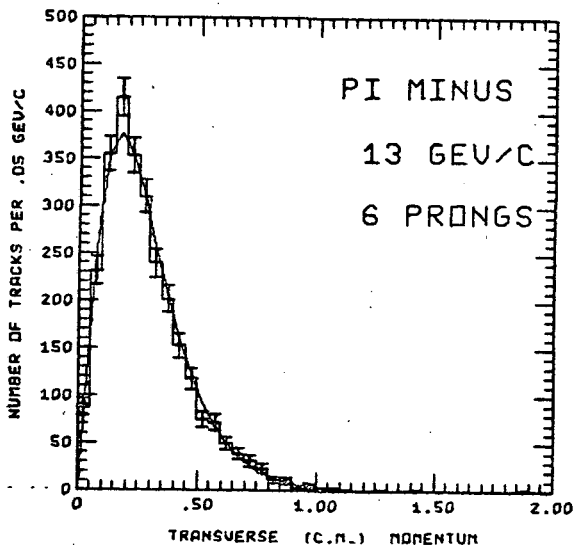
PI MINUS
13 GEV/C
6 PRONGS
NUMBER OF TRACKS PER .05 GEV/C
TRANSVERSE (C.M.) MOMENTUM
0
50
100
150
200
250
300
350
400
450
500
.50
1.00
1.50
2.00

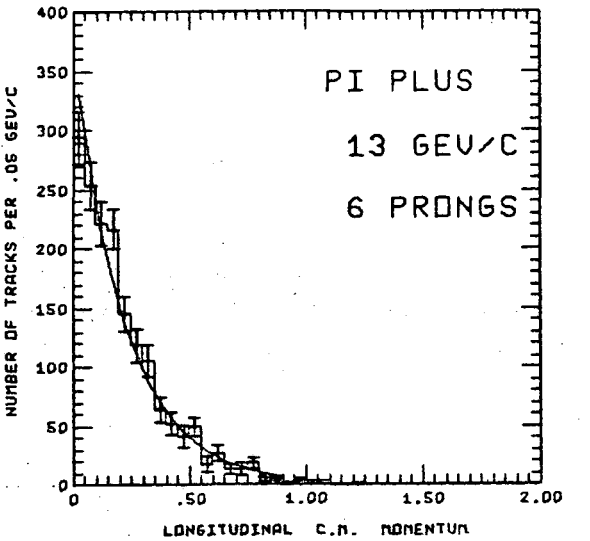
PI PLUS
13 GEV/C
6 PRONGS
NUMBER OF TRACKS PER .05 GEV/C
LONGITUDINAL C.M. MOMENTUM
0
50
100
150
200
250
300
350
400
.50
1.00
1.50
2.00

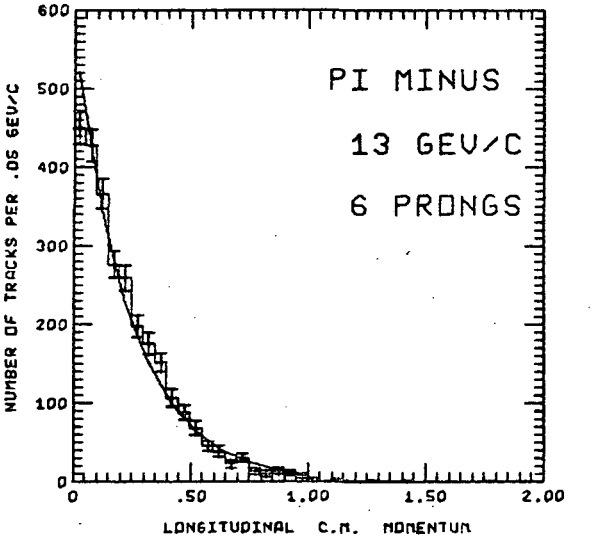
PI MINUS
13 GEV/C
6 PRONGS
NUMBER OF TRACKS PER .05 GEV/C
LONGITUDINAL C.M. MOMENTUM
0
100
200
300
400
500
600
.50
1.00
1.50
2.00

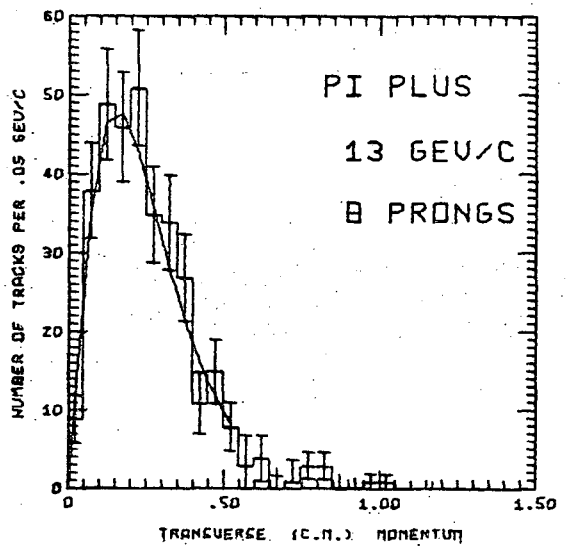
PI PLUS
13 GEV/C
8 PRONGS
NUMBER OF TRACKS PER .05 GEV/C
TRANSVERSE (C.M.) MOMENTUM
0
10
20
30
40
50
60
.50
1.00
1.50

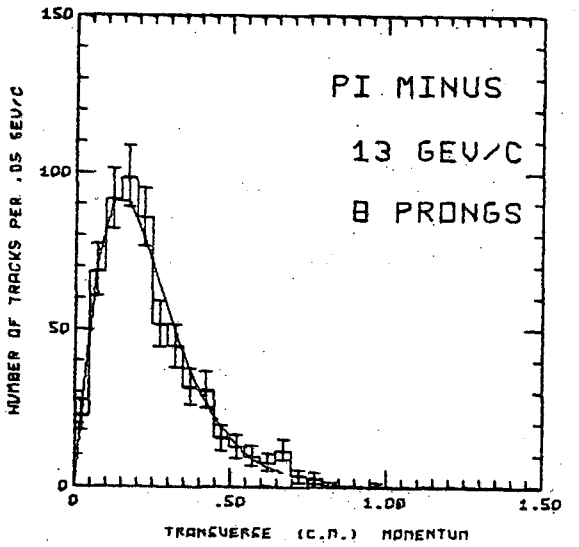
PI MINUS
13 GEV/C
8 PRONGS
NUMBER OF TRACKS PER .05 GEV/C
TRANSVERSE (C.M.) MOMENTUM
0
50
100
150
.50
1.00
1.50

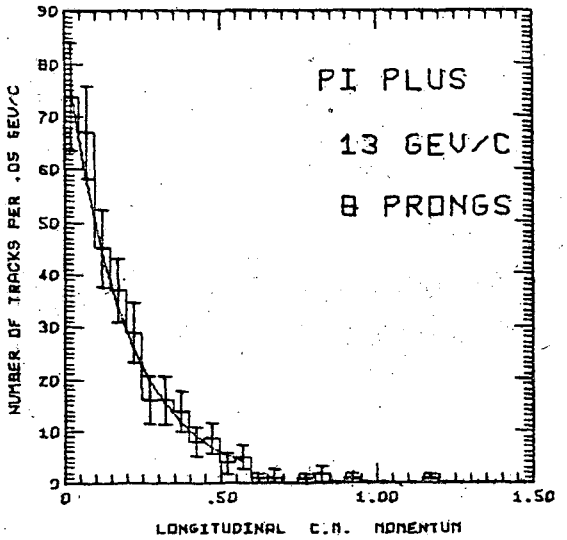
PI PLUS
13 GEV/C
8 PRONGS
NUMBER OF TRACKS PER .05 GEV/C
LONGITUDINAL C.M. MOMENTUM
0
10
20
30
40
50
60
70
80
90
.50
1.00
1.50

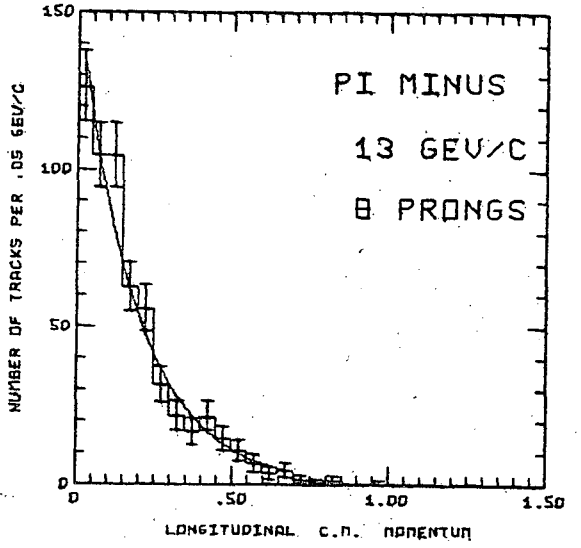
PI MINUS
13 GEV/C
8 PRONGS
NUMBER OF TRACKS PER .05 GEV/C
LONGITUDINAL C.M. MOMENTUM
0
50
100
150
.50
1.00
1.50

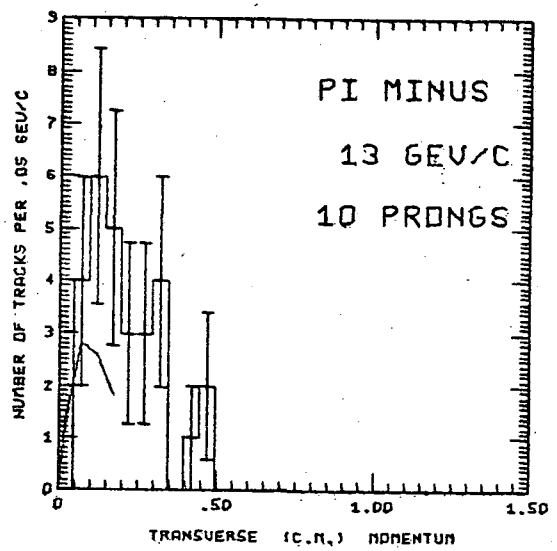
PI MINUS
13 GEV/C
10 PRONGS
NUMBER OF TRACKS PER .05 GEV/C
TRANSVERSE (C.M.) MOMENTUM
0
.50
1.00
1.50
1
2
3
4
5
6
7
8
9

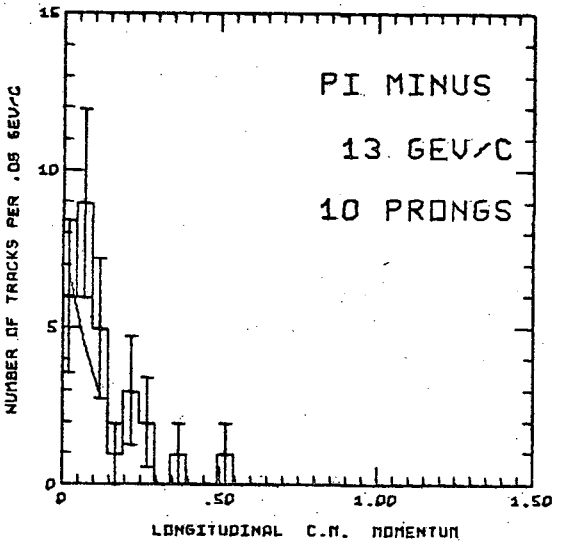
PI MINUS
13 GEV/C
10 PRONGS
NUMBER OF TRACKS PER .05 GEV/C
LONGITUDINAL C.M. MOMENTUM
0
.50
1.00
1.50
5
10
15

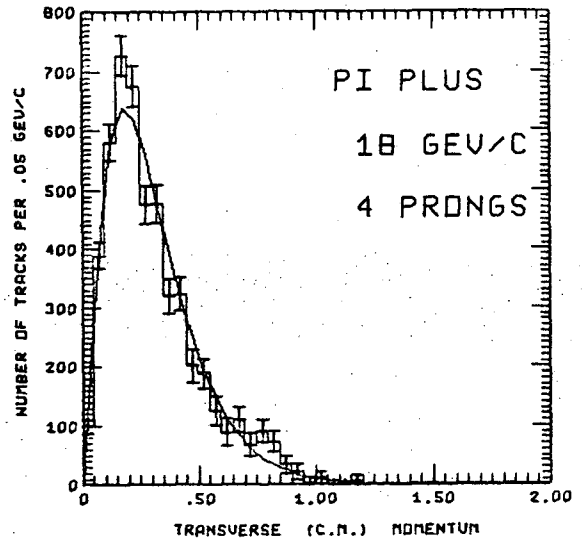
PI PLUS
18 GEV/C
4 PRONGS
NUMBER OF TRACKS PER .05 GEV/C
TRANSVERSE (C.M.) MOMENTUM
0
100
200
300
400
500
600
700
800
.50
1.00
1.50
2.00

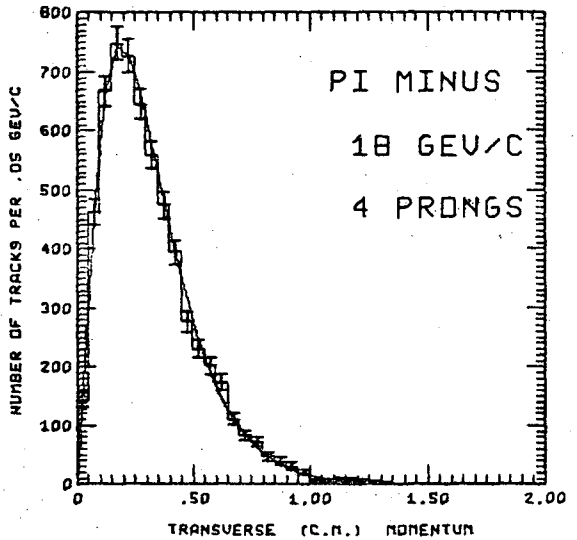
PI MINUS
18 GEV/C
4 PRONGS
NUMBER OF TRACKS PER .05 GEV/C
TRANSVERSE (C.M.) MOMENTUM
0
100
200
300
400
500
600
700
800
.50
1.00
1.50
2.00

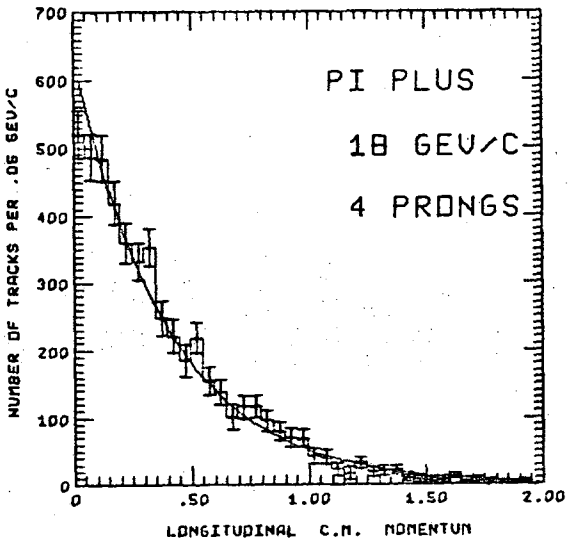
PI PLUS
18 GEV/C
4 PRONGS
NUMBER OF TRACKS PER .05 GEV/C
LONGITUDINAL C.M. MOMENTUM
0
100
200
300
400
500
600
700
.50
1.00
1.50
2.00

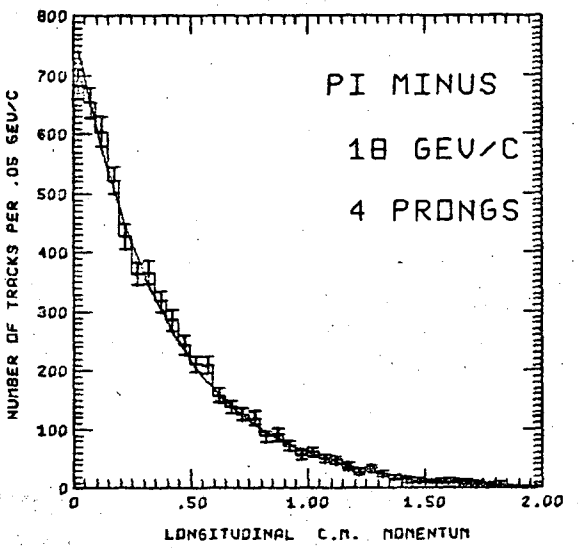
PI MINUS
18 GEV/C
4 PRONGS
NUMBER OF TRACKS PER .05 GEV/C
LONGITUDINAL C.M. MOMENTUM
0
100
200
300
400
500
600
700
800
.50
1.00
1.50
2.00

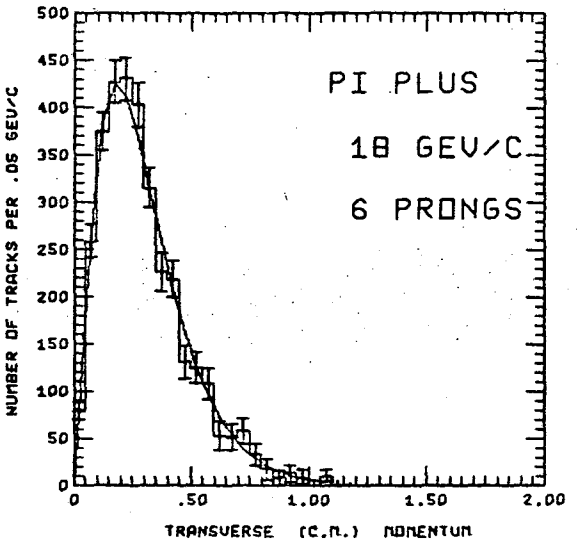
PI PLUS
18 GEV/C
6 PRONGS
NUMBER OF TRACKS PER .05 GEV/C
TRANSVERSE (C.M.) MOMENTUM
0
50
100
150
200
250
300
350
400
450
500
.50
1.00
1.50
2.00

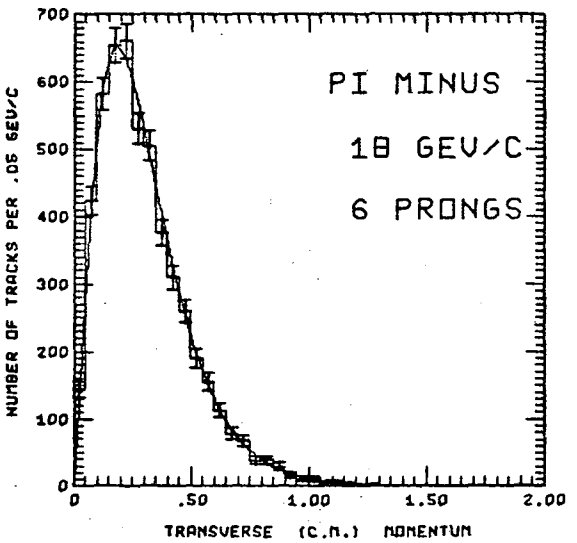
PI MINUS
18 GEV/C
6 PRONGS
NUMBER OF TRACKS PER .05 GEV/C
TRANSVERSE (C.M.) MOMENTUM
0
100
200
300
400
500
600
700
.50
1.00
1.50
2.00

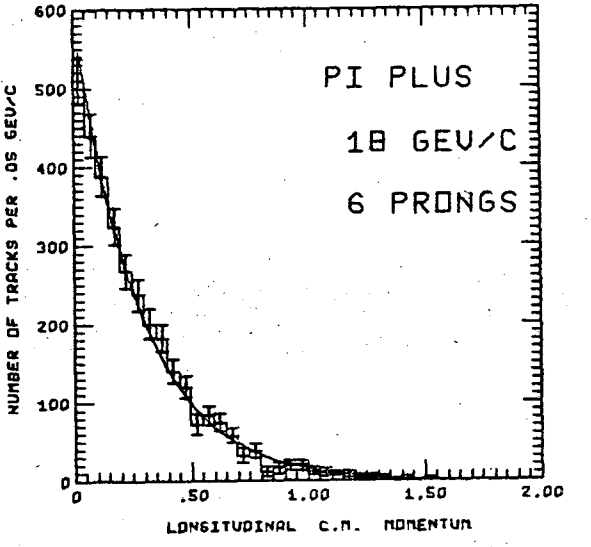
PI PLUS
18 GEV/C
6 PRONGS
NUMBER OF TRACKS PER .05 GEV/C
LONGITUDINAL C.M. MOMENTUM
0
100
200
300
400
500
600
.50
1.00
1.50
2.00

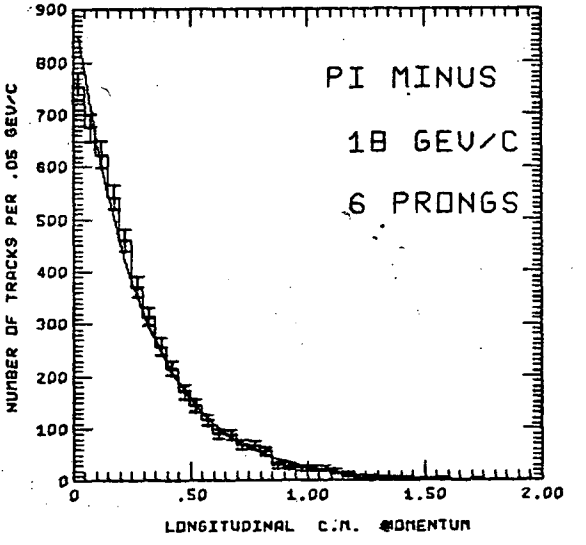
PI MINUS
18 GEV/C
6 PRONGS
NUMBER OF TRACKS PER .05 GEV/C
LONGITUDINAL C.M. MOMENTUM
0
100
200
300
400
500
600
700
800
900
.50
1.00
1.50
2.00

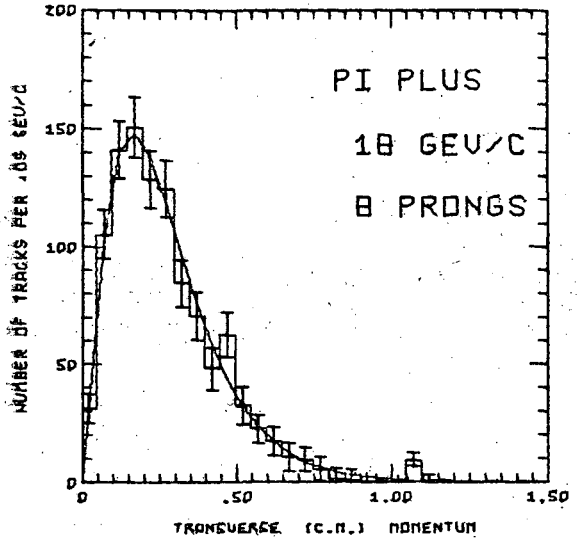
PI PLUS
18 GEV/C
8 PRONGS
NUMBER OF TRACKS PER .05 GEV/C
TRANSVERSE (C.M.) MOMENTUM
0
50
100
150
200
.50
1.00
1.50

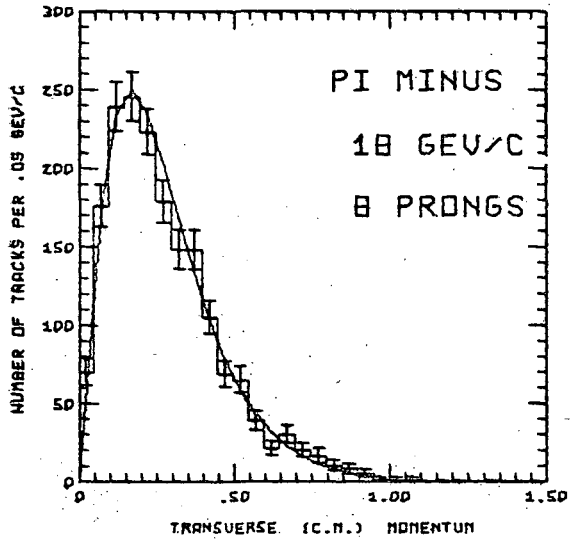
PI MINUS
18 GEV/C
8 PRONGS
NUMBER OF TRACKS PER .05 GEV/C
TRANSVERSE (C.M.) MOMENTUM
0
50
100
150
200
250
300
.50
1.00
1.50

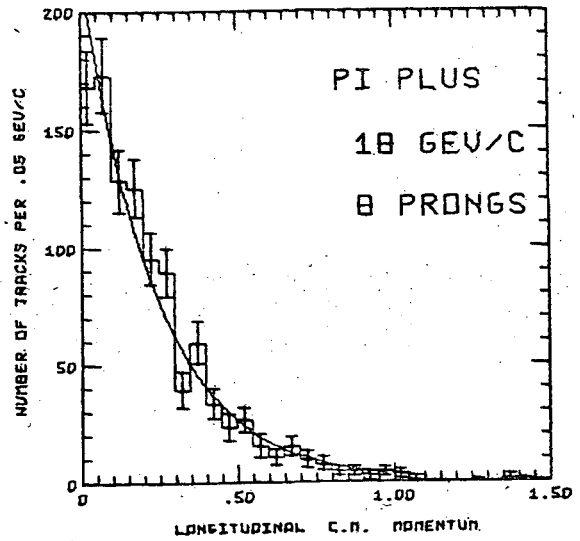
PI PLUS
18 GEV/C
8 PRONGS
NUMBER OF TRACKS PER .05 GEV/C
LONGITUDINAL C.M. MOMENTUM
0
50
100
150
200
.50
1.00
1.50

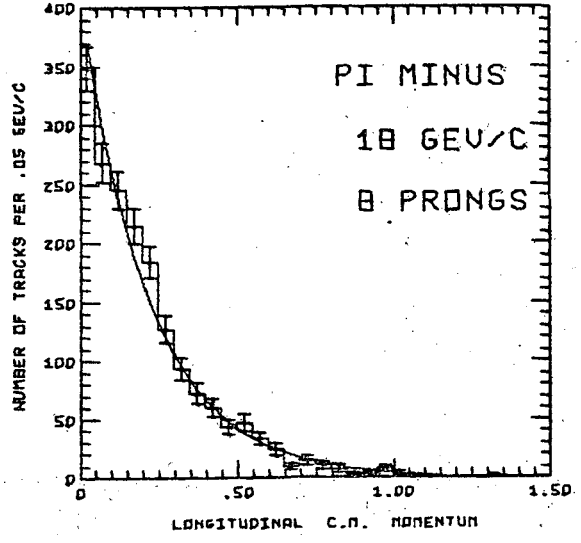
PI MINUS
18 GEV/C
8 PRONGS
NUMBER OF TRACKS PER .05 GEV/C
LONGITUDINAL C.M. MOMENTUM
0
50
100
150
200
250
300
350
400
.50
1.00
1.50

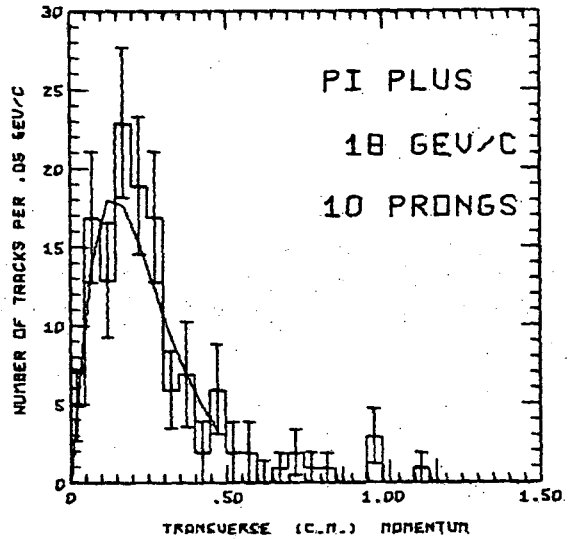
PI PLUS
18 GEV/C
10 PRONGS
NUMBER OF TRACKS PER .05 GEV/C
TRANSVERSE (C.M.) MOMENTUM
0
5
10
15
20
25
30
.50
1.00
1.50

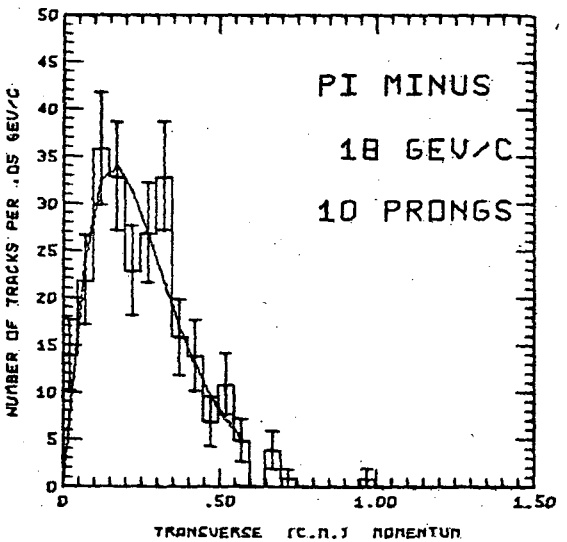
PI MINUS
18 GEV/C
10 PRONGS
NUMBER OF TRACKS PER .05 GEV/C
TRANSVERSE (C.M.) MOMENTUM
0
5
10
15
20
25
30
35
40
45
50
.50
1.00
1.50

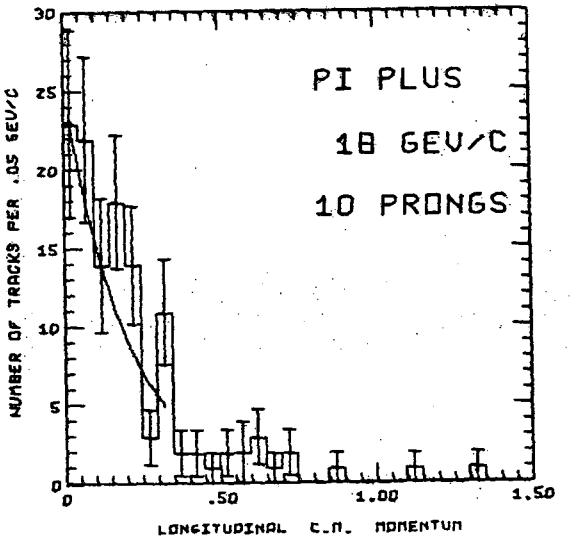
PI PLUS
18 GEV/C
10 PRONGS
NUMBER OF TRACKS PER .05 GEV/C
LONGITUDINAL C.M. MOMENTUM
0
5
10
15
20
25
30
.50
1.00
1.50

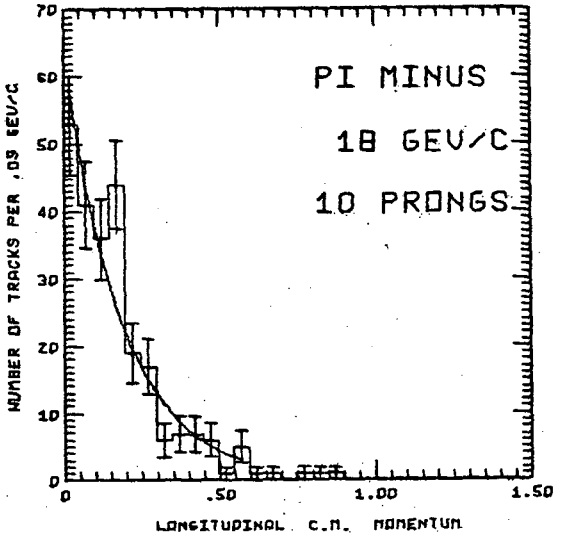
PI MINUS
18 GEV/C
10 PRONGS
NUMBER OF TRACKS PER .05 GEV/C
LONGITUDINAL C.M. MOMENTUM
0
10
20
30
40
50
60
70
.50
1.00
1.50

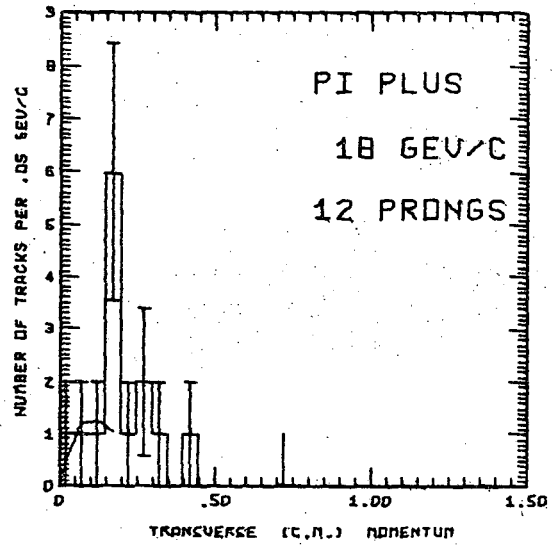
PI PLUS
18 GEV/C
12 PRONGS
NUMBER OF TRACKS PER .05 GEV/C
TRANSVERSE (C.M.) MOMENTUM
0
.50
1.00
1.50

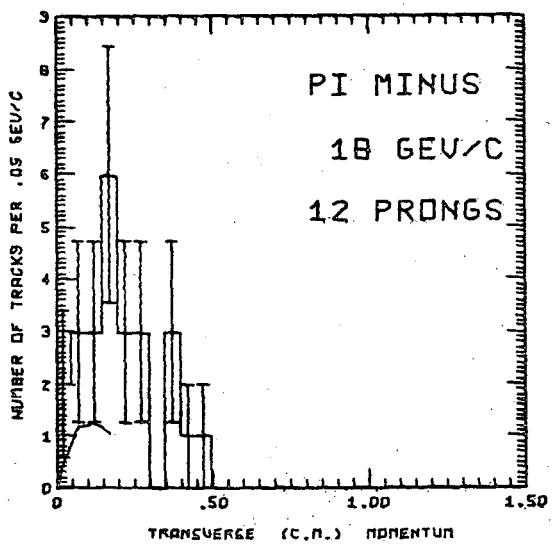
PI MINUS
18 GEV/C
12 PRONGS
NUMBER OF TRACKS PER .05 GEV/C
TRANSVERSE (C.M.) MOMENTUM
0
.50
1.00
1.50

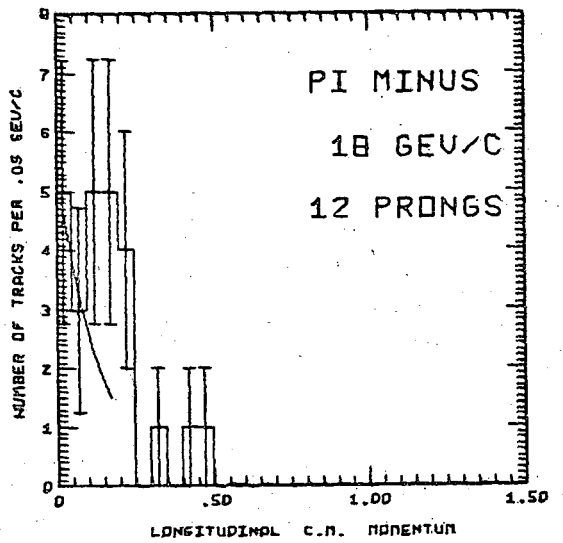
PI MINUS
18 GEV/C
12 PRONGS
NUMBER OF TRACKS PER .05 GEV/C
LONGITUDINAL C.M. MOMENTUM
0
.50
1.00
1.50

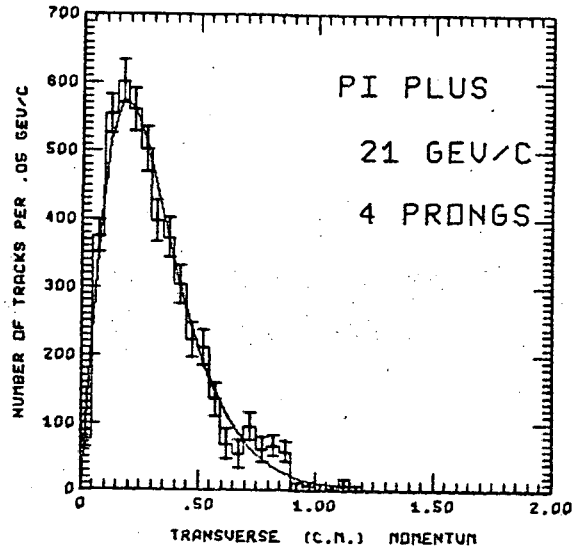
PI PLUS
21 GEV/C
4 PRONGS
NUMBER OF TRACKS PER .05 GEV/C
TRANSVERSE (C.M.) MOMENTUM
0
100
200
300
400
500
600
700
.50
1.00
1.50
2.00

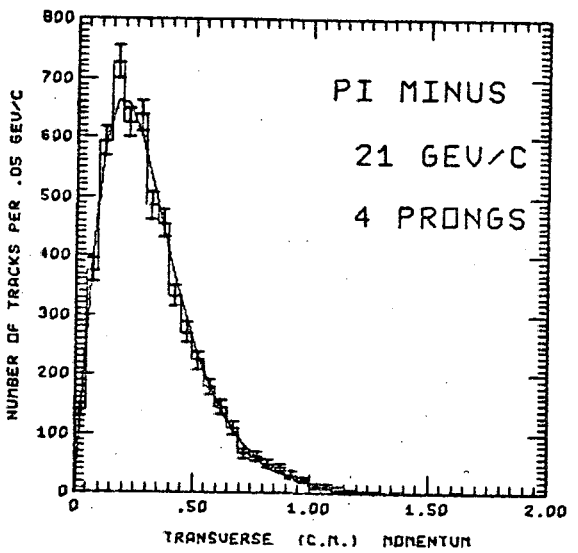
PI MINUS
21 GEV/C
4 PRONGS
NUMBER OF TRACKS PER .05 GEV/C
TRANSVERSE (C.M.) MOMENTUM
0
100
200
300
400
500
600
700
800
.50
1.00
1.50
2.00

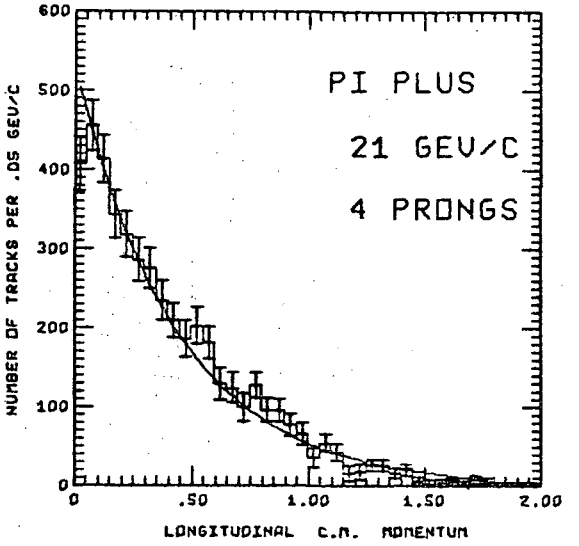
PI PLUS
21 GEV/C
4 PRONGS
NUMBER OF TRACKS PER .05 GEV/C
LONGITUDINAL C.M. MOMENTUM
0
100
200
300
400
500
600
.50
1.00
1.50
2.00

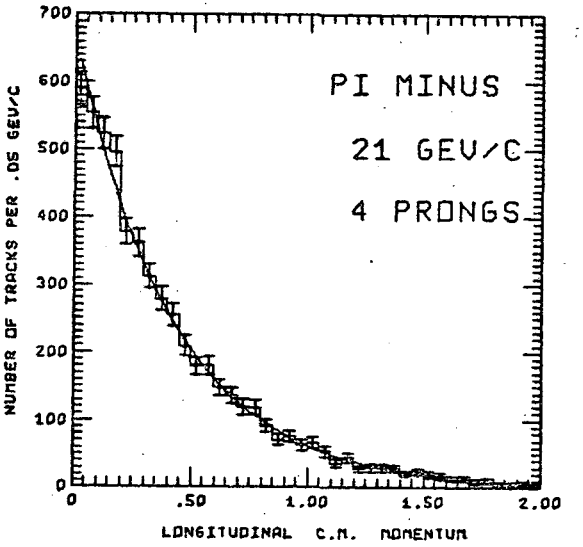
PI MINUS
21 GEV/C
4 PRONGS
NUMBER OF TRACKS PER .05 GEV/C
LONGITUDINAL C.M. MOMENTUM
0
100
200
300
400
500
600
700
.50
1.00
1.50
2.00

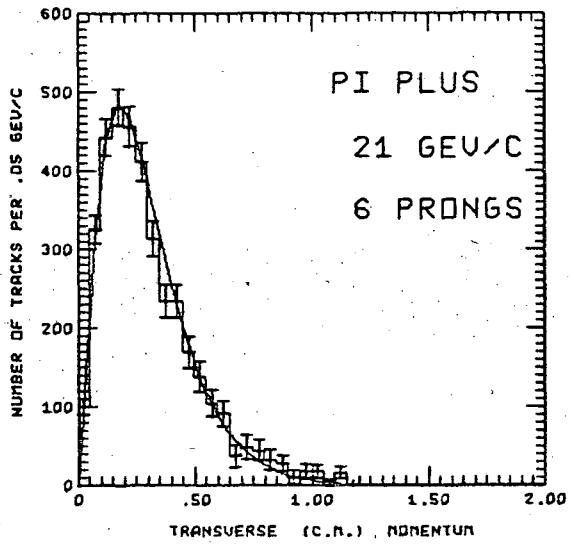
PI PLUS
21 GEV/C
6 PRONGS
NUMBER OF TRACKS PER .05 GEV/C
TRANSVERSE (C.M.) MOMENTUM
0
100
200
300
400
500
600
.50
1.00
1.50
2.00

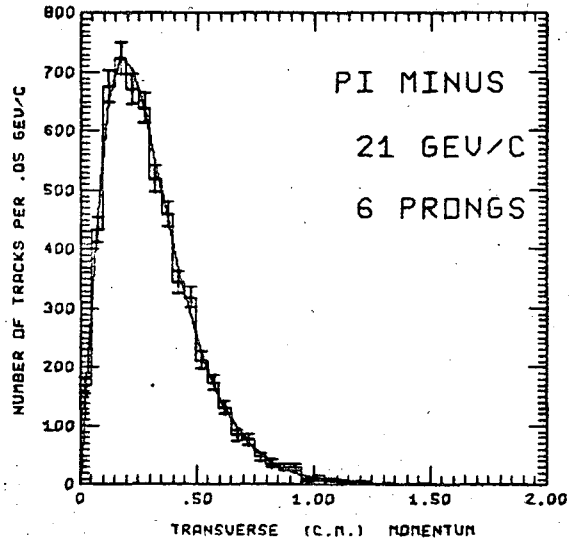
PI MINUS
21 GEV/C
6 PRONGS
NUMBER OF TRACKS PER .05 GEV/C
TRANSVERSE (C.M.) MOMENTUM
0
100
200
300
400
500
600
700
800
.50
1.00
1.50
2.00

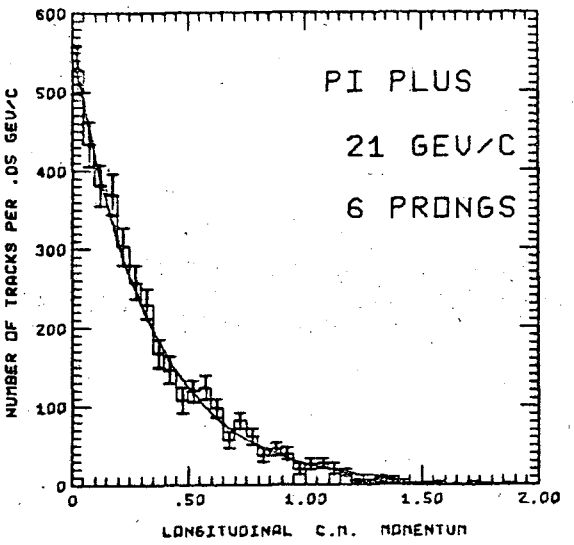
PI PLUS
21 GEV/C
6 PRONGS
NUMBER OF TRACKS PER .05 GEV/C
LONGITUDINAL C.M. MOMENTUM
0
100
200
300
400
500
600
.50
1.00
1.50
2.00

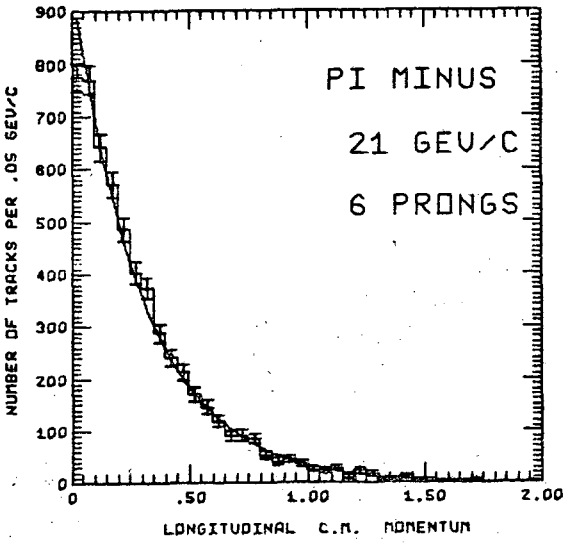
PI MINUS
21 GEV/C
6 PRONGS
NUMBER OF TRACKS PER .05 GEV/C
LONGITUDINAL C.M. MOMENTUM
0
100
200
300
400
500
600
700
800
900
.50
1.00
1.50
2.00

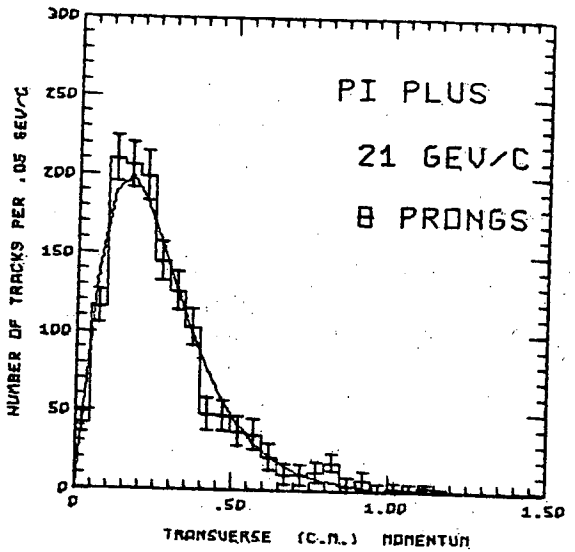
PI PLUS
21 GEV/C
8 PRONGS
NUMBER OF TRACKS PER .05 GEV/C
TRANSVERSE (C.M.) MOMENTUM
0
50
100
150
200
250
300
.50
1.00
1.50

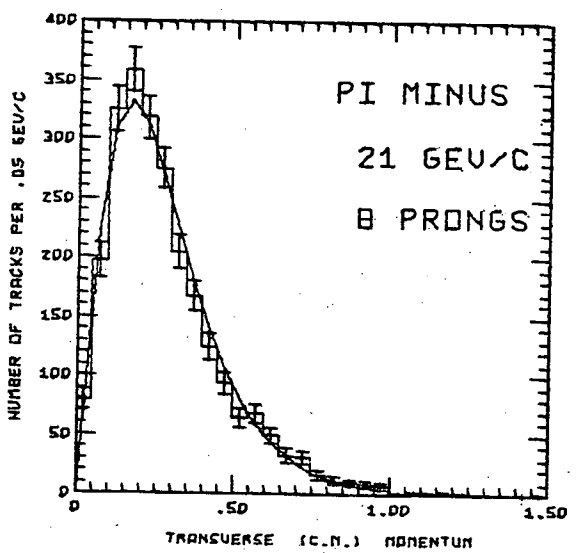
PI MINUS
21 GEV/C
8 PRONGS
NUMBER OF TRACKS PER .05 GEV/C
TRANSVERSE (C.M.) MOMENTUM
0
50
100
150
200
250
300
350
400
.50
1.00
1.50

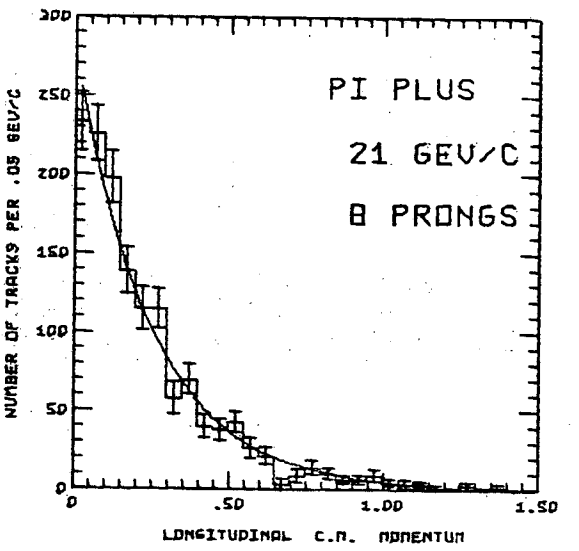
PI PLUS
21 GEV/C
8 PRONGS
NUMBER OF TRACKS PER .05 GEV/C
LONGITUDINAL C.M. MOMENTUM
0
50
100
150
200
250
300
.50
1.00
1.50

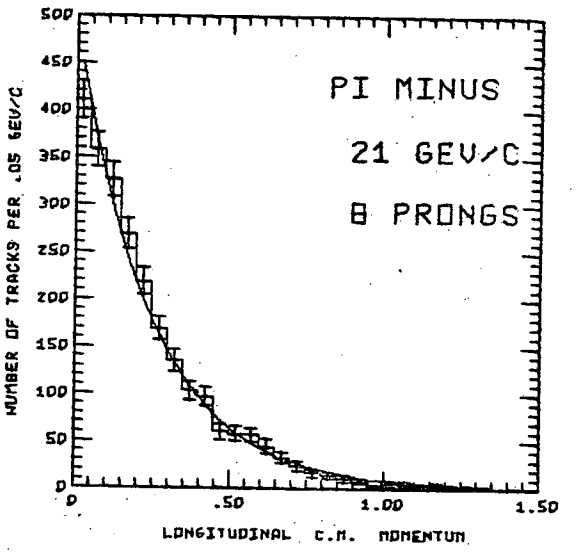
PI MINUS
21 GEV/C
8 PRONGS
NUMBER OF TRACKS PER .05 GEV/C
LONGITUDINAL C.M. MOMENTUM
0
50
100
150
200
250
300
350
400
450
500
.50
1.00
1.50

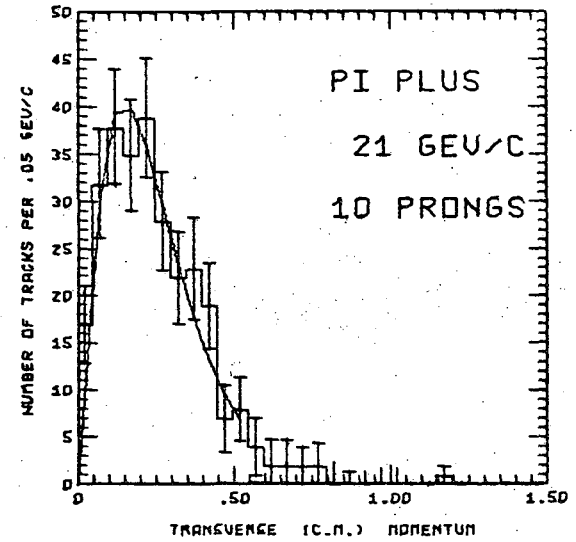
PI PLUS
21 GEV/C
10 PRONGS
NUMBER OF TRACKS PER .05 GEV/C
TRANSVERSE (C.M.) MOMENTUM
0
.50
1.00
1.50
5
10
15
20
25
30
35
40
45
50

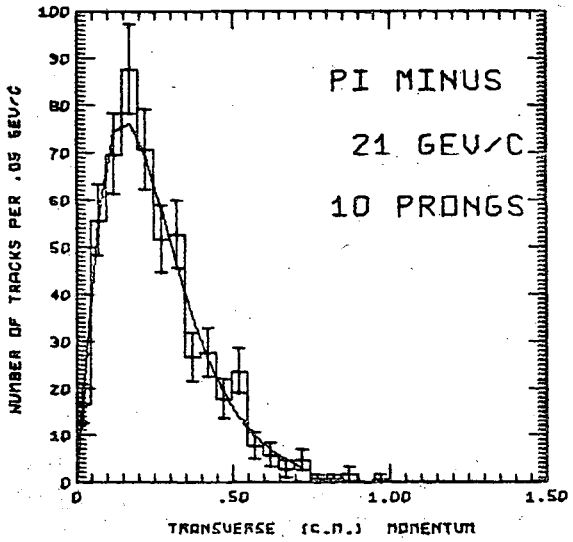
PI MINUS
21 GEV/C
10 PRONGS
NUMBER OF TRACKS PER .05 GEV/C
TRANSVERSE (C.M.) MOMENTUM
0
.50
1.00
1.50
10
20
30
40
50
60
70
80
90
100

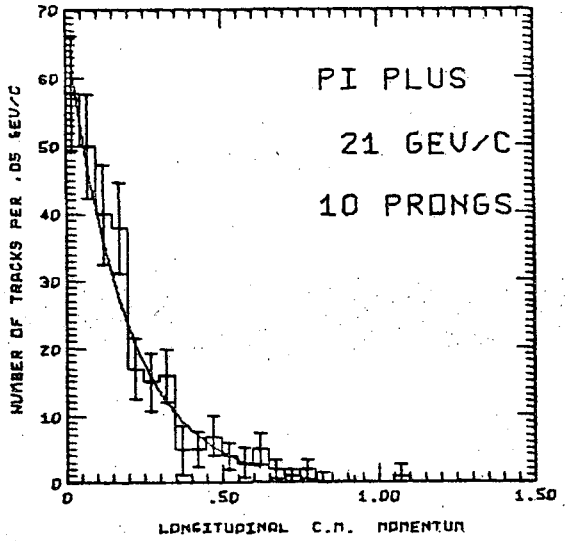
PI PLUS
21 GEV/C
10 PRONGS
NUMBER OF TRACKS PER .05 GEV/C
LONGITUDINAL C.M. MOMENTUM
0
.50
1.00
1.50
10
20
30
40
50
60
70

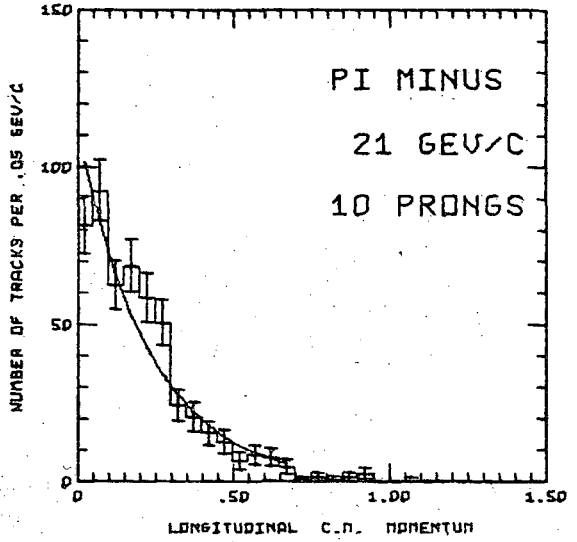
PI MINUS
21 GEV/C
10 PRONGS
NUMBER OF TRACKS PER .05 GEV/C
LONGITUDINAL C.M. MOMENTUM
0
.50
1.00
1.50
50
100
150

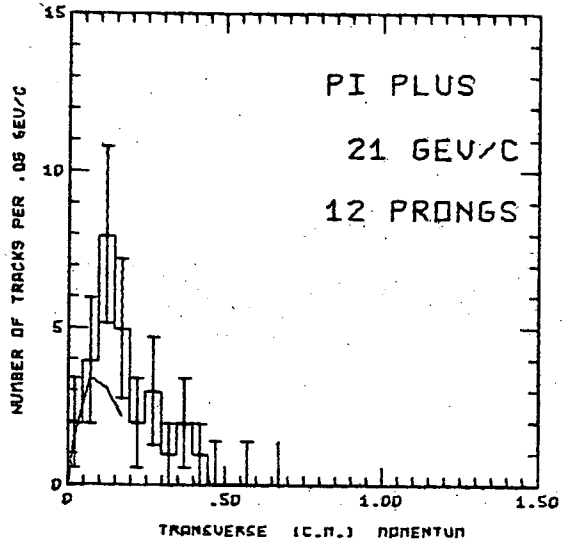
PI PLUS
21 GEV/C
12 PRONGS
NUMBER OF TRACKS PER .05 GEV/C
TRANSVERSE (C.M.) MOMENTUM
0
5
10
15
.50
1.00
1.50

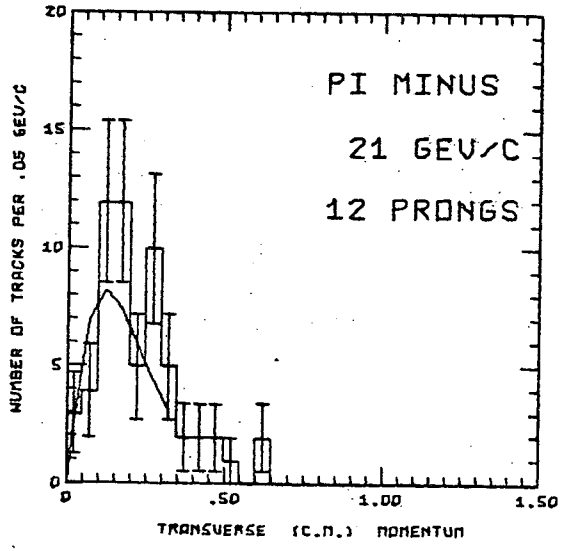
PI MINUS
21 GEV/C
12 PRONGS
NUMBER OF TRACKS PER .05 GEV/C
TRANSVERSE (C.M.) MOMENTUM
0
5
10
15
20
.50
1.00
1.50

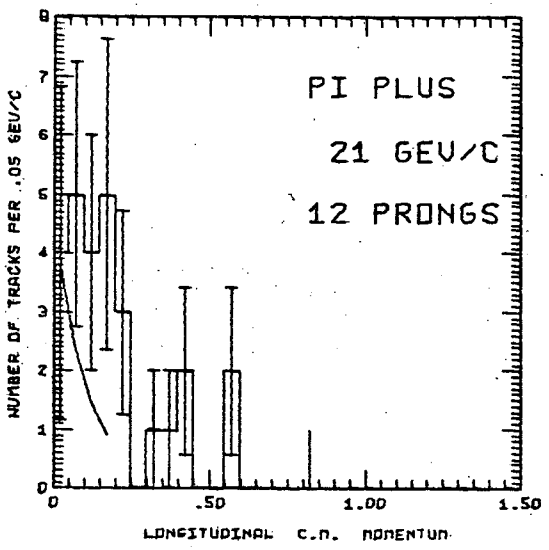
PI PLUS
21 GEV/C
12 PRONGS
NUMBER OF TRACKS PER .05 GEV/C
LONGITUDINAL C.M. MOMENTUM
0
1
2
3
4
5
6
7
8
.50
1.00
1.50

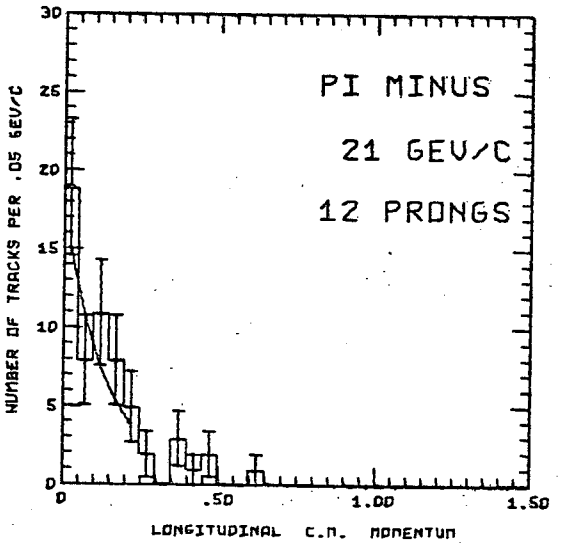
PI MINUS
21 GEV/C
12 PRONGS
NUMBER OF TRACKS PER .05 GEV/C
LONGITUDINAL C.M. MOMENTUM
0
5
10
15
20
25
30
.50
1.00
1.50

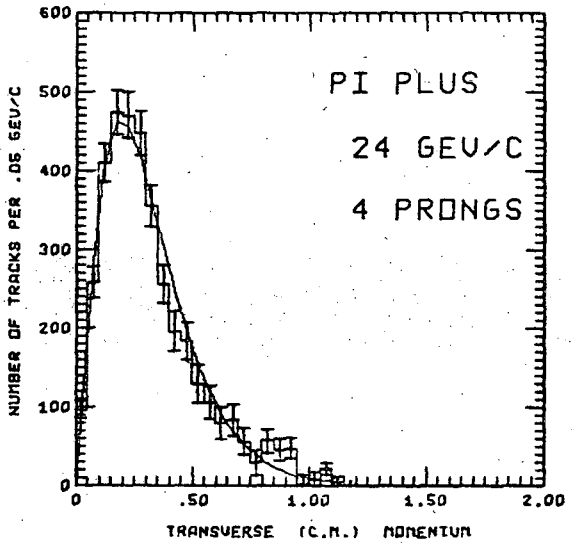
PI PLUS
24 GEV/C
4 PRONGS
NUMBER OF TRACKS PER .05 GEV/C
TRANSVERSE (C.M.) MOMENTUM
0
100
200
300
400
500
600
.50
1.00
1.50
2.00

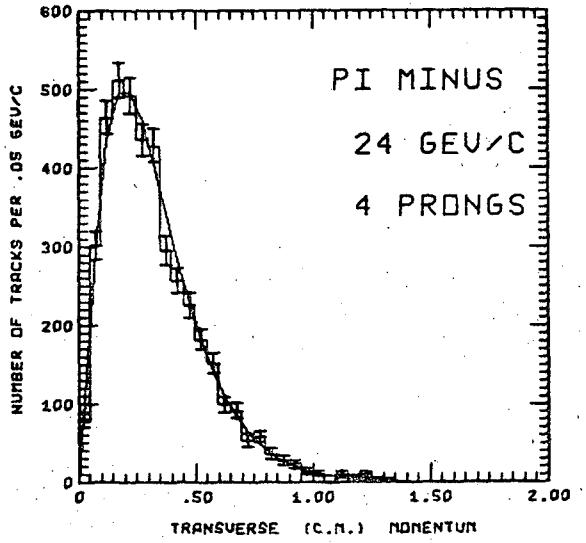
PI MINUS
24 GEV/C
4 PRONGS
NUMBER OF TRACKS PER .05 GEV/C
TRANSVERSE (C.M.) MOMENTUM
0
100
200
300
400
500
600
.50
1.00
1.50
2.00

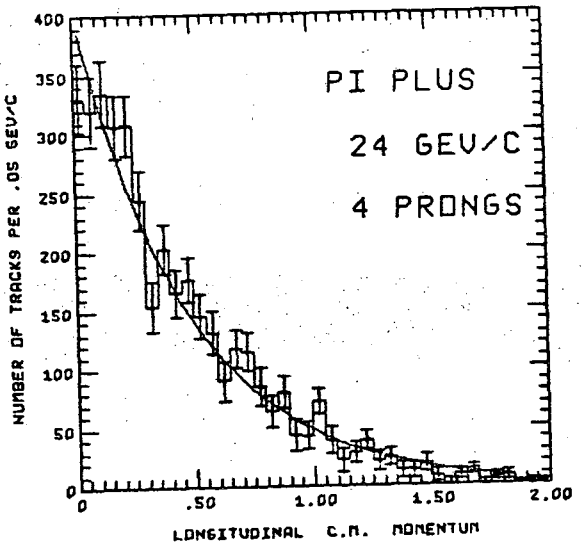
PI PLUS
24 GEV/C
4 PRONGS
NUMBER OF TRACKS PER .05 GEV/C
LONGITUDINAL C.M. MOMENTUM
0
50
100
150
200
250
300
350
400
.50
1.00
1.50
2.00

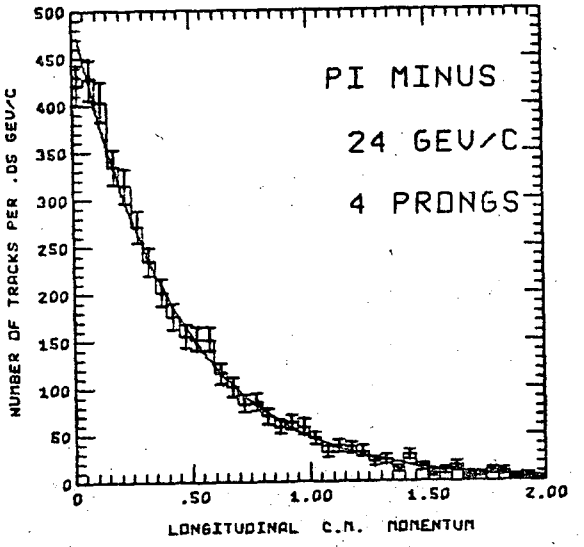
PI MINUS
24 GEV/C
4 PRONGS
NUMBER OF TRACKS PER .05 GEV/C
LONGITUDINAL C.M. MOMENTUM
0
50
100
150
200
250
300
350
400
450
500
.50
1.00
1.50
2.00

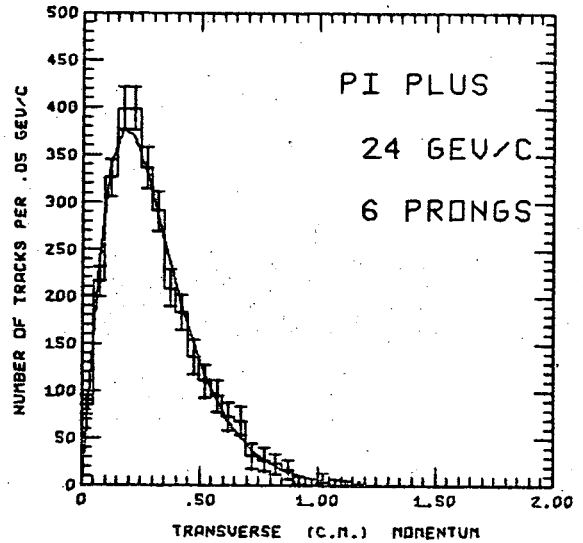
PI PLUS
24 GEV/C
6 PRONGS
NUMBER OF TRACKS PER .05 GEV/C
TRANSVERSE (C.M.) MOMENTUM
0
50
100
150
200
250
300
350
400
450
500
.50
1.00
1.50
2.00

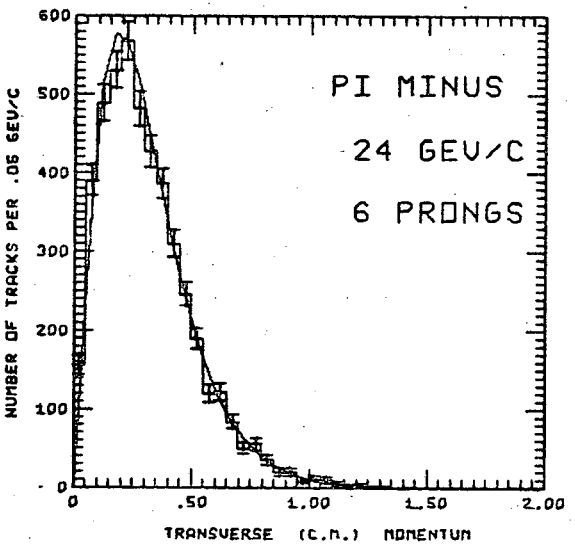
PI MINUS
24 GEV/C
6 PRONGS
NUMBER OF TRACKS PER .05 GEV/C
TRANSVERSE (C.M.) MOMENTUM
0
100
200
300
400
500
600
.50
1.00
1.50
2.00

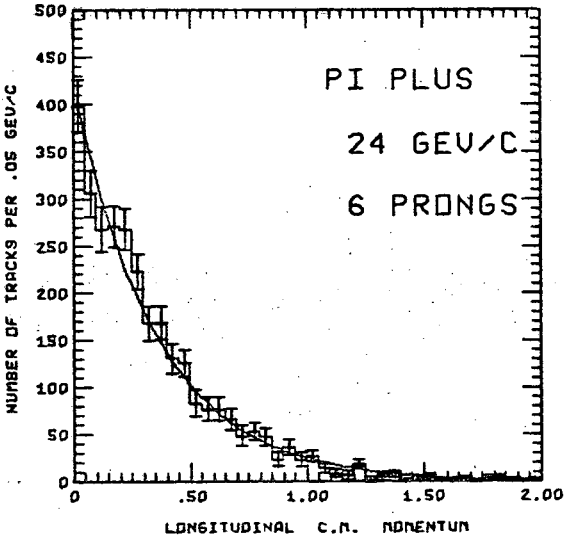
PI PLUS
24 GEV/C
6 PRONGS
NUMBER OF TRACKS PER .05 GEV/C
LONGITUDINAL C.M. MOMENTUM
0
50
100
150
200
250
300
350
400
450
500
.50
1.00
1.50
2.00

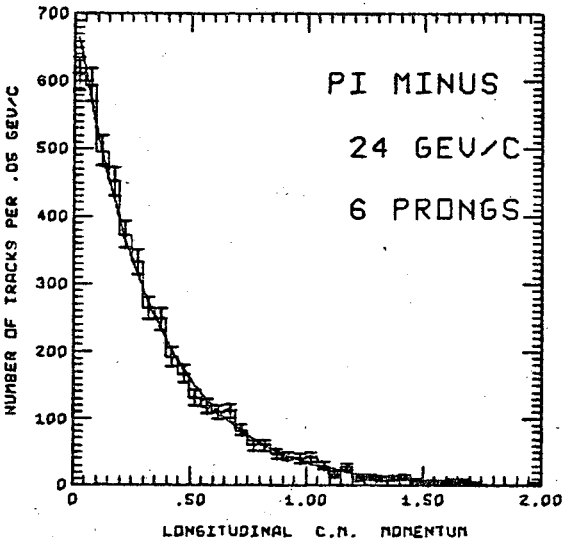
PI MINUS
24 GEV/C
6 PRONGS
NUMBER OF TRACKS PER .05 GEV/C
LONGITUDINAL C.M. MOMENTUM
0
100
200
300
400
500
600
700
.50
1.00
1.50
2.00

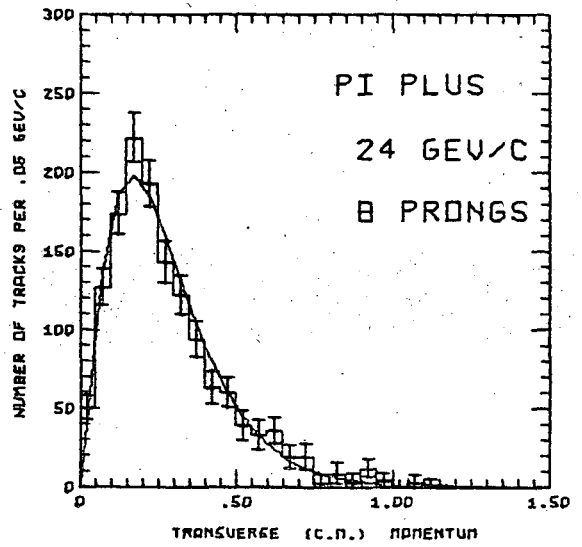
PI PLUS
24 GEV/C
8 PRONGS
NUMBER OF TRACKS PER .05 GEV/C
TRANSVERSE (C.M.) MOMENTUM
0
50
100
150
200
250
300
.50
1.00
1.50

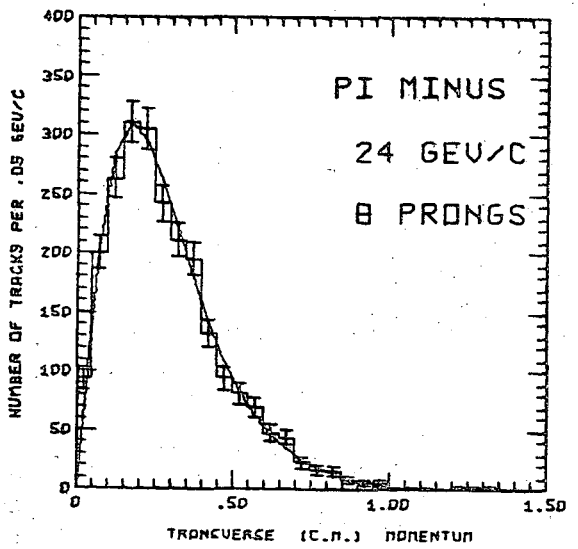
PI MINUS
24 GEV/C
8 PRONGS
NUMBER OF TRACKS PER .05 GEV/C
TRANSVERSE (C.M.) MOMENTUM
0
50
100
150
200
250
300
350
400
.50
1.00
1.50

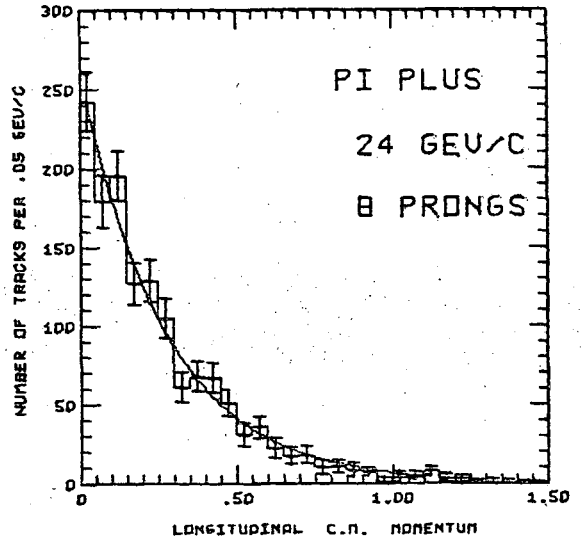
PI PLUS
24 GEV/C
8 PRONGS
NUMBER OF TRACKS PER .05 GEV/C
LONGITUDINAL C.M. MOMENTUM
0
50
100
150
200
250
300
.50
1.00
1.50

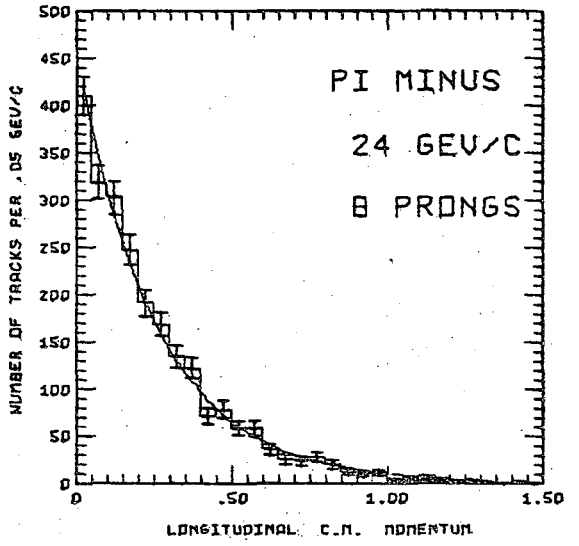
PI MINUS
24 GEV/C
8 PRONGS
NUMBER OF TRACKS PER .05 GEV/C
LONGITUDINAL C.M. MOMENTUM
0
50
100
150
200
250
300
350
400
450
500
.50
1.00
1.50

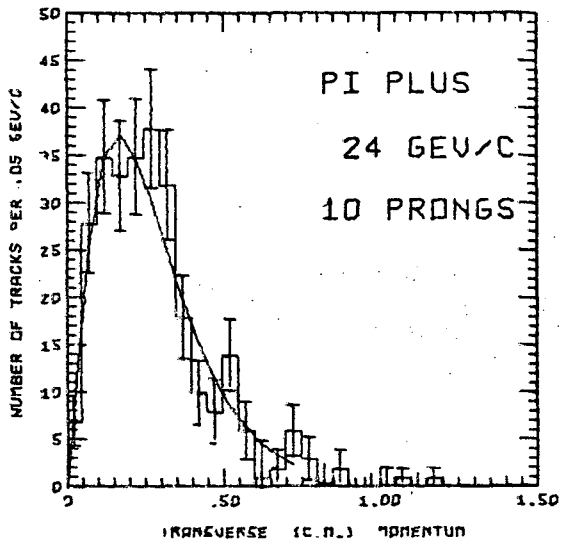
PI PLUS
24 GEV/C
10 PRONGS
NUMBER OF TRACKS PER .05 GEV/C
TRANSVERSE (C.M.) MOMENTUM

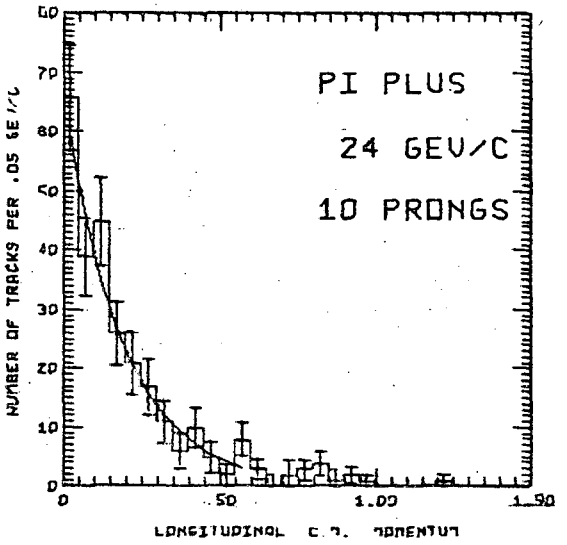
PI PLUS
24 GEV/C
10 PRONGS
NUMBER OF TRACKS PER .05 GEV/C
LONGITUDINAL C.M. MOMENTUM

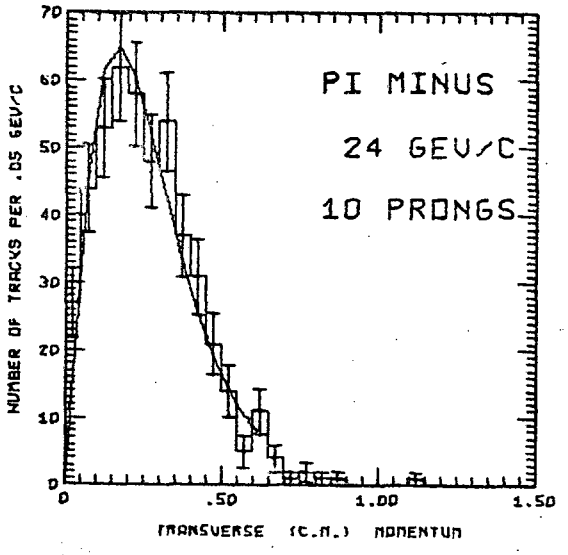
PI MINUS
24 GEV/C
10 PRONGS
NUMBER OF TRACKS PER .05 GEV/C
TRANSVERSE (C.M.) MOMENTUM

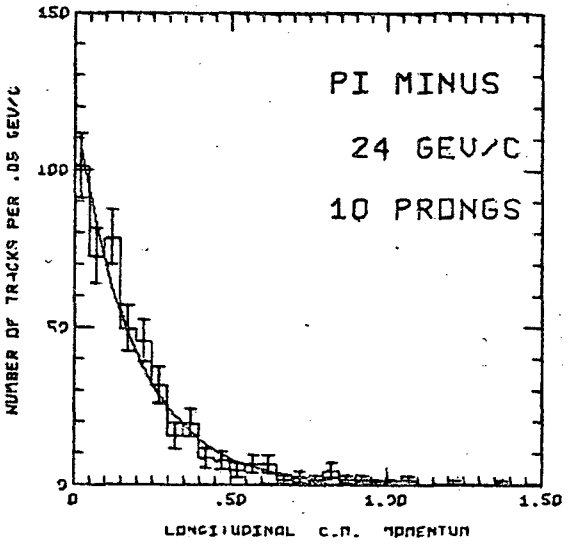
PI MINUS
24 GEV/C
10 PRONGS
NUMBER OF TRACKS PER .05 GEV/C
LONGITUDINAL C.M. MOMENTUM

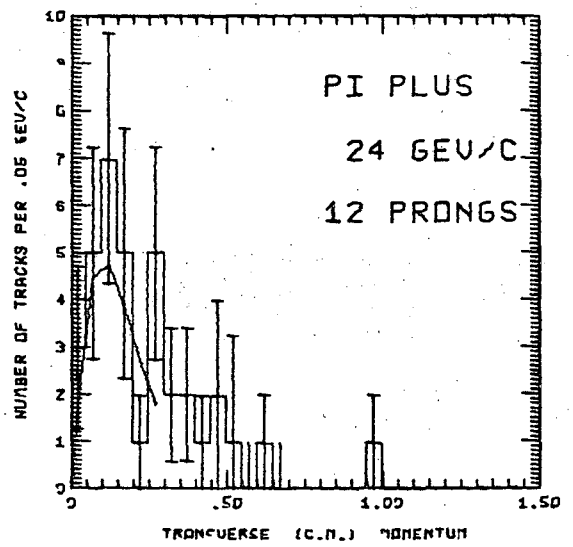
PI PLUS
24 GEV/C
12 PRONGS
NUMBER OF TRACKS PER .05 GEV/C
TRANSVERSE (C.M.) MOMENTUM
0
.50
1.00
1.50

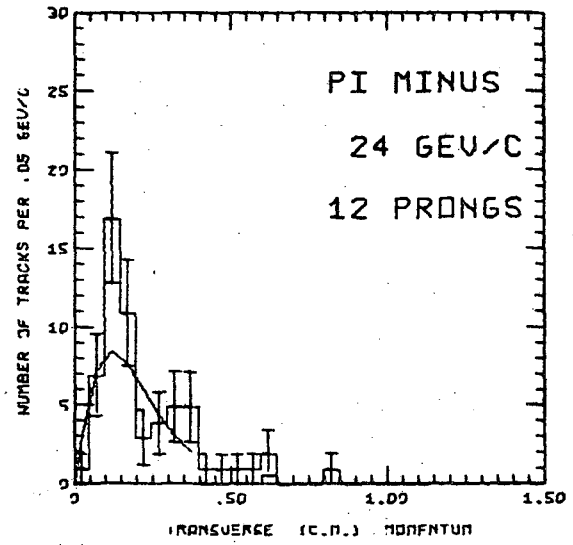
PI MINUS
24 GEV/C
12 PRONGS
NUMBER OF TRACKS PER .05 GEV/C
TRANSVERSE (C.M.) MOMENTUM
0
.50
1.00
1.50

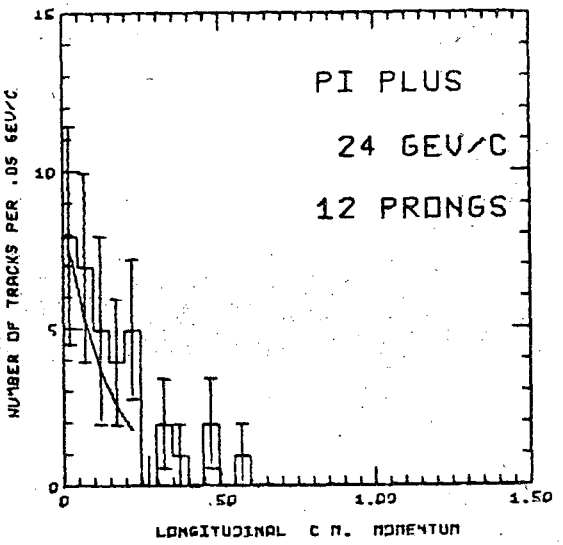
PI PLUS
24 GEV/C
12 PRONGS
NUMBER OF TRACKS PER .05 GEV/C
LONGITUDINAL C.M. MOMENTUM
0
.50
1.00
1.50

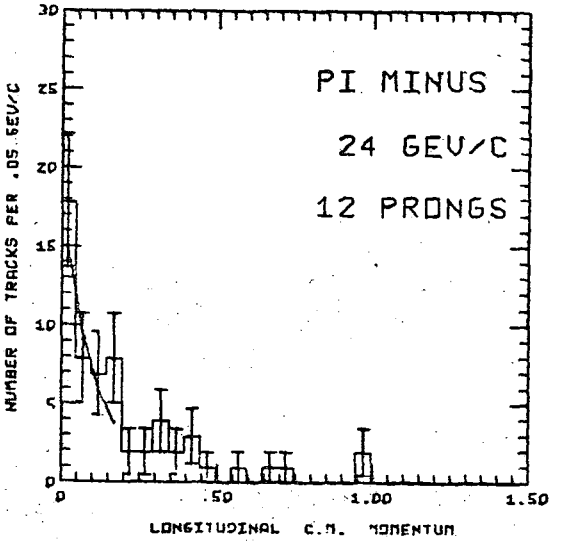
PI MINUS
24 GEV/C
12 PRONGS
NUMBER OF TRACKS PER .05 GEV/C
LONGITUDINAL C.M. MOMENTUM
0
.50
1.00
1.50

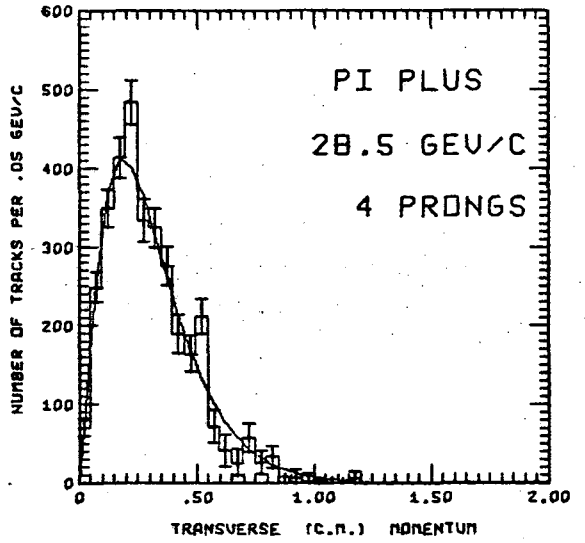
PI PLUS
28.5 GEV/C
4 PRONGS
NUMBER OF TRACKS PER .05 GEV/C
TRANSVERSE (C.M.) MOMENTUM
0
100
200
300
400
500
600
.50
1.00
1.50
2.00

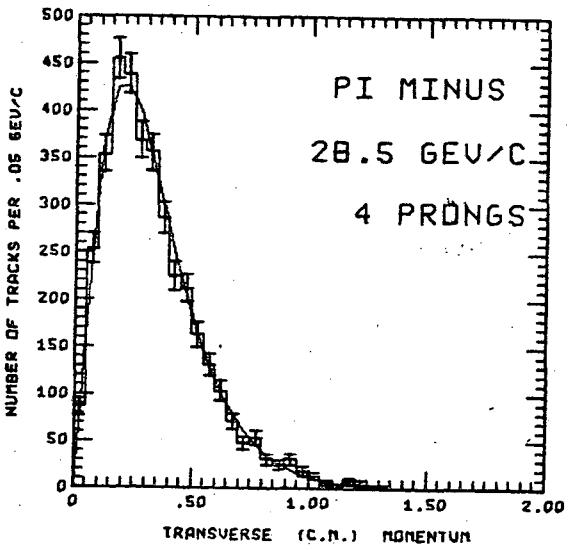
PI MINUS
28.5 GEV/C
4 PRONGS
NUMBER OF TRACKS PER .05 GEV/C
TRANSVERSE (C.M.) MOMENTUM
0
50
100
150
200
250
300
350
400
450
500
.50
1.00
1.50
2.00

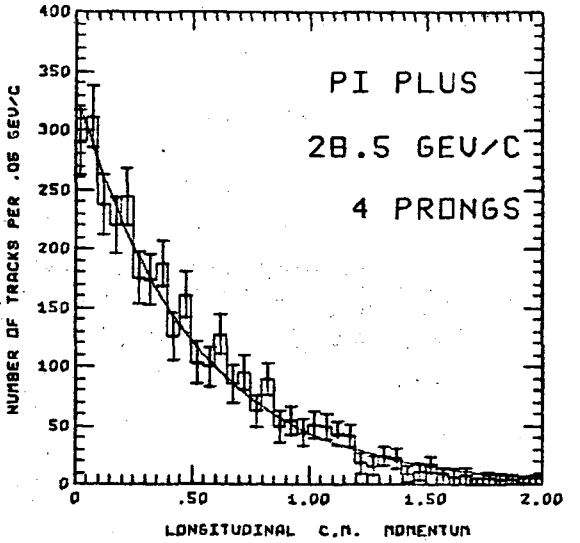
PI PLUS
28.5 GEV/C
4 PRONGS
NUMBER OF TRACKS PER .05 GEV/C
LONGITUDINAL C.M. MOMENTUM
0
50
100
150
200
250
300
350
400
.50
1.00
1.50
2.00

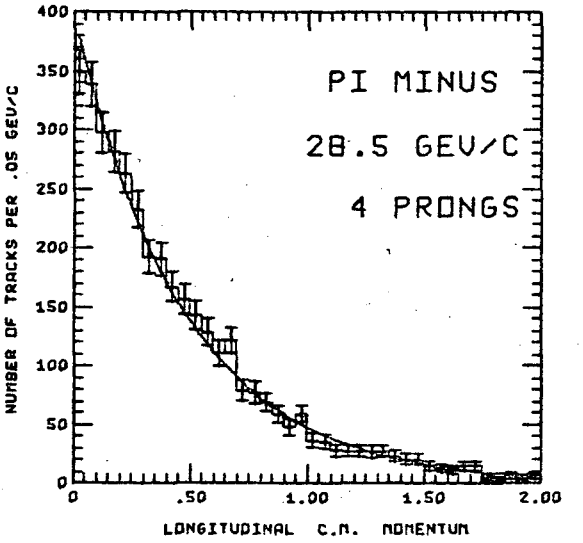
PI MINUS
28.5 GEV/C
4 PRONGS
NUMBER OF TRACKS PER .05 GEV/C
LONGITUDINAL C.M. MOMENTUM
0
50
100
150
200
250
300
350
400
.50
1.00
1.50
2.00

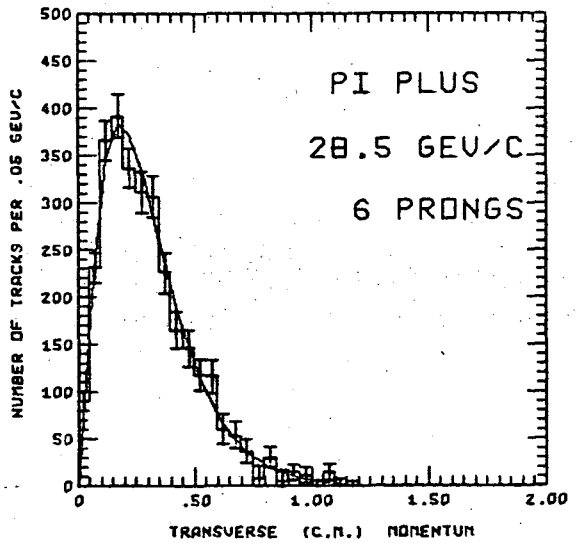
PI PLUS
28.5 GEV/C
6 PRONGS
NUMBER OF TRACKS PER .05 GEV/C
TRANSVERSE (C.M.) MOMENTUM
0
50
100
150
200
250
300
350
400
450
500
.50
1.00
1.50
2.00

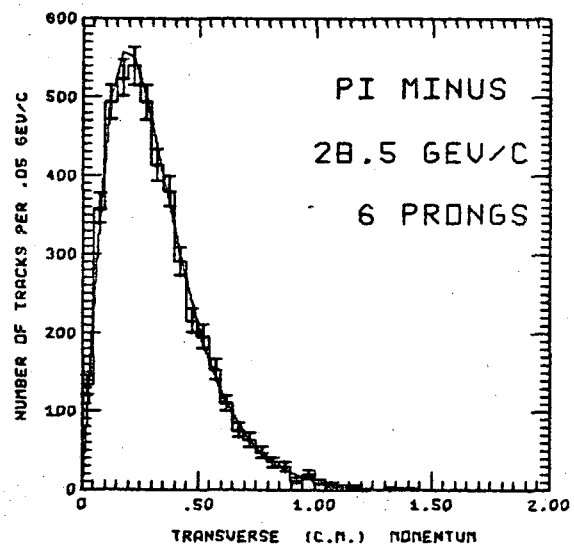
PI MINUS
28.5 GEV/C
6 PRONGS
NUMBER OF TRACKS PER .05 GEV/C
TRANSVERSE (C.M.) MOMENTUM
0
100
200
300
400
500
600
.50
1.00
1.50
2.00

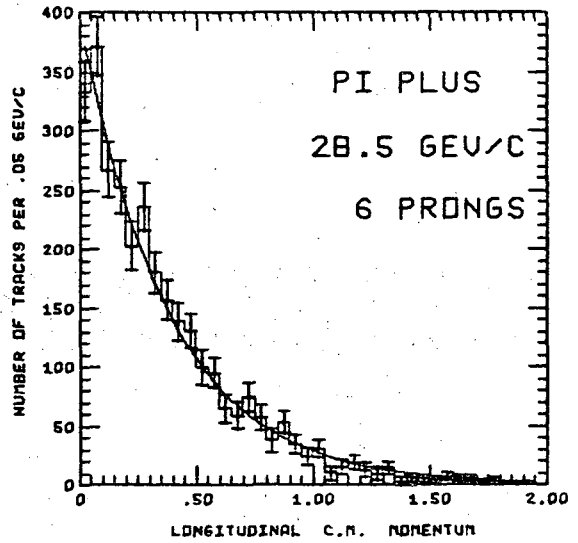
PI PLUS
28.5 GEV/C
6 PRONGS
NUMBER OF TRACKS PER .05 GEV/C
LONGITUDINAL C.M. MOMENTUM
0
50
100
150
200
250
300
350
400
.50
1.00
1.50
2.00

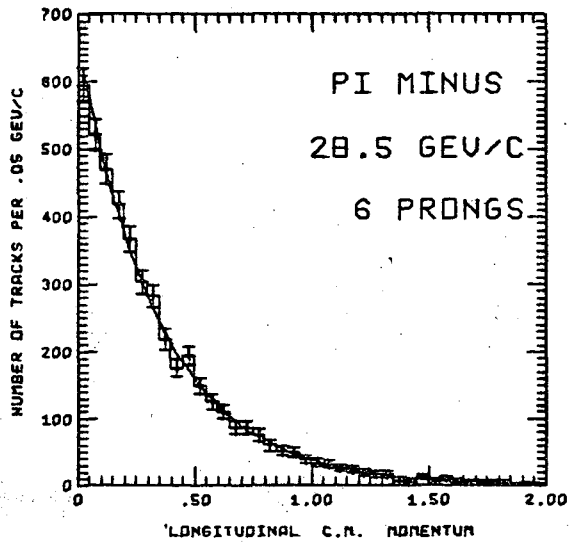
PI MINUS
28.5 GEV/C
6 PRONGS
NUMBER OF TRACKS PER .05 GEV/C
LONGITUDINAL C.M. MOMENTUM
0
100
200
300
400
500
600
700
.50
1.00
1.50
2.00

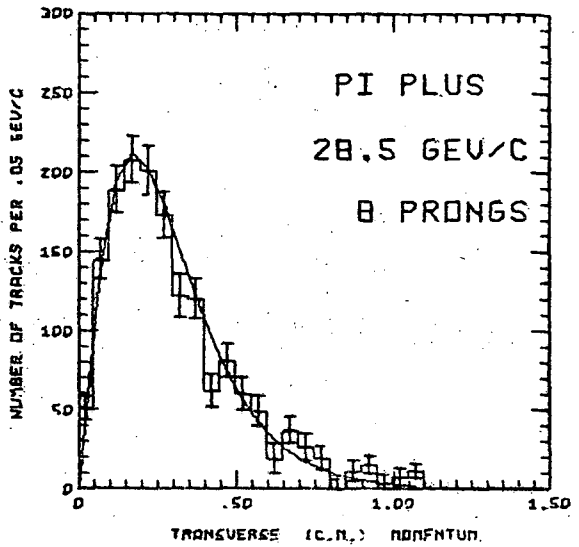
PI PLUS
28.5 GEV/C
8 PRONGS
NUMBER OF TRACKS PER .05 GEV/C
TRANSVERSE (C.M.) MOMENTUM
0
50
100
150
200
250
300
.50
1.00
1.50

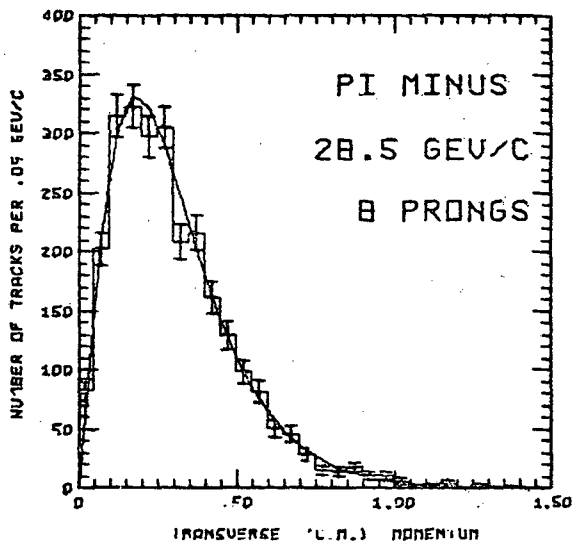
PI MINUS
28.5 GEV/C
8 PRONGS
NUMBER OF TRACKS PER .05 GEV/C
TRANSVERSE (C.M.) MOMENTUM
0
50
100
150
200
250
300
350
400
.50
1.00
1.50

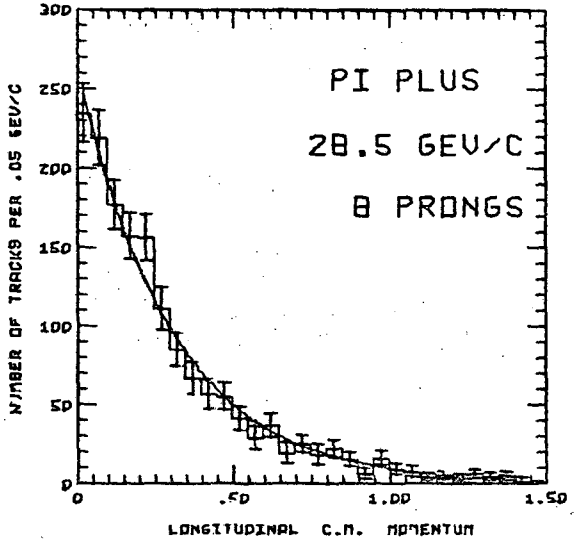
PI PLUS
28.5 GEV/C
8 PRONGS
NUMBER OF TRACKS PER .05 GEV/C
LONGITUDINAL C.M. MOMENTUM
0
50
100
150
200
250
300
.50
1.00
1.50

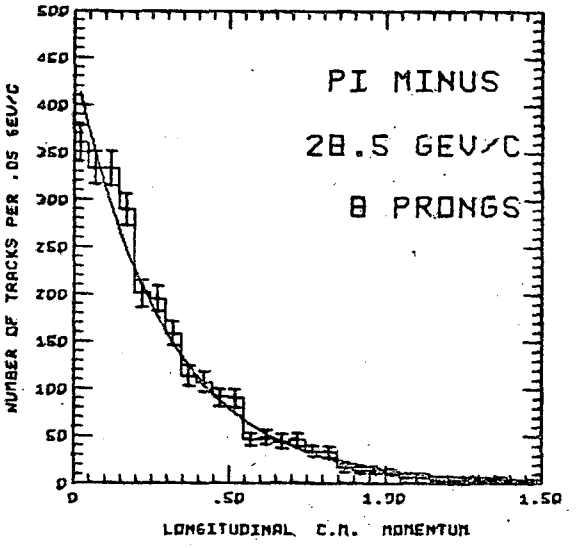
PI MINUS
28.5 GEV/C
8 PRONGS
NUMBER OF TRACKS PER .05 GEV/C
LONGITUDINAL C.M. MOMENTUM
0
50
100
150
200
250
300
350
400
450
500
.50
1.00
1.50

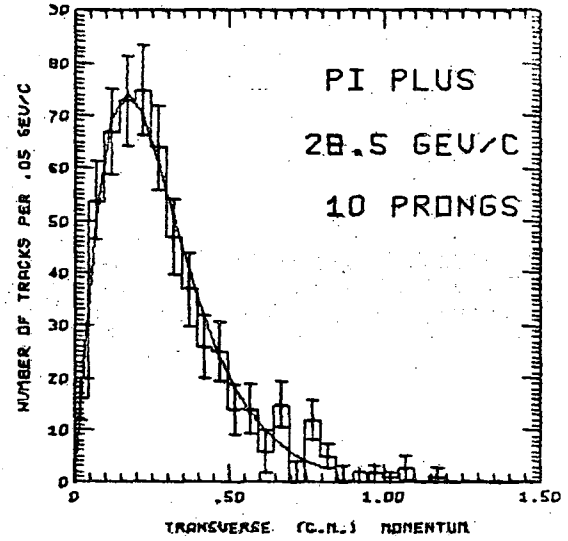
PI PLUS
28.5 GEV/C
10 PRONGS
NUMBER OF TRACKS PER .05 GEV/C
TRANSVERSE (C.M.) MOMENTUM
0
10
20
30
40
50
60
70
80
90
.50
1.00
1.50

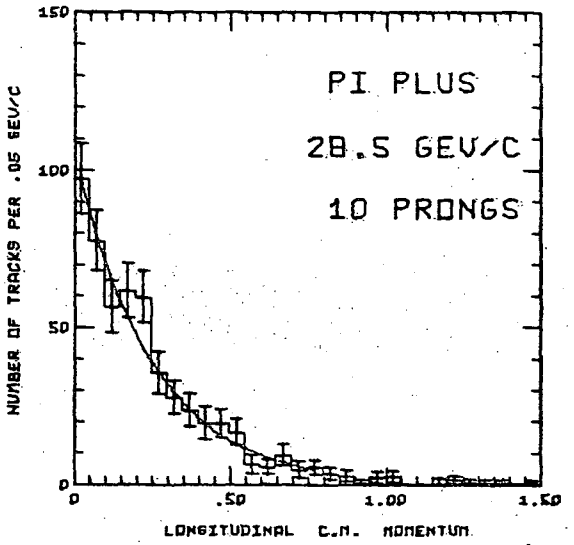
PI PLUS
28.5 GEV/C
10 PRONGS
NUMBER OF TRACKS PER .05 GEV/C
LONGITUDINAL C.M. MOMENTUM
0
50
100
150
.50
1.00
1.50

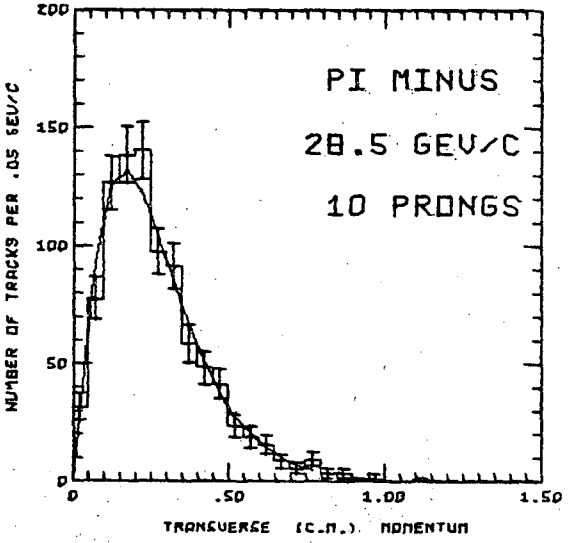
PI MINUS
28.5 GEV/C
10 PRONGS
NUMBER OF TRACKS PER .05 GEV/C
TRANSVERSE (C.M.) MOMENTUM
0
50
100
150
200
.50
1.00
1.50

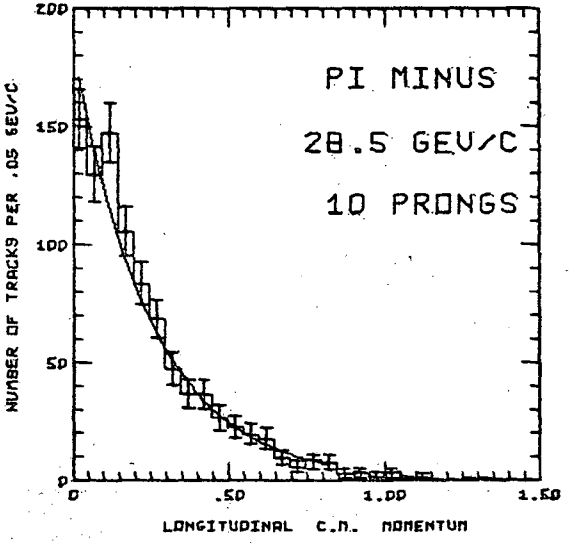
PI MINUS
28.5 GEV/C
10 PRONGS
NUMBER OF TRACKS PER .05 GEV/C
LONGITUDINAL C.M. MOMENTUM
0
50
100
150
200
.50
1.00
1.50

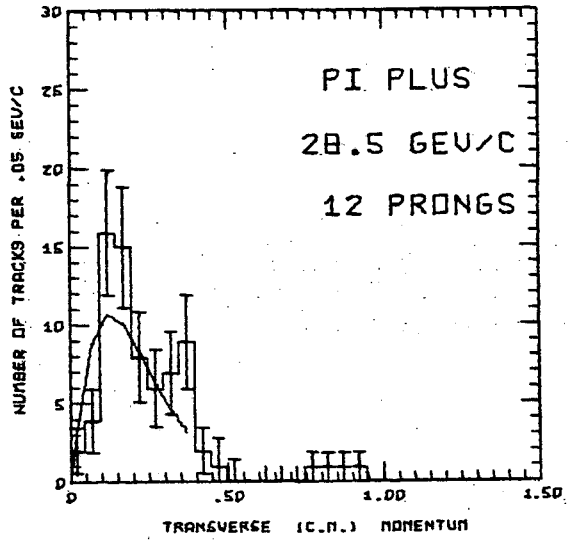
PI PLUS
28.5 GEV/C
12 PRONGS
NUMBER OF TRACKS PER .05 GEV/C
TRANSVERSE (C.M.) MOMENTUM
0
.50
1.00
1.50
5
10
15
20
25
30

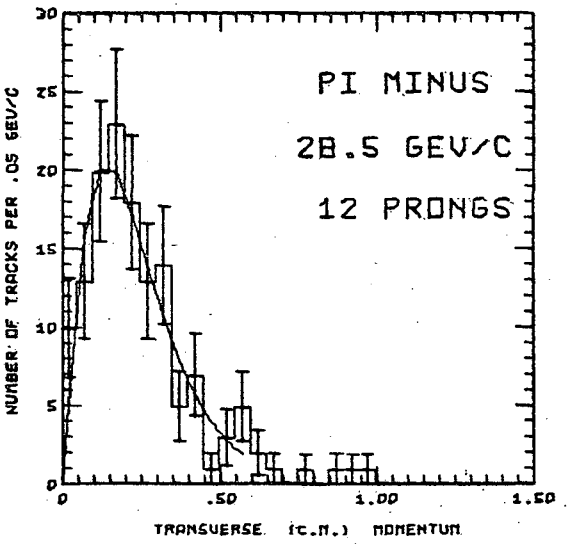
PI MINUS
28.5 GEV/C
12 PRONGS
NUMBER OF TRACKS PER .05 GEV/C
TRANSVERSE (C.M.) MOMENTUM
0
.50
1.00
1.50
5
10
15
20
25
30

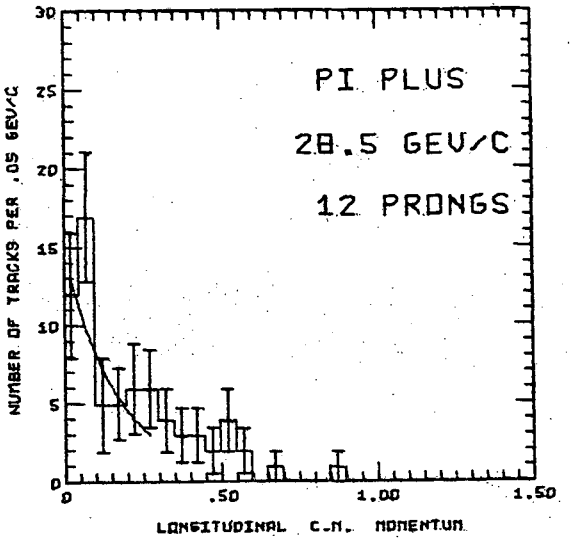
PI PLUS
28.5 GEV/C
12 PRONGS
NUMBER OF TRACKS PER .05 GEV/C
LONGITUDINAL C.M. MOMENTUM
0
.50
1.00
1.50
5
10
15
20
25
30

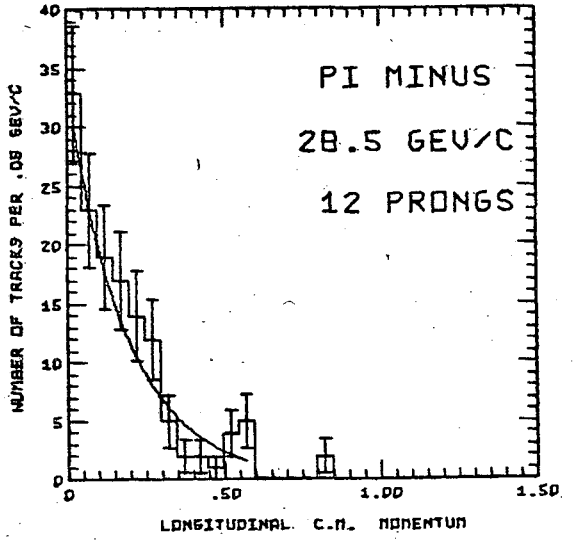
PI MINUS
28.5 GEV/C
12 PRONGS
NUMBER OF TRACKS PER .05 GEV/C
LONGITUDINAL C.M. MOMENTUM
0
.50
1.00
1.50
5
10
15
20
25
30
35
40

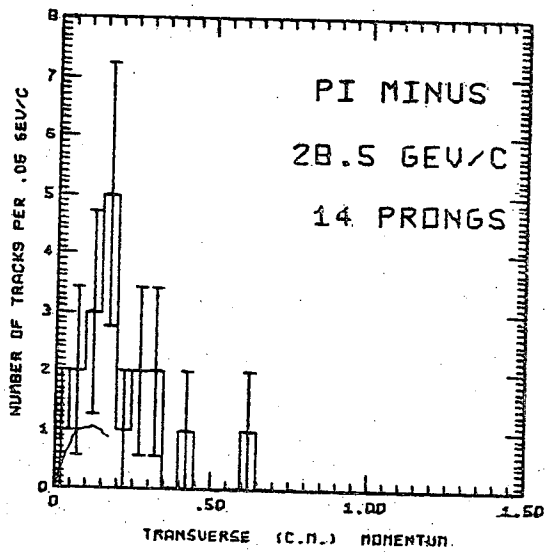
PI MINUS
28.5 GEV/C
14 PRONGS
NUMBER OF TRACKS PER .05 GEV/C
TRANSVERSE (C.M.) MOMENTUM
0
.50
1.00
1.50

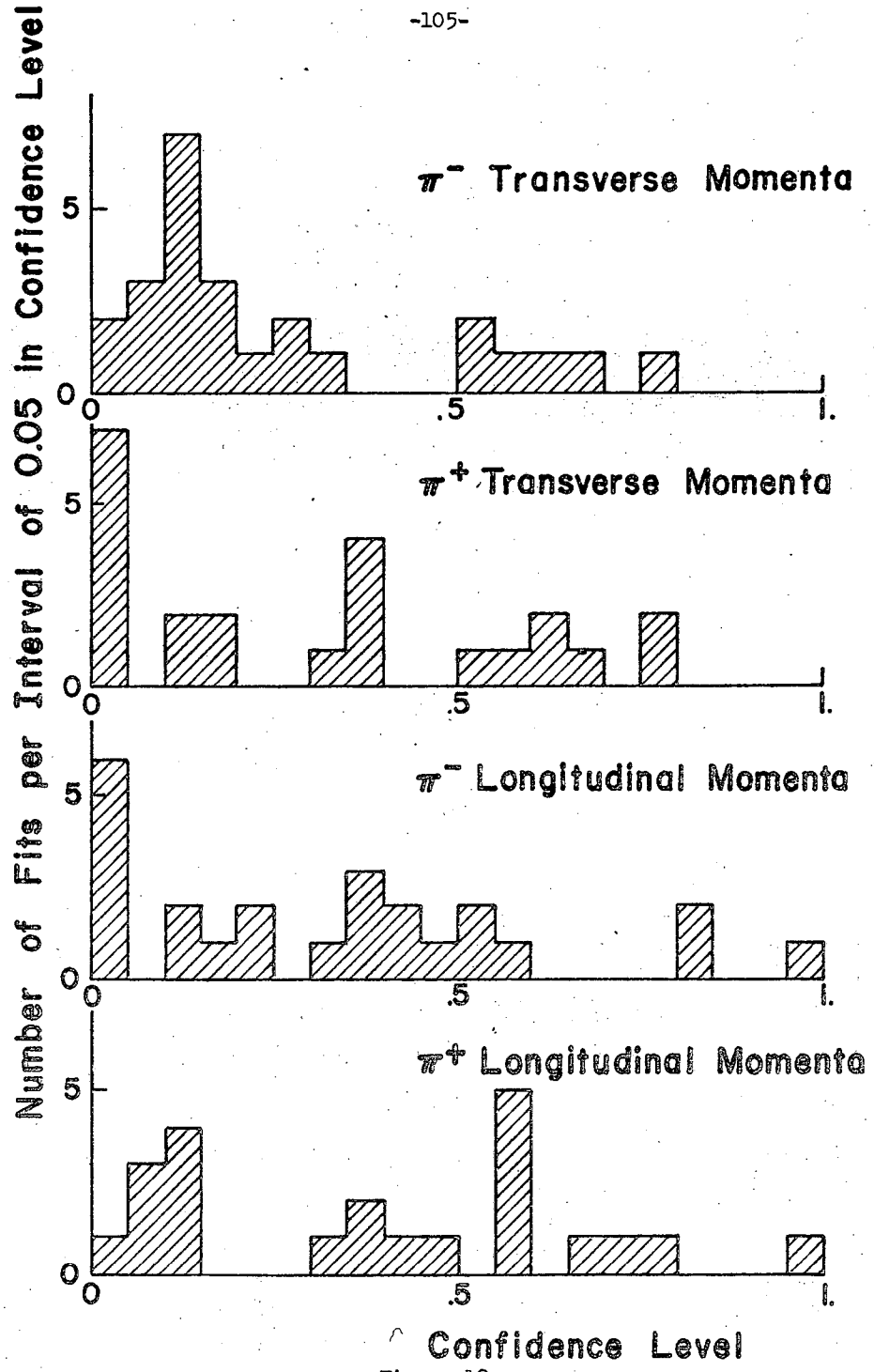
Number of Fits per Interval of 0.05 in Confidence Level
π⁻ Transverse Momenta
π⁺ Transverse Momenta
π⁻ Longitudinal Momenta
π⁺ Longitudinal Momenta
0
.5
1.
5
Confidence Level

Figure 12.

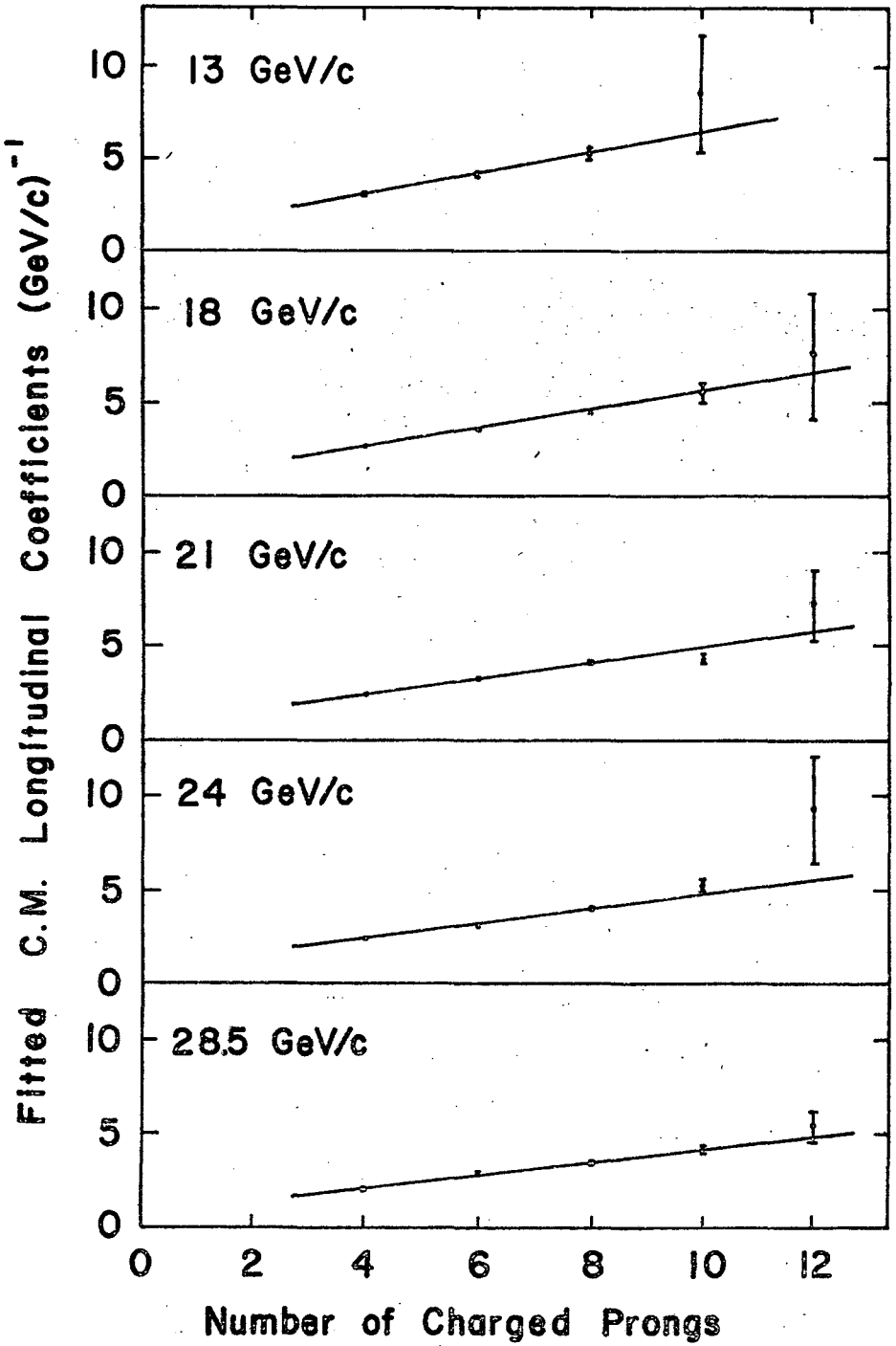
13 GeV/c
18 GeV/c
21 GeV/c
24 GeV/c
28.5 GeV/c
Fitted C.M. Longitudinal Coefficients (GeV/c)$^{-1}$
Number of Charged Prongs

Figure 13a.

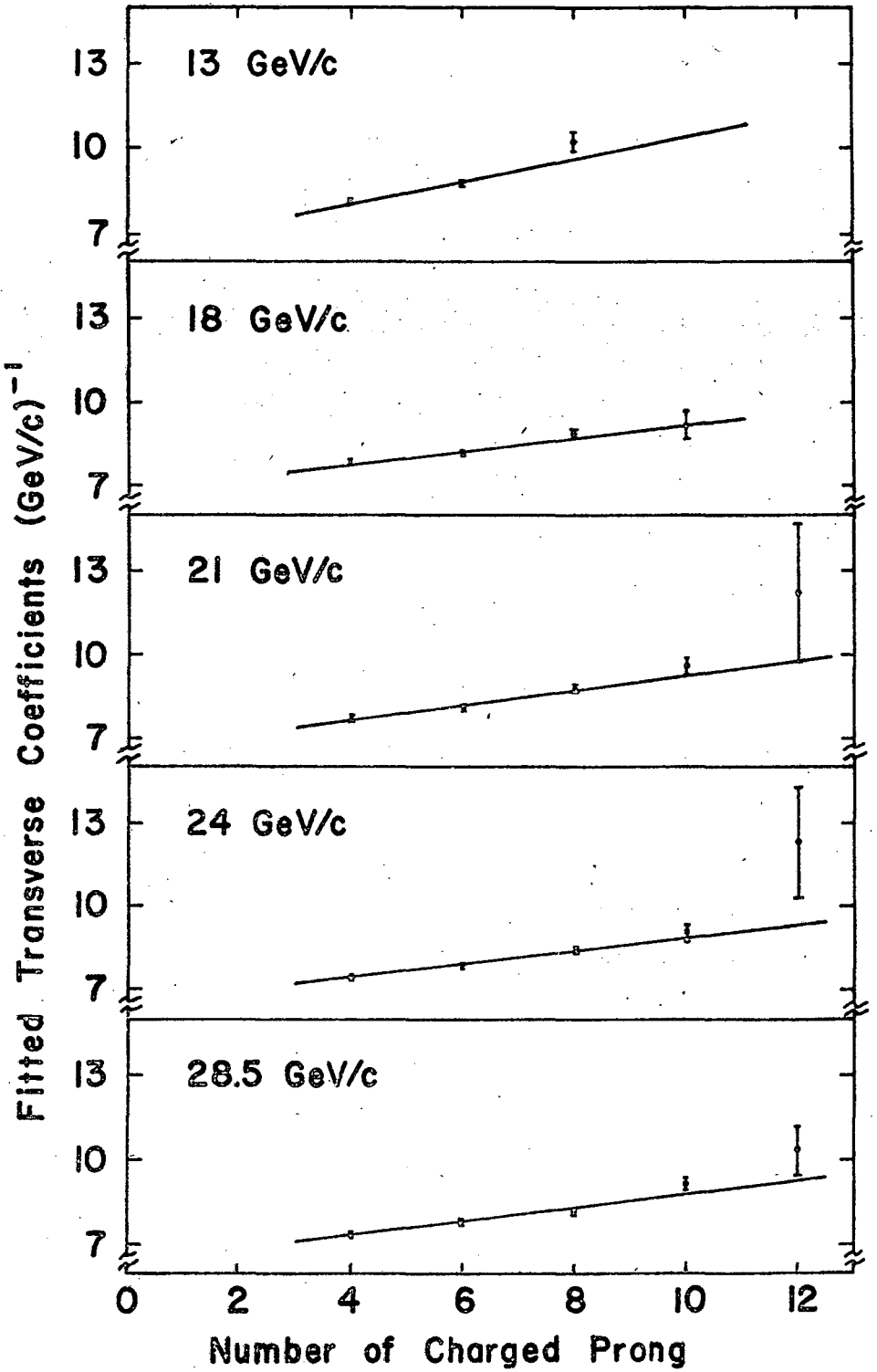
13 GeV/c
18 GeV/c
21 GeV/c
24 GeV/c
28.5 GeV/c
Fitted Transverse Coefficients (GeV/c)$^{-1}$
Number of Charged Prong

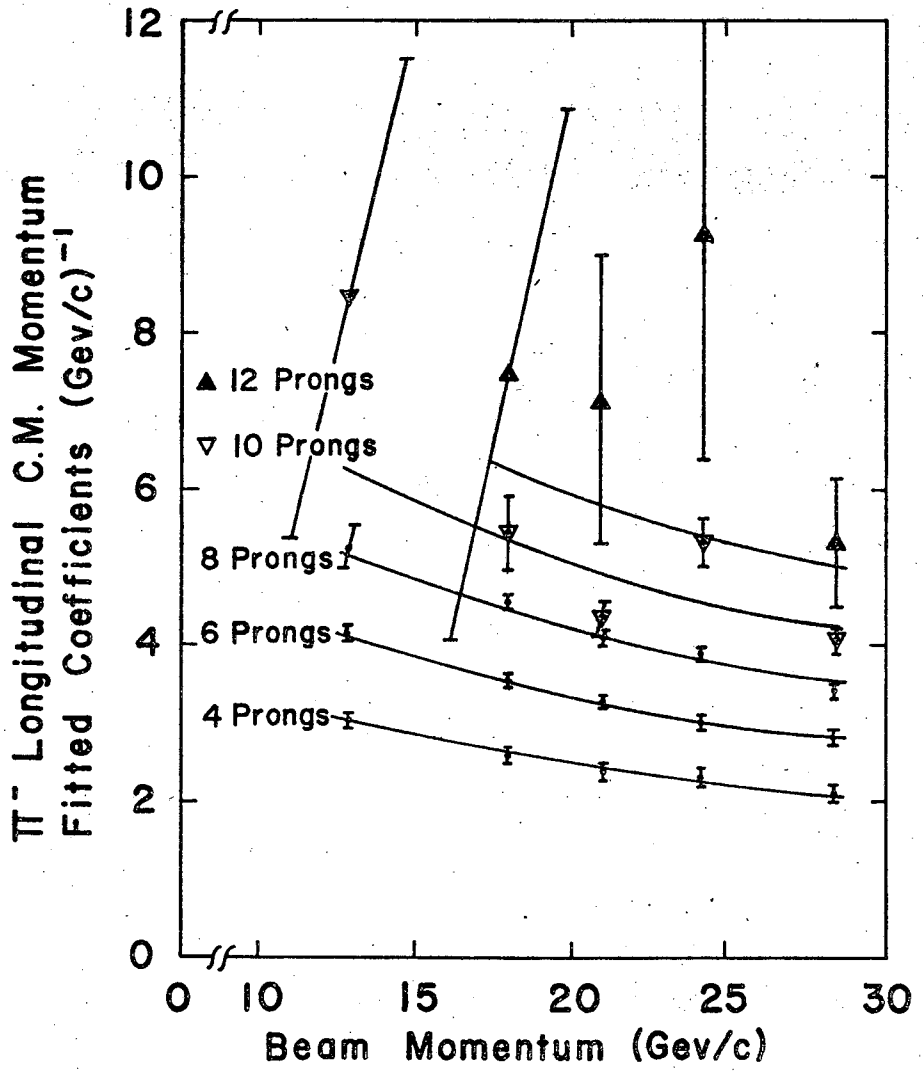

Figure 14.

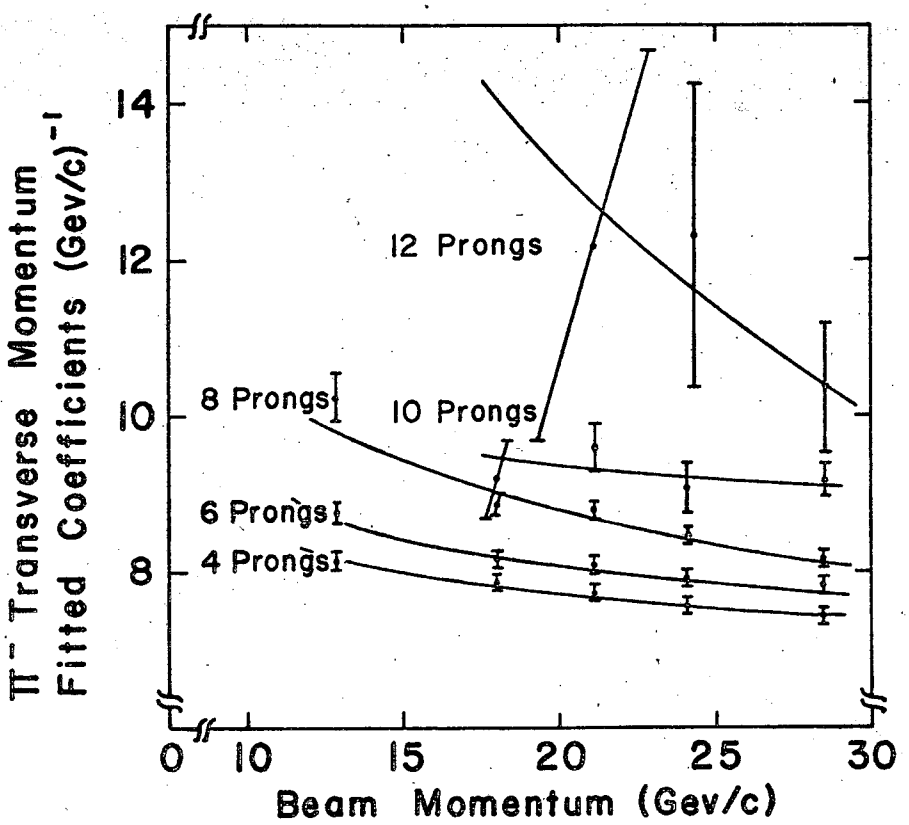

Figure 15.

TECHNICAL INFORMATION DIVISION
LAWRENCE RADIATION LABORATORY
UNIVERSITY OF CALIFORNIA
BERKELEY, CALIFORNIA 94720